JOURNAL OF MADENAT ALELEM COLLEGE

REFEREED SCIENTIFIC JOURNAL Published
by the University College of Madenat al-elem , Iraq , Baghdad , AlKadmyia

Vol:4 No:1 year: 2012 ISSN: 2073-2295

كلية مدينة العلم الجامعة

Madenat Alel em Uni versity College

مجلة كلية مدينة العلم

العراق - بغداد - الكاظمية المقدسة

Journal of Madenat Al-elem College
(JMAC)

E-mail: Jmac2009m@yahoo.com

P.O,Box (9216) Tel:5238850

WWW.madenatalelem.com

INSTRUCTIONS to AUTHERS

Submitted articles to the Journal of Madinat Al-Elem University College can be published in all fields related to the Academic Departments of the College (Biology, Law, programming Engineering Sciences, and Computer Techniques Engineering).

Written request for publication and signing a consent form to publish must be for articles which have not been published or submitted for publication to other journals. Three copies with CD are needed. Manuscripts should be typed on: A4 white paper, double spaced, written in Times New Roman font size 14. Margins should be 3cm from top, bottom, left and right. The main title should be in: bold Times New Roman font size 14. Author names should be written in the following sequence: first name, middle name, the family name, followed by the names of departments and institutions of work. A footnote accompanies the first page stating the full address of correspondence author.

Articles need to contain the following items:

- Abstract in English and Arabic not more than 300 words.
- Article includes the following items: Introduction, Materials and Methods, Results and Discussion, Conclusion and References.
- References should be numbered in the text according to the sequence appeared in the text and listed in order.
- Tables and figures should be appropriately titled with size not exceed an A4 page.

The editor reserves the right to reject or accept any article submitted.

Contents

Proposal New Approach for Blowfish Algorithm by Using Random Key Generator

Israa Tahseen[1]and Shatha Habeeb[2]
University of Technology, Computer Sciences Department
[1]Israa80atar@yahoo.com, [2]ShathaHabeeb@yahoo.com

Abstract

There are three basic encryption methods: hashing, symmetric cryptography, and asymmetric cryptography. Each of these encryption methods has their own uses, advantages, and disadvantages. All the three of these encryption methods use cryptography or the science of scrambling data. Although there are several pieces to an encryption process, the two main pieces are the algorithms and the keys. Blowfish, a symmetric block cipher and a Feistel network which follows simple Enciphering and Deciphering functions of 16 times each. The strength of the Blowfish algorithm relies on its sub-key generation and its basic confusion and diffusion based design. The proposed method are generate key drawn from parts of the image and by the size of key used with Blowfish.

Key word: Blowfish, symmetric, key, encryption, ciphertext.

المستخلص

طرق التشفير الأساسية ثلاثة: التجزئة والتشفير المتناظر والتشفير غير المتناظر. كل من هذه الأساليب للتشفير لها استخدامات خاصة ومزايا وعيوب. كل هذه الأساليب تتضمن استخدام التشفي أو علم هرولة البيانات. على الرغم من أن يكون هناك عدة اجزاء لعملية التشفير، والاجزاء الرئيسية هي الخوارزميات والمفاتيح blowfish. تشفيركتلة متماثل وشبكة تتبع التشفيرالبسيط وفك التشفير ويتكون من 16 مرة لكل منهما. قوة خوارزمية Blowfish يعتمد على المفتاح الفرعي. في هذا البحث تم اقتراح وسيلة لتوليد مفتاح مستخلص من أجزاء من الصورة ويحدد حجم االمفتاح المستخدم مع blowfish الخوارزمية المستخدمة في تشفير النص.

1. Introduction

The algorithms used in computer systems are complex mathematical formulas that dictate the rules of how the plaintext will be turned into ciphertext. A key is a string of random bits that will be used by the algorithm to add to the randomness of the encryption process. The entities to be able to communicate via encryption, they must use the same algorithm, many times, and the same key. In some encryption technologies, the receiver and the sender use the same key, and in other encryption technologies, they must use different but related keys for encryption and decryption purposes [1].

2. Blowfish Algorithm

Blowfish, a symmetric block cipher and a Feistel network which follows simple Enciphering and Deciphering functions of 16 times each. The strength of the Blowfish algorithm relies on its sub-key generation and its basic confusion and diffusion based design.[2] Blowfish cipher uses 18 each of 32-bit Permutation arrays precisely known as P-Boxes and 4 Substitution boxes referred as S-Box each of 32 bit size and having 256 entries each. It uses a Feaster cipher which is a general method of transforming a function into another function by using the concept of permutation, diffusion, confusion [3].

The working of blowfish cipher can be illustrated as follows, It splits the 64 bit block into two equal blocks having 32 bit size each, left block is XORed with first Sub array P1 and thus obtained result is fed in to a function called F-function. Inside the F-function substitution operations are carried out which in turn converts 32 bit blocks in to another 32 bit blocks. Thus resulted 32bit entries are XORed with the right half and the result obtained is swapped as the left half for the next round. The Fiestal Structure of Blowfish Algorithm with 16 rounds of encryption is shown in the following Figs.1, 2, and 3.

3. Related work of key generator

A key generator is used in many cryptographicprotocols to generate a sequence with many pseudo-random characteristics. This sequence is used as an encryption key at one end of communication, and as a decryption key at the other.

The initial value of the LFSR is called the seed, and because the operation of the register isdeterministic, the stream of values produced by the register is

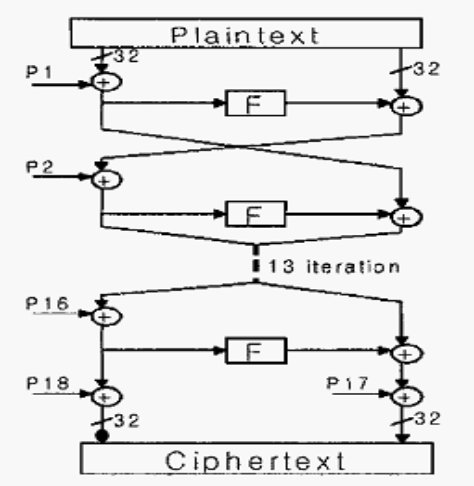

Figure (1) blowfish algorithm.

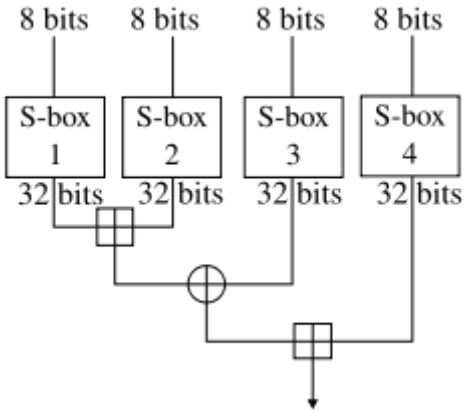

Figure (2) s-boxes to blowfish.

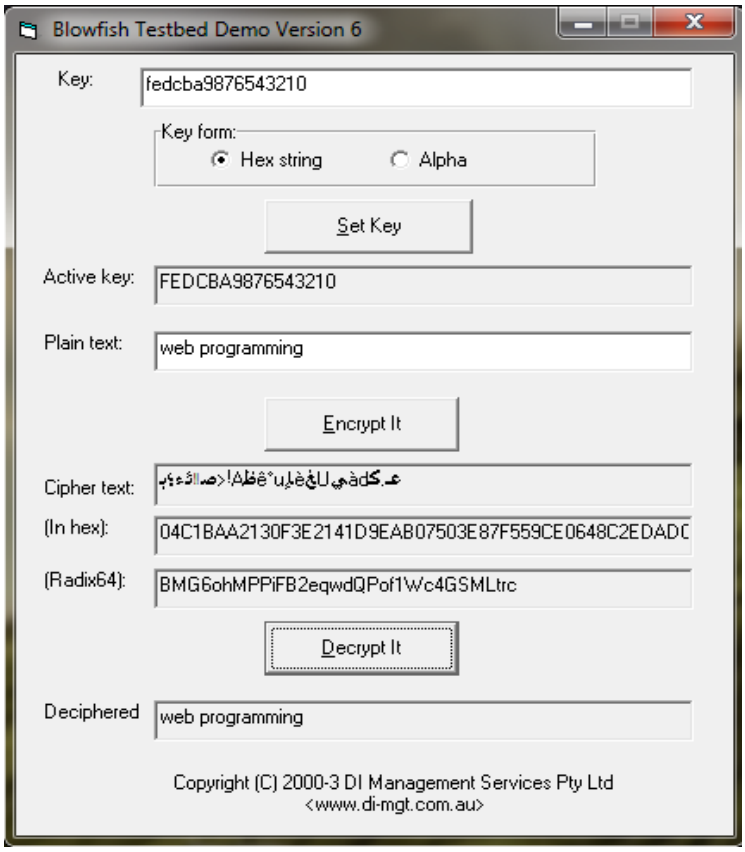

Figure (3) implementation of blowfish.

completely determined by its current(or previous) state. Likewise, because the register has a finite number of possible states, it must eventually enter a repeating cycle. However, an LFSR with a well-chosen feedback function can produce a sequence of bits which appears random and which has a very long cycle [3,4].

Refer to a technique, its objective is the blending between the two encryption methods. Data Encryption Standard (DES) and Diffie Hellman to make DES more safe and secure. That by propose two options first one include injection the encryption DES after the seventh round with Diffie-Hellman just as key distribution algorithm then the results of the last back to the eighth round to complete the encryption process of DES. The second include injection the encryption DES after the eighth round with Diffie-Hellman just as key distribution algorithm to generate key the results of the eighth round will be encrypted using stream cipher then back to the ninth round to complete the encryption process of DES [5].

This tool generates a WPA encryption key that can be used to secure your Wireless network. Generate the WPA Encryption key, copy it and paste it into your wireless router's configuration panel. Restart your DSL modem/router.

WPA is designed for use with an 802.1X authentication server, which distributes different keys to each user. However, it can also be used in a less secure "pre-shared key" (PSK) mode, where every user is given the same passphrase. The Wi-Fi Alliance calls the pre-shared key version WPA-Personal or WPA2-Personal and the 802.1X authentication version WPA-Enterprise or WPA2-Enterprise[6].

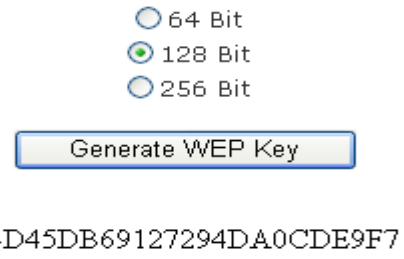

Fig.(4) web key generator 64,128,or 256 bit

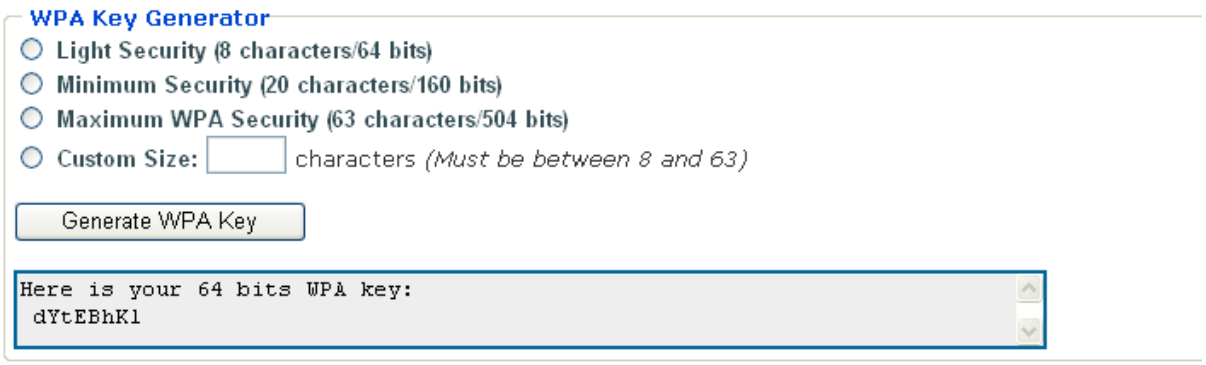

Fig. (5). Web key generator between 8-63 characters.

4. The Design of the Proposal

The proposed system suggests technique to derive the encryption key of any image are set by the user and determines the location of the points drawn from the key and depends on the colors red and blue and taking x or between the red and blue and a series of numbers is the key and determines its length according to Blowfish algorithm between 32-448 bit size.

Algorithm of proposal

Step 1: Load picture
Step 2: read picture by pixel and RGB
Step 3: get the key 32-448 bit size
Step 4: convert key to ASCII or Hex
Step5: use key to Blowfish Algorithm End

5. The Implementation of the Proposal System

The implementation of the proposal is using VB6 language. The application consists of several interfaces start to upload a photo as the user's choice and read the points and pull the two colors red, blue and the work of XOR. Then determines the length of the key according to the method used between 32-448 bit, (Figs. 6-10) to explain the proposal.

6. Conclusion

By studying the Blowfish algorithms and analysis its work, this research presents some modification on it. By implementing the proposed modified key of Blowfish there is some point concluded, these are:

The encryption of Blowfish has something danger, that it is an algorithm depend on symmetric key, so if the key is discovered that will destroy the Blowfish security. From previous point, the research proposes key generation method aim to reduce the danger of symmetric keys by

taking short key and from it the | overall key will be generated.

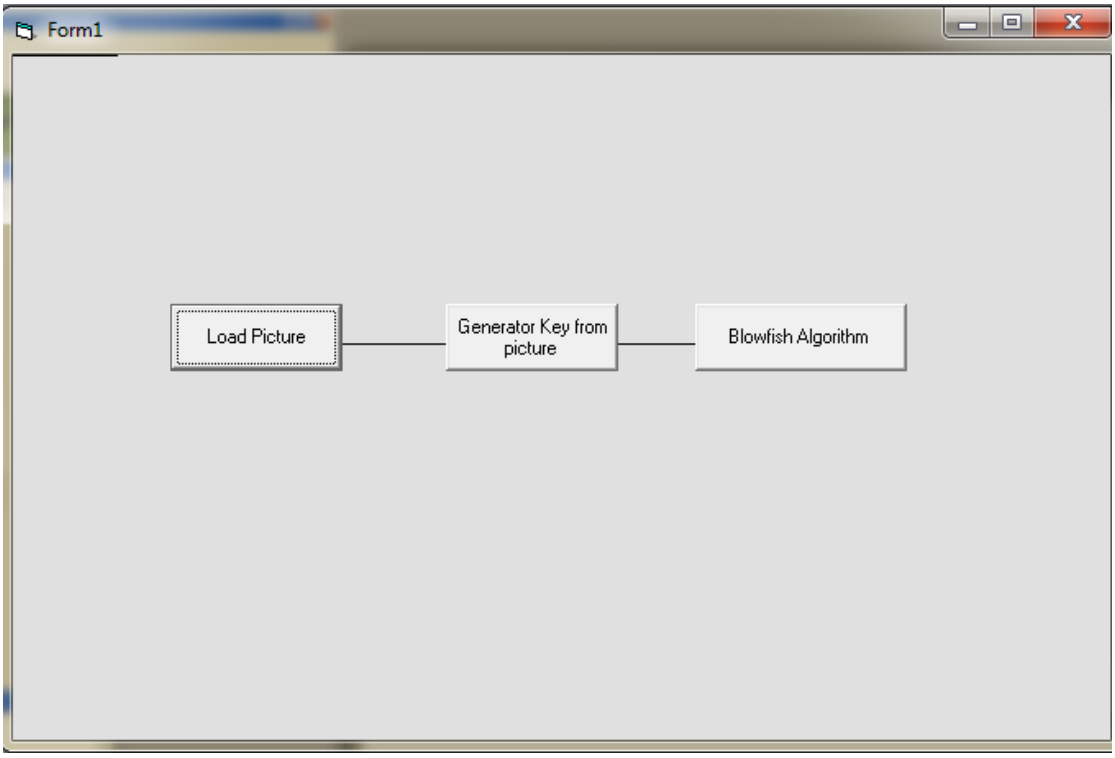

Figure (6) main proposal system.

In figure(7) The main application interface.

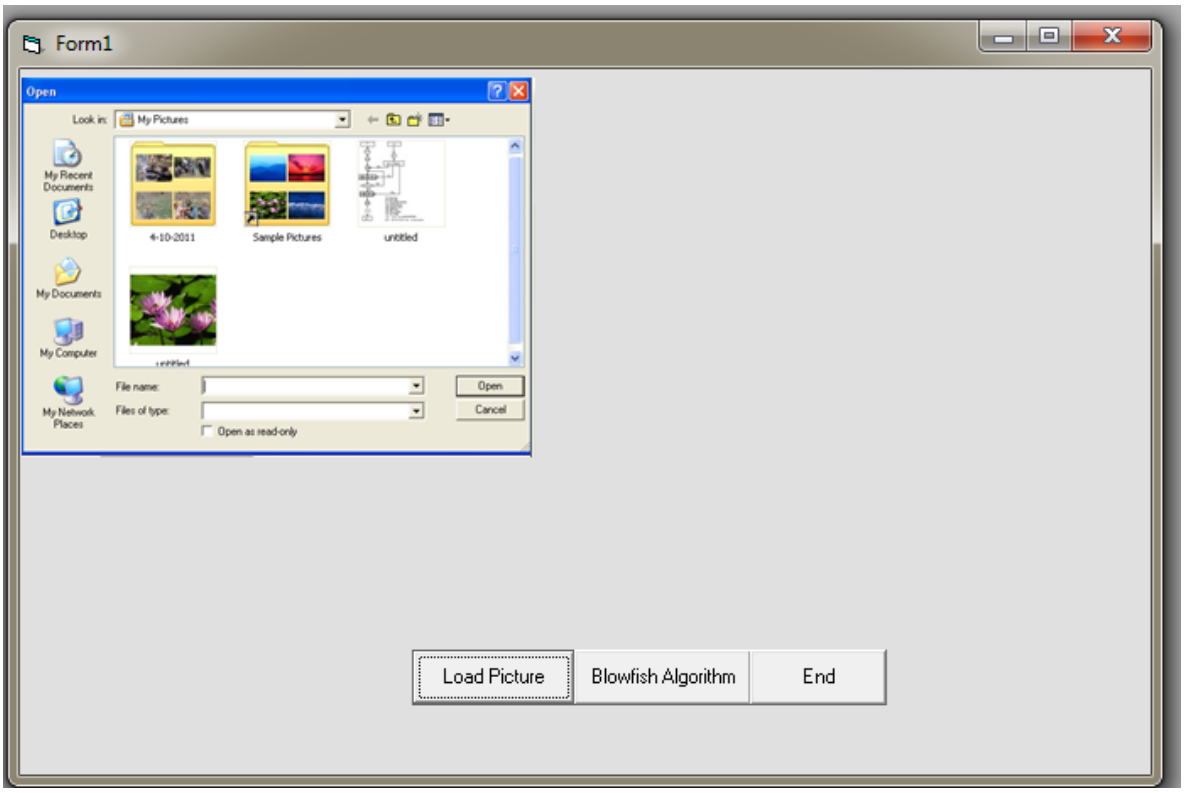

Fig.(7) main implementation load image

In figure (8) the second interface choose Key size

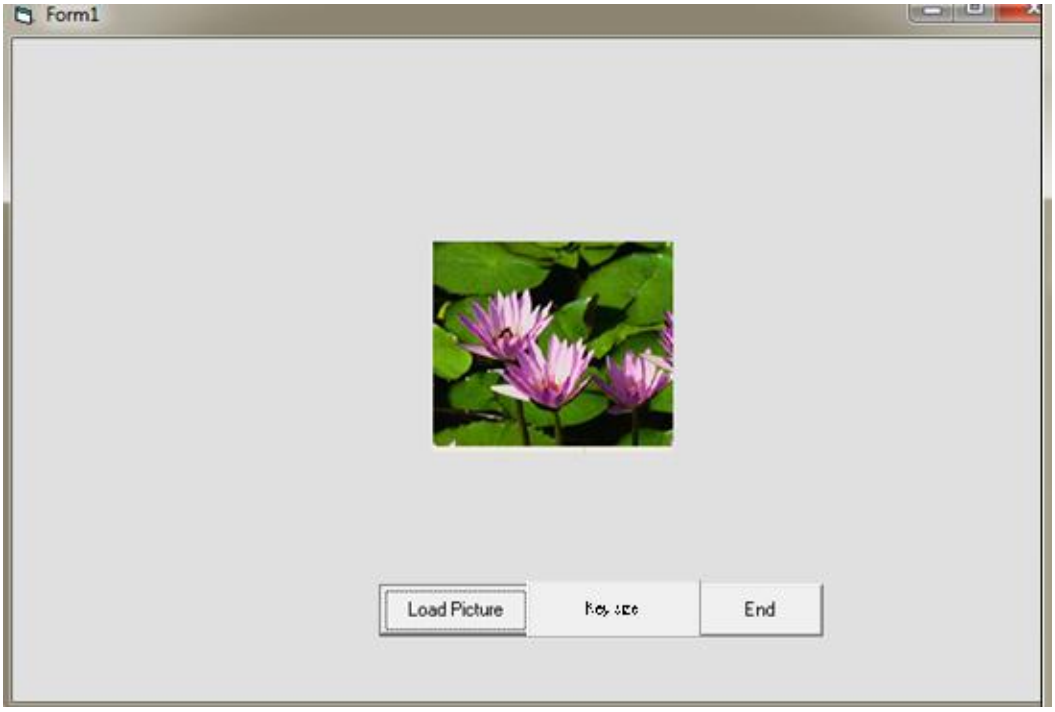

Fig. (8) Choose size of key.

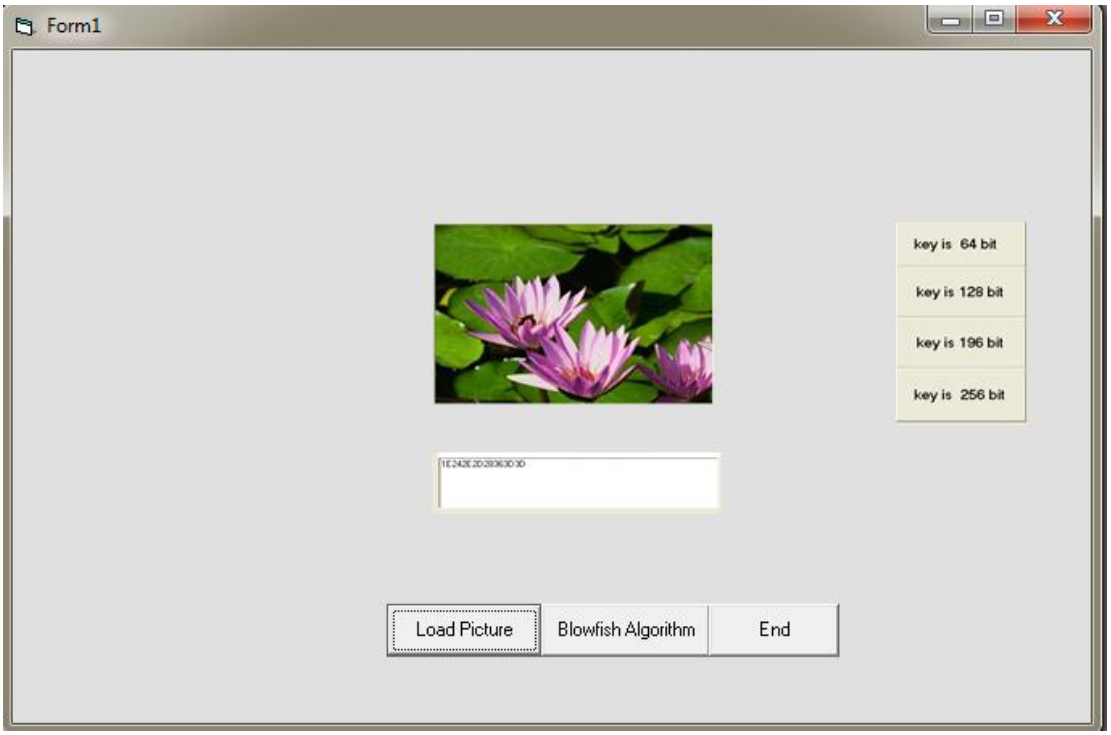

Fig. (9) Generator key.

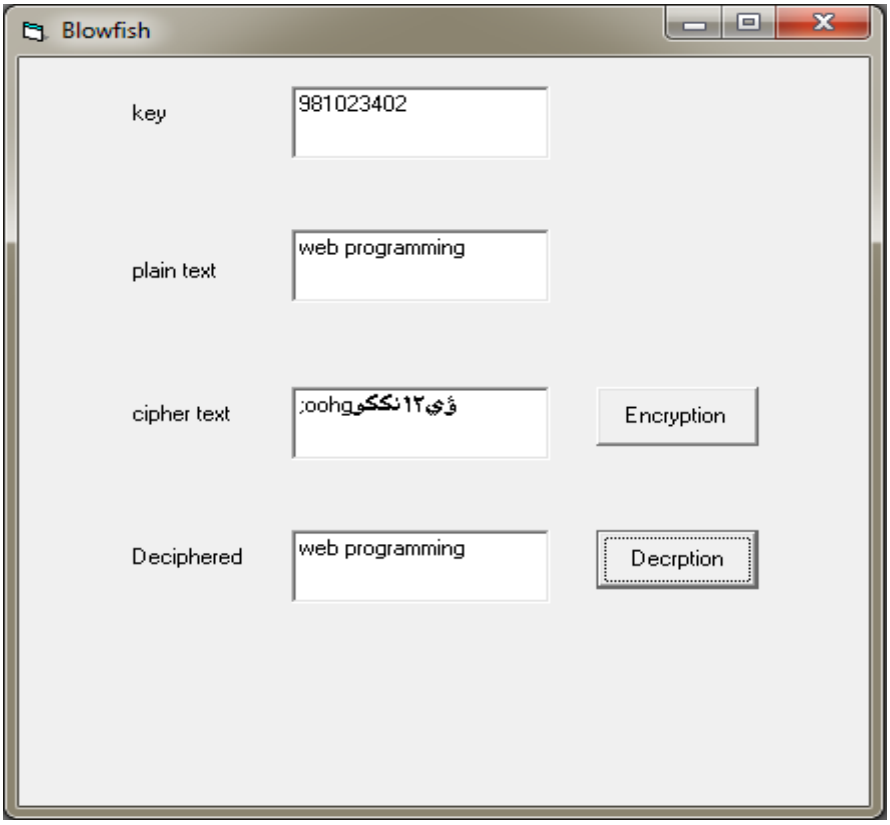

Figure (6) Blowfish proposal system.

References

1. Blowfish, http://en.wikipedia.org/wiki/Blowfish_(cipher)
2. "Type-3 Feistel Network of The 128-bits Block Size Improved Blowfish Cryptographic Encryption", Ashwaq T. Hashim Received on: 28/5/2008 Accepted on: 6/11/2008
3. Adam Young. "Mitigating insider threats to RSA key generation". Crypto Bytes, 7(1):1–15, 2004.
4. Encryption & decryption,

   http://www.encryptionanddecryption.com/encryption/
5. "Modification to Improve the Mobile-Commerce Security" A Dissertation Submitted to the department of computer science of university of technology in partial fulfillment of the requirement for degree of Doctor of philosophy in computer science by Soukaena Hassan Hashem, 2002 (77-90).
6. R.Satheesh Kumar, E.Pradeep, K.Naveen and R.Gunasekaran "**A Novel** Approach for Enciphering Data of Smaller Bytes" International Journal of Computer Theory and Engineering, Vol. 2, No. 4, August, 2010.
7. Shatha Habeeb " *Proposal to Complex DES Security Using Diffie Hellman Injection* **",(**1216-1226) Engineering & Technology Journal Vol. 29, No. 6, 2011.

Assessment of Soil Contamination in Area Surrounding Tuwaitha Nuclear Facilities

Ali A. Fahad Al-Taii, Shakir M. Al-Jobori, and Jabbar F. Al-Maadhidi

University College of Madenat Elem, Kadimiya, Baghdad, Iraq

Abstract

The wide spread looting of the Tuwaitha Nuclear Facilities as well as damaging of some buildings in 2003, had offered possibilities of contamination of soil environment inside the Site. The objective of the present work was to investigate soil contamination to help in future decontamination programs. A total of 25 soil surface samples (including one reference sample) covered different locations in the Site were collected in March 2011. High purity Ge detector was used for gamma spectrometry of soil samples. Data of total and spectral gamma for U series, Th series, ^{40}K and ^{137}Cs are presented. Slight variations were observed in specific activity of the U series (^{214}Bi or ^{214}Pb and ^{226}Ra) among measured soil samples where the range was 10.3-12.7 for ^{214}Bi as compared with 12.2-33.4 Bq/kg for ^{226}Ra. Values of both ^{214}Bi and ^{226}Ra are in the range of reference sample specific activity indicating that no evidence of contamination had occurred in the investigated area. Results of activity concentrations of thorium series (^{228}Ac or ^{208}Tl, ^{212}Pb, and ^{212}Bi) are in the range of reference sample and close to those values given worldwide for natural uranium in soil. The levels of ^{40}K in soil are within the natural abundance of this isotope in the soil where the range was 207.6-266.1 with 220.3 Bq/kg for the reference sample. On the other hand, ^{137}Cs specific activities showed great variation among measured samples. The minimum value for ^{137}Cs was 0.6 and the maximum 7.6 compared with 0.8 Bq/kg for the control soil sample. The non-uniformity of radioactivity concentration of ^{137}Cs suggest the presence of contamination in some locations although this level is considered as an acceptable level and no hazardous effect will be generated.

Key words: Tuwaitha site, soil contamination, natural isotopes, U series, Th series, K-40, Cs-137.

تقييم تلوث التربة في المساحة المحيطة بالمنشآت النووية في التويثة

المستخلص

إن اعمال النهب الواسع التي حدثت في المنشآت النووية في التويثة فضلاً عن تدمير بعض البنايات في عام 2003 وفر احتمال تلوث التربة المحيطة بالمنشآت النووية. يهدف العمل الحالي الى دراسة تلوث التربة المحيطة بهذه المنشآت للمساعدة في برامج ازالة التلوث في المستقبل. تم جمع 25 عينة تربة تمثل مواقع مختلفة في المنشآت (من ضمنها عينة من تربة المرجع بعيداً عن التويثة) في آذار 2011. استخدم عداد الجيرمانيوم عالي النقاوة لتحليل طيف أشعة كاما في عينات التربة. بينت نتائج النشاط الإشعاعي النوعي لسلسلة اليورانيومU والثوريومTh وكذلك البوتاسيوم ^{40}K والسيزيوم^{137}Cs. لوحظ وجود تغايرات بسيطة في النشاط النوعي لسلسلة اليورانيومU (^{214}Bi أو ^{214}Pb و ^{226}Ra) في عينات التربة المقاسة حيث وصل المدى الى 10.3–12.7 للبيزموث^{214}Bi مقارنة بـ 12.2–33.4 بكريل/كغم للراديوم ^{226}Ra. كانت قيم ^{214}Bi و ^{226}Ra ضمن مدى عينة المرجع والذي يؤشر الى عدم وجود تلوث التربة بهذه النظائر. أشارت نتائج النشاط الإشعاعي لسلسلة الثوريوم Th (^{228}Ac أو ^{208}Tl و ^{212}Pb و ^{221}Bi) أن المدى كان ضمن عينة المرجع وهي قريبة من القيم المذكورة عن اليورانيوم الطبيعي في العالم. كانت مستويات البوتاسيوم ^{40}K ضمن التواجد الطبيعي لهذا النظير في التربة حيث وصل المدى الى 207.6–266.1 مقارنة مع 220.3 بكريل/كغم لعينة المرجع. من جهة أخرى، أظهر النشاط النوعي الإشعاعي للسيزيوم ^{137}Cs تغاير كبير في العينات المقاسة. حيث كانت أقل قيمة 0.6 وأعلى قيمة 7.6 مقارنة بـ 0.8 بكريل/كغم لعينة المرجع. يعود عدم الإنتظام في تركيز الـ ^{137}Cs الى وجود تلوث في بعض المواقع رغم أن هذه المستويات تكون مقبولة ولا تسبب خطورة.

الكلمات الدالة: موقع التويثة، تلوث التربة، النظائر الطبيعية، سلسلة اليورانيوم ، سلسلة الثوريوم، البوتاسيوم–40، السيزيوم–137.

Introduction

The Tuwaitha Nuclear Facilities (TNF), about 20 km south of Baghdad, had been damaged or destroyed in 1981 (Israel attack), 1991 (First Gulf War), and 2003 (US military operation). The TNF had partially enriched uranium, along with quantities of highly radioactive medical and industrial isotopes, sensitive equipment, chemical stores, and radioactive waste materials. The wide spread looting of the Site as well as damaging of some buildings in 2003, had offered possibilities of contamination of soil environment inside the Site.

Next to air and water, soil is generally considered as the main environmental component. Handling

of potential pollution problems in soil must be based on the prediction of the functioning of soil. Soil may act as a sink for deposited fallout radionuclides [1] and/or contaminants reached from many possible sources. Also, soil that is heavily contaminated with pollutants will be a source for contamination [2]. Therefore, the dual functions of soil in this process, acting as sink and being a source of pollutants are connected. Consequently, predictions on the retaining factors and decontamination of radionuclides are possible with detailed investigation of the complicated system.

Soil is a valuable environmental monitoring medium because it can accumulate contaminants from both current air emissions and resuspended materials. Hence, soil sampling and analysis evaluates long-term contamination trends and monitors environmental radionuclide inventories [3]. Radioactivity observed in soil could be originated from fall-out radionuclides (^{137}Cs and ^{90}Sr), natural isotopes (Uranium series and ^{40}K), fission products (^{137}Cs, ^{60}Co, and others), or contaminants reached soil due to accidents or mishandling of radioactive materials [1].

Cesium-137 was introduced into the environment mainly through atmospheric nuclear tests, in the 1950s and 1960s and the Chernobyl accident in 1986 [4] where significant amounts of fallout ^{137}Cs were deposited worldwide on the landscape. Cesium-137 is a gamma and beta emitter with a relatively long half-life of 30.2 years. Therefore, ^{137}Cs is expected to persist for some time. However, it is relatively immobile in the environment and is expected to sorb strongly to soils and sediment, especially those with high clay or organic content [5]. In this respect, Fahadet. al. [2] found most of ^{137}Cs in the liquid waste applied to soil columns taken from Tuwaitha Site and leached for 180 days with water, remained in the upper 10 cm of soil. Also, 96% of ^{137}Cs applied to soil columns in the form of CsCl and in concentration of 18.5 MBq/column remained in the upper 1.0 cm even leached with 240 cm of water for 115 days [6]. Results of these experiments suggest that the Tuwaitha soil is highly reactive to ^{137}Cs and other radionuclides and when they present, they will be strongly adsorbed by soil particles in essentially nonexchangeable or irreversible forms.

Natural uranium (U) occurs in soils in typical concentrations of a few parts per million. Uranium-238 is the most abundant isotope in natural uranium (fraction by weight in natural uranium is 99.28%) and decays into other radioactive elements [7]. In surface soils, its concentration ranges from 0.1 to 20 mg/kg with a world average value of 2.8 mg/kg [8]. Natural uranium

consists of a mixture of three radioactive isotopes which are identified by the mass numbers ^{238}U (99.2836% by mass), ^{235}U (0.711%) and ^{234}U (0.0054%).These radionuclides have very long half-lives: 4.5 x 10^9, 7 x 10^8 and 2.5 x 10^5 years, respectively [9]. Uaranium-238 decays into series of isotopes, ^{234}Th, ^{234}Pa, ^{234}U, etc. down the decay chain [10].

Potassium is an important constituent of fertile soil and is an essential nutrient for plant growth; it is widely distributed in nature and is present in all plant and animal tissues [11]. Potassium-40 is a naturally occurring radioactive isotope of potassium which has a very long half-life of 1.248 ×10^9 years [12]. It decays to ^{40}Ca by emitting a beta particle with no attendant gamma radiation (with branching time of 89%) and to the gas ^{40}Ar by electron capture with emission of an energetic gamma ray (with branching time of 11%).

This paper presents results of soil contaminations with radionuclides in area surrounding Site of the Tuwaitha Nuclear Facilities. The information presented here will aid in understanding the real situation of contamination of the area and in future decontamination programs.

Materials and Methods

Study Site:

The area under investigation is located 20 km southeast Baghdad, Iraq in the Tigris valley with coordinates of 33° 12" latitude and 44° 30" longitude and elevation of 39.3 m. Average annual precipitation in the area is about 150 mm, and the prevailing wind direction is from the northeast.

The soils of the area are recent alluvium without any horizons differentiation. These are entisols with an ochricepipedon as result of plowing. Organic matter content in the upper soil surface did not exceed 1.5% and lime content was relatively high and may be observed as a fine fraction in non-active form. The salinity status depends upon many factors including environmental conditions, soil texture, landscape features, and groundwater table [13].

Water table depth is in the range 130-400 cm and is not a fixed level; it rather increases in summer to the greatest depth from the soil surface, while it decreases in winter [13]. The fluctuation in water table levels may be due to i) absence of efficient drainage system in the area and ii) effect of water levels in the Tigris and Diyala rivers on the groundwater level.

Sampling and characterization of soil:

Sampling of soil was carried out on an area of nearly 2 hectare surrounding nuclear facilities and buildings in March 2011. Surface soil samples (0-25 cm depth) were taken by auger and transferred to laboratory. A total number of 24 samples were collected from the area with one sample taken far from the investigated area (Zaafraniya, 1.0 km south of the Tuwaitha Site) to represent a reference sample (control). Location map of the samples is given in Figure 1. List of samples locations is given in Table 1.

Some physical and chemical characteristics of the investigated soils (Location 10 and 15) are given in Table 2. For characterization of soils, standard procedures of soil analysis have been used [14].

Measuring of radioactivity (gamma-ray spectrometry):

Soil samples were air dried, ground by rubber hammer, and screened through a 2.00 mm sieve. Exactly 1000 g were taken from each bulk soil sample and placed in plastic sheet for gamma spectrometry.

For gamma spectrometry analysis of soil samples, high purity germanium detector, Canberra was used for this purpose. The relative efficiency of the system was 30% with energy resolution of 2 keV for 1.33 MeV gamma line of ^{60}Co. The system was calibrated using reference source ^{152}Eu Marnelii beaker geometry for the reference and samples. The counting time was 60 min for each soil sample. Analysis of gamma spectrometry was accomplished by the Faculty of Radiation Protection Center, Ministry of Environment.

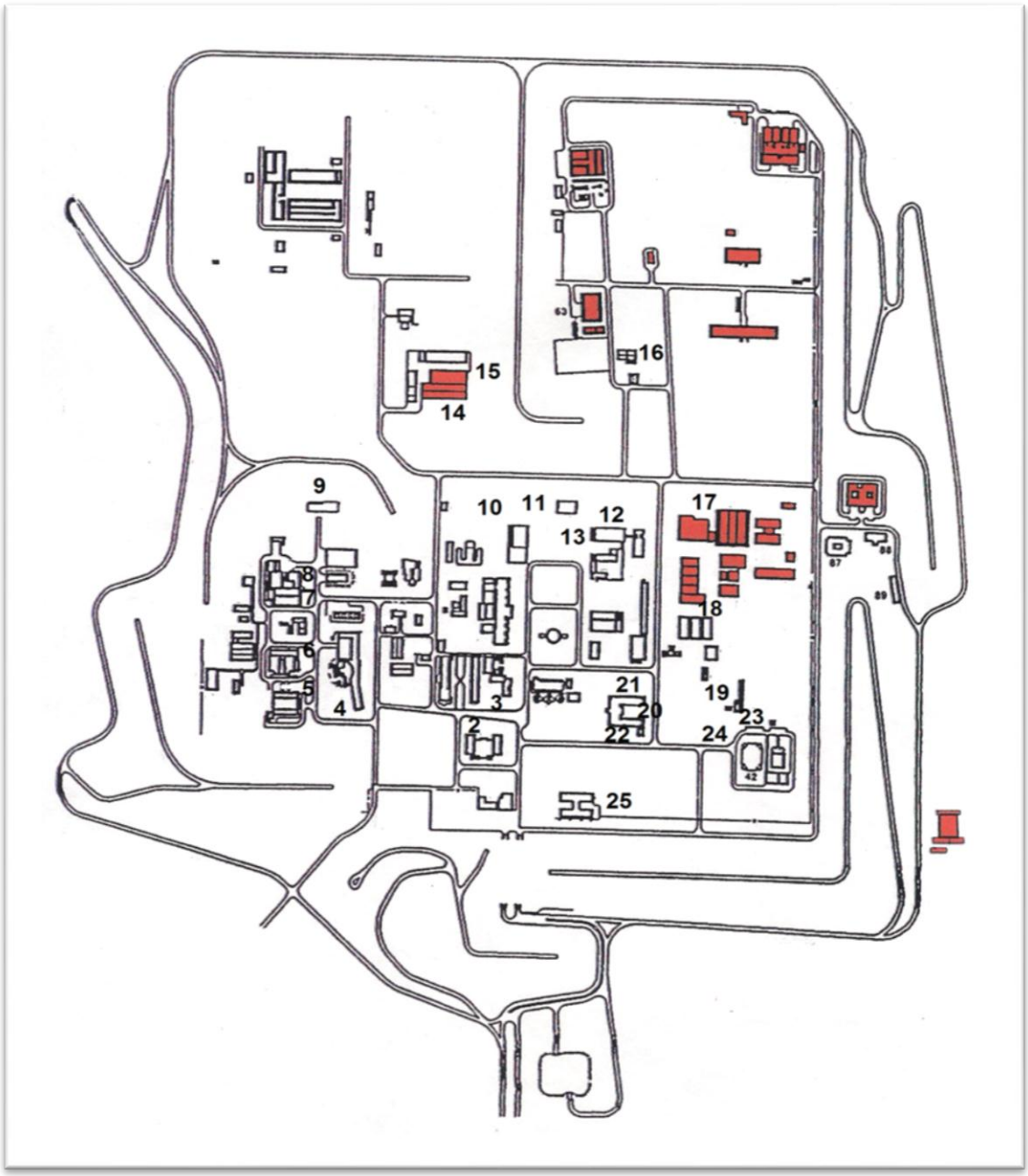

Fig. 1. Lay out of the Tuwaitha Site where the numbers indicate the location of soil sampling.

Table 1. Number of soil sample and the corresponding building or activity at the Tuwaitha Site.

Sample Number	Location in the Tuwaitha Site
1	Reference sample (Control) taken from Zaafaraniya, 1.0 km south of Baghdad
2	Restaurant
3	Radiochemistry Labs
4	Tamuz-2, zero power reactor (destroyed)
5	Laboratory Work Building
6	Hot Laboratory (LAMA)
7	RWTS, North
8	RWTS, Northwest
9	Waste Storage for Tamuz-1 Reactor
10	Tamuz-1 (IRT-5000), West
11	Tamuz-1 (IRT-5000), Northwest
12	Isotope Production, West
13	Isotope Production, South
14	Chemical Waste Treatment, East
15	Chemical Waste Treatment, North
16	Sewage Station
17	Health Physics
18	Green Houses
19	Water Treatment Station
20	Agriculture and Biology, North
21	Agriculture and Biology, West
22	Agriculture and Biology, East
23	Main Library, West
24	Main Library, Southwest
25	Administration Building, North

Table 2. Some physical and chemical characteristics of the soils.

Characteristics	Sample Location 1 (Reference)	Sample Location 10	Sample Location 15
Clay (g kg^{-1})	312	293	315
Silt (g kg^{-1})	490	303	490
Sand (g kg^{-1})	198	304	195
Soil Textural Class	Silty Clay Loam	Clay Loam	Silty Clay Loam
Electrical conductivity (dS/m)$^{+}$	3.1	2.5	2.6
pH^{+}	8.0	8.1	8.1
Lime (g kg^{-1})	255	386	246
Organic Matter (g kg^{-1})	12.6	11.4	14.0
Cation Exchange Capacity (cmol kg^{-1})	26.2	27.6	25.9
Soluble Cations (mg kg^{-1})			
Ca^{++}	138.1	81.2	122.4
Mg^{++}	50.5	36.9	48.6
Na^{+}	56.8	12.8	45.5
K^{+}	27	12.5	28

+ Measurements were made on saturation extract.

Results and Discussion

Uranium and thorium series in soil samples:

Data on specific activity of uranium and thorium series measured by high purity Ge detector are presented in Table 3. Total gamma and spectral gamma provide a direct measurement of uranium progeny isotopes in the soil [10]. Uranium undergoes radioactive decay to lead via a series of radioactive progeny or daughter radionuclides. Some nuclides emit gamma radiation as the nucleons and electrons reconfigure to a more stable form during or shortly after an alpha or beta decay [10]. Only data of 10 samples (selected randomly) are given in Table 3 including the reference sample (sample taken from area far from the investigated one). It is evident that slight variations were observed in specific activity of the U series (^{214}Bi or ^{214}Pb and ^{226}Ra). For these 10 locations, the minimum specific activity for ^{214}Bi was 10.7 Bq/kg (nearly 0.86 mg/kg in unit of mass concentration) (Sample 21) and

a maximum of 12.7 Bq/kg (nearly 1.02 mg/kg) (Sample 12); the reference (or the control) sample was 12.0 Bq/kg (nearly 0.97 mg/kg). The ^{226}Ra showed higher values than ^{214}Bi in those 10 samples. Specific activities of ^{214}Bi and ^{226}Ra in all samples (25 samples) are best evaluated by the statistical parameters given in Table 4. Less variation was obtained for ^{214}Bi than for ^{226}Ra where the range (minimum and maximum) was 10.3, 12.7 for ^{214}Bi as compared with 12.2, 33.4 Bq/kg for ^{226}Ra. Values of both ^{214}Bi and ^{226}Ra are in the range of reference sample specific activity indicating that no evidence of contamination had occurred in the investigated area. The current values of both isotopes are close to those values given worldwide for natural uranium in soil. United Nation SCEAR [15) reported values in the range from 0.3 to 11.7 mg/kg of uranium in soil worldwide. Bleise et al. [16] showed that values for concentration of uranium in soil were from 0.7 to 11 and to 15 mg/kg in farmland soil due to use of phosphate fertilizers. Also, Gilday and Edick [17] reported values of 0.9-2.3 for ^{226}Ra (U chain) and 1.1-2.7 pCi/g for ^{228}Ra (Th chain) in soil of New York State, USA.

Results of activity concentrations of thorium series (^{228}Ac or ^{208}Tl, ^{212}Pb, and ^{212}Bi) for only 10 samples (locations) are given in Table 3. Statistical parameters (mean, min, max, and standard deviation) of these isotopes for all samples are given in Table 4. Apparently, variations among samples for the same isotope were minimal. At the same time, values are close to the control sample indicating that the radioactivity of these isotopes was in the range of background readings. For instance, the minimum and maximum specific activity of ^{228}Ac was 9.0 and 14.6 as compared to 12.8 Bq/kg for the control sample. Similarly, the ^{212}Pb showed values of 7.8 and 15.7 for minimum and maximum with 9.1 Bq/kg for the control sample. The magnitude of the specific activity of U and Th series (^{226}Ra, ^{214}Pb, ^{228}Ac, ^{212}Pb, and ^{212} Bi) for the 25 soil samples is given in Figure 2. In general, ^{226}Ra showed the highest magnitudes among the measured 25 soil samples followed by ^{228}Ac, ^{212}Pb, and ^{212}Pb with the lowest magnitude was for ^{212} Bi.

Table 3. Specific activities of U series and Th series for 10 soil samples including the reference sample.

No.	Location No.	Specific Activity (Bq/kg)				
		U series		Th series		
		Bi-214 or Pb-214	Ra-226	Ac-228 or Tl-208	Pb-212	Bi-212
1	Reference (Control)	**12**	**21.8**	**12.8**	**9.1**	**8.6**
2	2	11.5	20.7	11.2	8.2	5.8
3	11	12.4	31.5	11.7	9.1	8.1
4	12	12.7	19.5	9.0	7.8	5.3
5	14	11.4	25.8	10.7	9.2	7.3
6	15	11.7	23.9	14.6	9.7	7.3
7	18	11.3	22.8	11.2	9.9	8.6
8	19	11.8	20.5	11.2	9.2	8.8
9	21	10.7	18.2	11.9	8.7	7.04
10	22	11.5	22.4	13.1	9.9	5.1

Table 4. Statistical parameters of the specific activity of uranium and thorium series for the 25 soil samples.

Statistical Parameter	Specific Activity (Bq/kg)				
	U series		Th series		
	Bi-214 or Pb-214	Ra-226	Ac-228 or Tl-208	Pb-212	Bi-212
mean	11.6	23.0	11.7	9.6	7.1
max	12.7	33.4	14.6	15.7	10.2
min	10.3	12.2	9.0	7.8	4.7
Stand. dev.	0.75	4.82	1.30	1.60	1.55
(Control)	**12**	**21.8**	**12.8**	**9.1**	**8.6**

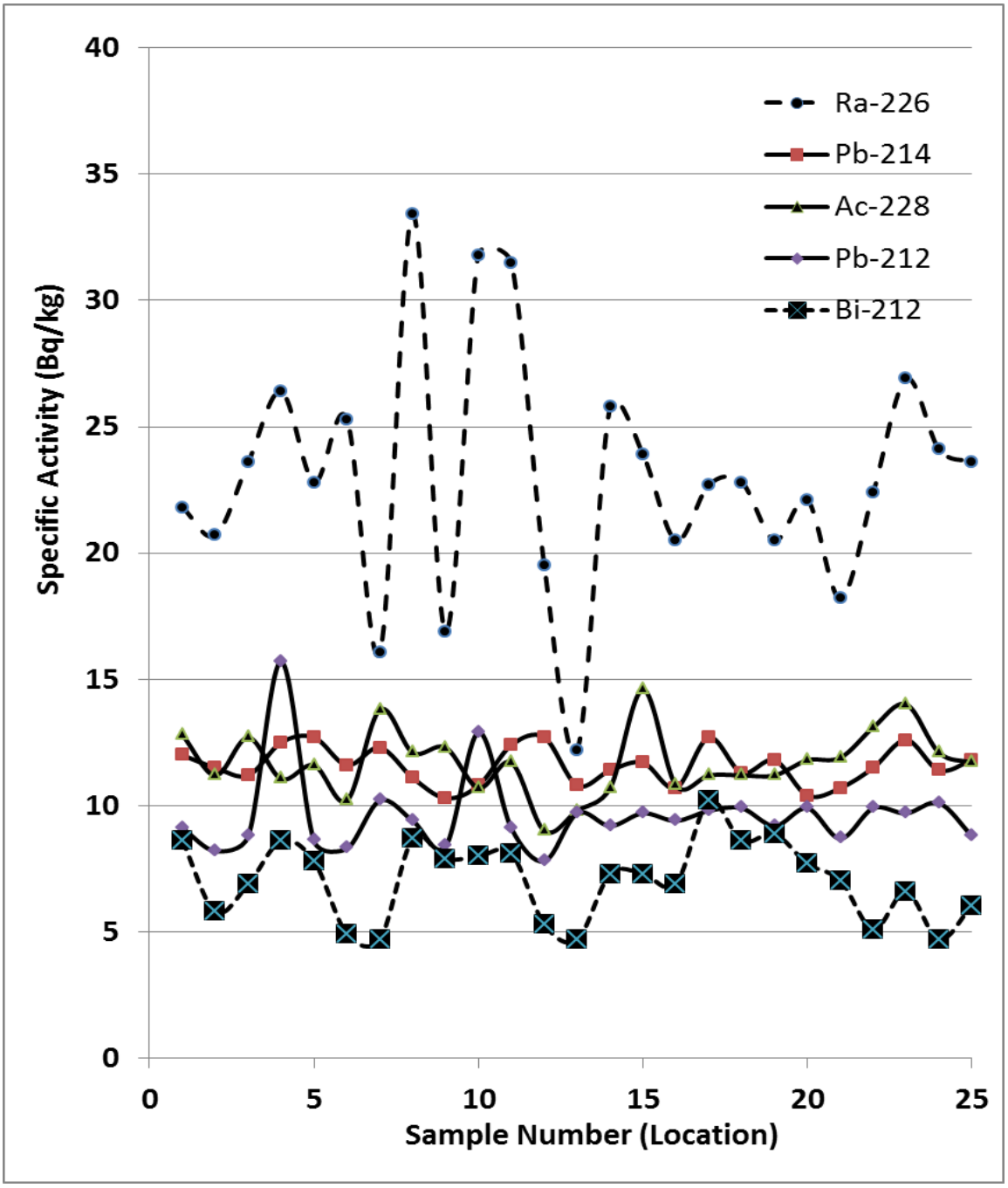

Fig. 2. Magnitudes of the specific activity of U and Th series (Ra-226, Pb-214, Ac-228, Pb-212, and Bi-212) for the 25 soil samples.

Potasium-40 and Cesium-137 in soil samples:

Specific activity of ^{40}K and ^{137}Cs for 10 soil samples selected randomly along with the statistical parameters for the 25 soil samples are given in Table 5. Data on ^{40}K indicate the presence of slight variations in specific activity among measured samples. Most of samples specific radioactivities were very close to the reference sample. The minimum specific activity was 207.6 and the maximum 266.1 with 220.3 Bq/kg for the reference sample. Therefore, it is expected that these levels of ^{40}K in soil are within the natural abundance of this isotope in the soil. Potassium is an important constituent of fertile soil and is an essential nutrient for plant growth and in the human diet. ^{40}K is an important radionuclide in terms of the dose associated with naturally occurring radionuclides and comprises a very small fraction (about 0.012%) of naturally occurring potassium [18].

Zhu et al. [19] showed that ^{40}K is a natural isotope present in soil and an essential plant's nutrient. Under field conditions, plants can suffer from potassium starvation (or potassium deficiency) periodically or constantly throughout the growing season, due to spatial and temporal variations in the potassium status of agricultural soil. Holmgen et al. [20] reported value of 51,800 mCi/km^2 (1,916 kBq/m^2 or nearly 5474 Bq/kg) for ^{40}K in soil of the USA and this value is not high enough to be hazardous.

Unlike ^{40}K, ^{137}Cs specific activities showed great variation among measured samples (Table 5). The minimum value for ^{137}Cs was 0.6 (Sample 7) and the maximum 7.6 (Sample 21) compared with 0.8 Bq/kg for the control soil sample. It is expected that ^{137}Cs was deposited as fallout primarily during the late 1950s and the 1960s and after Chernobyl accident in 1986 and in most environments was rapidly and strongly absorbed by soil particles at the ground surfaces [21]. Figure 3 presents histograms of the magnitudes of both ^{40}K and ^{137}Cs among the 25 soil samples. The greater deviation in ^{137}Cs values among the investigated soil samples is evident. On the other hand, very slight deviation was observed for ^{40}K.

Since the distribution of fallout ^{137}Cs is assumed to be uniform on soil surface, the variability of radioactivity concentration observed in soil samples reflected the presence of an input other than the fallout deposition. Even though the maximum specific activity observed was 7.6 Bq/kg (Location 21), this

level is considered an acceptable level and no hazardous effect will be generated. The locations which have shown the highest radioactivity of ^{137}Cs (much greater than the reference sample) are in ascending order: 21 (Agriculture and Biology Building), 18 (Green houses), 12 (Isotope production), and 4 (Tamuz-2 destroyed reactor). It is believed that the source of ^{137}Cs in Locations 18 and 21 was the looting which occurred in 1991 and 2003. This looting resulted in spreading contaminated soils and/or containers of liquid ^{137}Cs. The high level of ^{137}Cs in Locations 4 and 12 is hard to be explained. In this respect, Holmgen et al. [20] reported an average value of 620 mCi/km^2 (22,940 Bq/m^2 or nearly 65.5 Bq/kg) for ^{137}Cs in the USA. In the arable part of the catchment area of central Europe, Van der Perk et al. [21] estimation was 8756 Bq/m^2 [25 Bq/kg) for ^{137}Cs.

Table 5. Specific activity of ^{40}K and ^{137}Cs for 10 soil samples and the statistical parameters for the 25 soil samples.

No.	Location No.	Specific Activity (Bq/kg)	
		K-40	Cs-137
Data for 10 Samples			
1	**Reference (Control)**	**220.3**	**0.8**
2	2	228.0	2.08
3	11	230.9	0.8
4	12	207.6	3.4
5	14	218.7	0.72
6	15	258.9	0.74
7	18	232.5	4.05
8	19	253.3	2.2
9	21	230.1	7.6
10	22	238.3	1.27
Statistical Parameters for 25 Samples			
mean		236.2	2.1
max		266.1	7.6 (Sample 21)
min		207.6	0.6 (Sample 7)
Stand. dev.		15.91	1.52

Gamma spectral analysis of soil samples:

Spectral analysis of gamma radiation measured by HPGe detector for only four selected soil samples are given in Fig. 4 (Sample 1, Reference sample and Sample 5, Laboratory Work Building) and Fig. 5 (Sample 15, Chemical Waste Treatment-North and Sample 21, Agriculture and Biology-West). In general, nearly the same spectrum was observed for the investigated 25 soil samples. The difference was in magnitude of energy peaks for ^{212}Pb, ^{137}Cs, and ^{40}K. The spectrum given is a natural-gamma energy spectrum, which is caused by the decay of uranium, thorium, and potassium-40, along with anthropogenic radioactive isotopes ^{137}Cs. Natural gamma rays are emitted by isotopes that are the natural products (daughter products) of the uranium decay series, the thorium decay series, and potassium-40 [22]. Uranium and thorium each decay into a series of unstable (radioactive) daughter products. The uranium decay series consists of several unstable elements in nature; this series of unstable isotopes finally decays to a stable (not radioactive) lead isotope. The decay of thorium forms a similar series of unstable elements. Potassium-40 decays into two stable isotopes, argon and calcium [22].

In Figures 4 and 5, the spectrum of gamma energy was plotted versus the count rates (counts the number of gamma emissions associated with each energy level), where the energy ranges from nearly 10 to 1,765 keV (for ^{214}Bi). The isotopes and the corresponding energy peak are presented in Table 6 in ascending order of their decay energy. Post-processing was used to determine the concentration of these isotopes in the investigated soils presented in Tables 2-5.

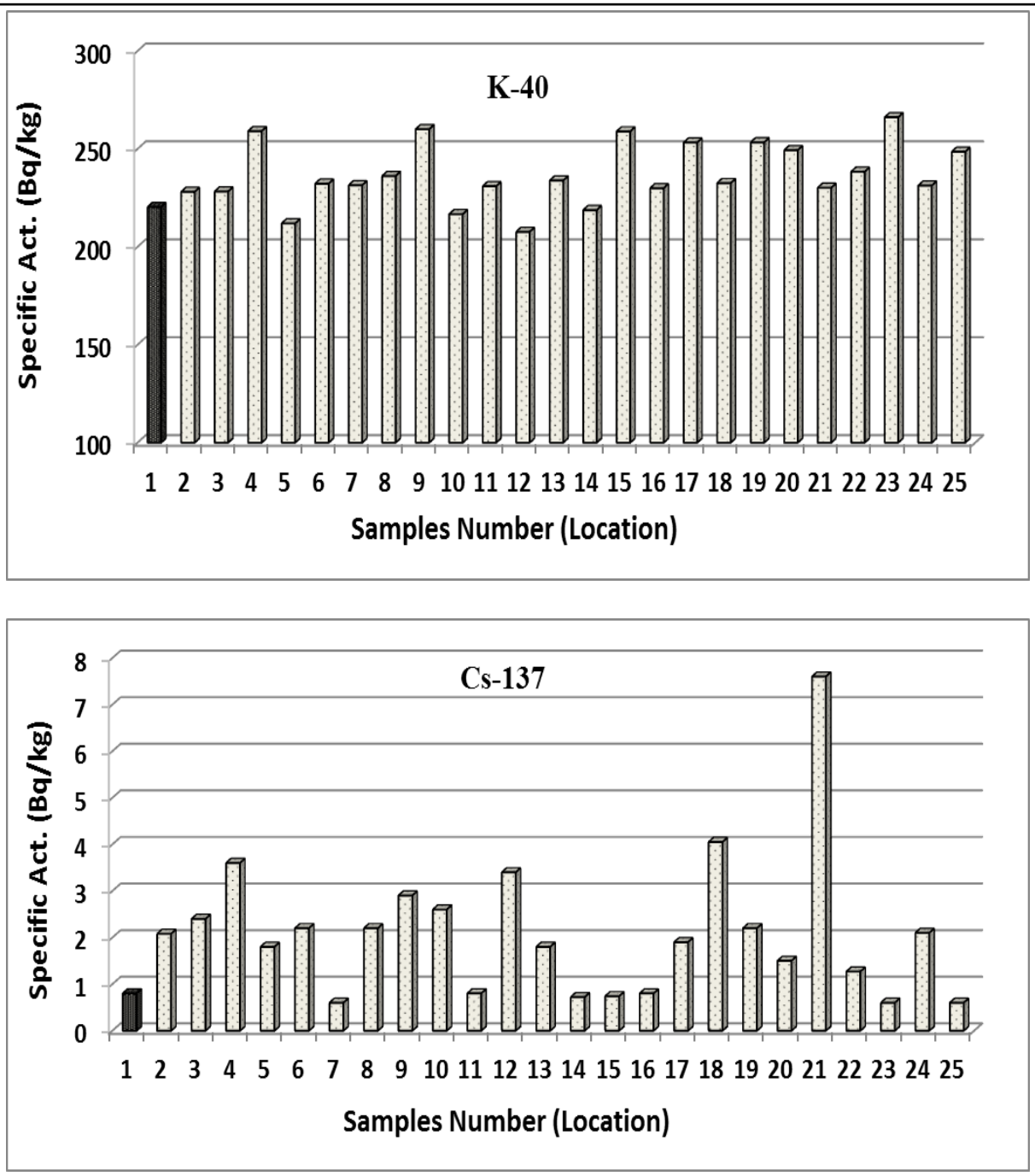

Fig. 3. Magnitude of specific activity of K-40 and Cs-137 among soil samples where sample number 1 refers to the reference (control)

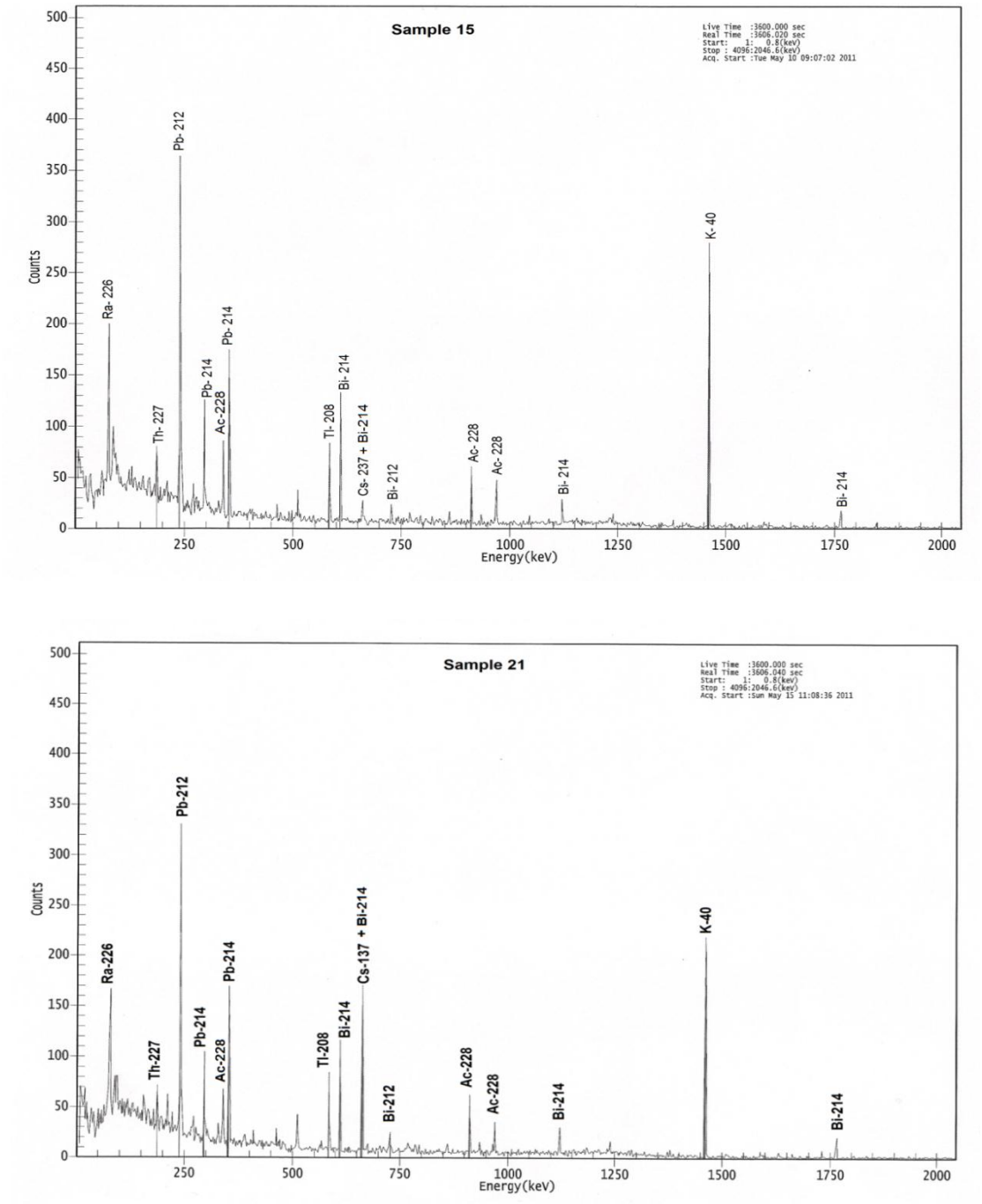

Fig. 5. Gamma spectral analysis of soil sample 15 (Chemical Waste Treatment, North) and sample 21 (Agriculture and Biology, West).

Table 6.Isotopes and the decay energy of gamma radiation of the investigated soil samples and their corresponding energy in ascending order.

No.	Isotopes	Energy (keV)
1	Ra-226	210.1
2	Th-227	210.1
3	Pb-212	239.1
4	Pb-214	296.1
5	Ac-208	339.0
6	Pb-214	352.0
7	Tl-208	583.3
8	Bi-214	609.3
9	Cs-137	661.8
10	Bi-212	727.7
11	Ac-228	911.0
12	Ac-228	969.0
13	Bi-214	1120.0
14	K-40	1460.0
15	Bi-214	1765.0

References

1. Gee, G.W., Rai D., and Serne R.E. (1983). Mobility of radionuclides in soil. In: Chemical Mobility and Reactivity in Soil Systems, 203-227, *Am. Soc. Agron.*, Madison, Wisconsin, USA.
2. Fahad, A.A., Razaq I.B., Shihab R.M., Ali A.W., and Tawfeek H.A. (1990). Migration of liquid waste ^{137}Cs and ^{60}Co in calcareous soils. *Waste Manage.* 10:117-124.
3. DOE, Department of Energy (2000). Guide of Good Practices for Occupational Radiological Protection in Uranium Facilities. Chapter 4– Contamination Control, DOE-STD-1136-2000.
4. Anspaugh, L.R., Catlin R.J., and Goldman M. (1988). The Chernobyl accident. *Science* 242:1513-1519.
5. Mabit, L., Benmansour M., and Walling D.E. (2002). Comparative advantages and limitations of the fallout radionuclides 137Cs, 210Pb, 7Be for assessing soil erosion and sedimentation. *J. Environ. Radioactivity* 99(12):1799-1807.

6. Fahad, A.A. (1987). Movement of Cs-137 in undisturbed calcareous soil and its extractability and association with soil particles. *Isotope & Rad. Res*. 19(2):153-161.
7. Stegnar, P. and Benedik L. (2001). Depleted uranium in the environment – an issue of concern. *Archive of Oncology 9*(4):251-255.
8. UN SCEAR , United Nations Scientific Committee on the Effects of Atomic Radiation (2000). Sources and Effects of Ionizing radiation. Report to the General Assembly, with scientific annexes.
9. Bem, B. and Bou-Rabee F. (2004). Environmental and health consequences of depleted uranium use in the 1991 Gulf War. *Environment International* 30:123-134.
10. US EPA, United States Environmental Protection Agency. "Depleted Uranium", Technical Brief, EPA 402-R-06-011, December 2006, Washington, DC 2046.
11. ANL, Argonne National Laboratory, EVS (2005). Human Health Fact Sheet, August 2005.
12. Green, M.G. (1978). A simple measurement of the isotopic abundance of ^{40}K. Phys. Educ. 13:348-350.
13. Al-Sanawy, K.I. (1974). Hydrological investigations, depth, and distance of field drain for the soils of Nuclear Research Centre in Tuwaitha. Report contributions to State Organization of Soils and Land Reclamation, Baghdad, Iraq.
14. Page, A.L., R.H. Miller, and D.R. Keeney (1982). Methods of Soil Analysis: Chemical and Microbiological Properties, Second Edition. Agronomy 9 (Part 2), Madison, Wisconsin, USA.
15. UN SCEAR, United Nations Scientific Committee on the Effects of Atomic Radiation (UNSCEAR), 1993. Report to the General Assembly, with scientific annexes, New York.
16. Bleise, A., Danesi, P., Burkart, W. 2003. Properties, use and health effects of depleted uranium (DU): A general overview. *Journal of Environmental Radioactivity* 64: 93-112.
17. Gilday, W.M. and Edick R.G. (1999). An investigation ofnaturally occurring radioactivity materials (NORM) in oil and gas wells in New York State. Division of Solid & Hazardous Materials, Bureau of Radiation and Hazardous Site Management, DEC Publication.
18. Ciuffo, L.E.C., Belli M., Pasqule A., Menegon S., and velasco H. (2002). ^{137}Cs and ^{40}K soil-to-plant relationship in natural grassland of the Giulie Alps, Italy. *The Science of the Total Environ.* 295(1-3) :69-80.

19. Zhu, Y. G. and Shaw G. (2000). Soil contamination with radionuclides and potential remediation. *Chemosphere* 41(2):121-128.

20. Holmgen G.G., Meyer M.W., Chaney R.L., and Daniels R.B (1993). Cadmium, Lead, Copper and Nickel in Agricultural soils. Agricultural soil in the United States of America, 1st Ed., Vol. 22: 335-348.

21. Van der Perk, M., Slavik O., and Fulajtar E. (2002). Assessment of spatial variation of cesium-137 in small catchments. *J. Environ. Quality* 31:1930-1939.

22. Pritchard. M. "Health Risks of Depleted Uranium: An Independent Review of the Scientific Literature. Students of Science for Peace", University of Toronto, 2004.

Effect of Oxidation of Some Aluminum Alloys on X-ray Attenuation Coefficients

Farid M. Mohammed[1], Raed N. Razooqi[2], and Sokayna E. Yusuf[3]

[1]Dept. of Physics/College of science ,University of Tikrit P.O.Box 42. Iraq, (dr_fr_2006@yahoo.com); [2]Dept. of Mechanical Engineering College of Engineering, University of Tikrit P. O. Box 42 . Iraq (Raidmousis@yahoo.com); [3]Dept. of Physics/College of Education , University of Tikrit P.O.Box 42. Iraq

Abstract

Characteristic X-ray of 35KV (Mo-Tube) was used to determine the attenuation coefficients of x-ray for some of aluminum alloys with different thicknesses after oxidized them at different times and temperatures. By graphic figures and the phases formation on each sample's surfaces, we studied the effect of oxidation circumstance on absorption. The phases (θ-Al_2O_3) and (GeO_2) were formatted on alloy A, (θ- Al_2O_3), (GeO_2) and ($AlGe_{0.0435}$) on alloy B, (MgO) and (Al_2SiO_5) on alloy C hence we found direct proportion between absorption logarithm with thickness and equivalent thickness for alloy C , while we got inverse proportions for alloys A and B which was due to the phases formation on their surfaces, we found absorption logarithm for alloy C increased with ratio 0.178% after 4 hours later comparing with the same sample at same circumstances after the first half hour. The relation between the half value thickness and mean free path with attenuation coefficients were determined also.

Keywords : x-ray absorption , attenuation coefficients , oxidation , mean free half thickness .

تأثير أكسدة بعض سبائك الألمنيوم على معاملات التوهين للأشعة السينية المستخلص

تم استخدام الأشعة السينية المميزة (35) kV مع (Mo –Tube) لحساب معاملات التوهين للأشعة السينية لبعض سبائك الألمنيوم بسماك مختلفة بعد أكسدتها بفترات ودرجات حرارة مختلفة. درسنا تأثير ظروف الأكسدة على الامتصاصية من خلال الأشكال البيانية والأطوار المتكونة على السطح . ان الأطوار المتكونة على السبيكة A هي (θ- Al_2O_3) و (GeO_2)، والسبيكة B (θ- Al_2O_3) و(GeO_2)، اما السبيكة C فكانت الاطوار هي ($AlGe_{0.0435}$) و(MgO) و(Al_2SiO_5). تم ايجاد علاقة خطية بين لوغاريتم الامتصاصية والسمك والسمك المكافئ للسبيكة C. وتكون العلاقة عكسية للسبيكتين A و B بسبب الأطوار المتكونة على سطوحها. يزداد لوغاريتم الامتصاصية بنسبة 0.178% بعد 4 ساعات من أكسدتها مقارنة مع نفس العينة تحت نفس الظروف بعد النصف ساعة الأولى من التأكسد. تم حساب العلاقة بين سمك النصف ومعدل المسار الحر لمعاملات التوهين.

1. Introduction

Uncovered tissue can be severely damaged if it was exposed to the X-ray for a long time. Long-term continual exposures at sensible levels can directly cause a variety of skin disorders , while a continual relatively low-level exposures may be considered as a factor in increased cancer risk exposed workers . Many early workers with X-rays developed serious ailments (from skin lesions to various forms of cancer) as a consequence of their work . Although there are safeguards associated with modern X-ray tools designed to minimize or attenuate radiation in the work surroundings , an awareness of the dangers of radiation exposure and associated safety issues is required for any worker using X-ray laboratories [1] .

2. Theory

X-ray:

The intensity of emitted X-ray by the anti-cathode is directly proportional to the current inside the tube and to the square of the applied voltage .However , the efficiency of the emission process is very low , and even in the best conditions , with a voltage of 100 kV, only 2% of the energy provided is transmitted to the X-rays. Roughly 98% of the electron beams energy is consumed by the Joule effect and heats up the anticathode, which is why it is important to set up a system to

evacuate heat. A cooling system by water circulation is used as shown in Fig. (1) [2 - 6] .

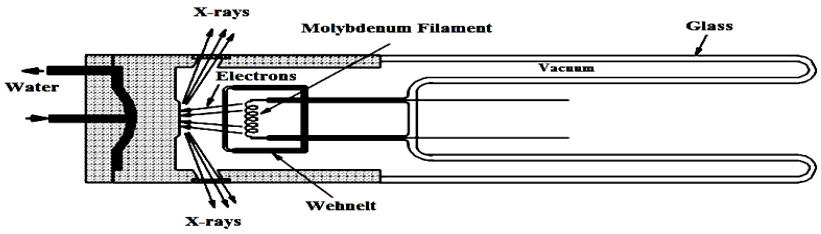

Fig.1 X-ray tube

The Oxidation:

The bulk structures of oxides of magnesium, aluminum, iron, titanium and silicon have been described in detail in several textbooks [7 - 11].

- The metals of the alloys have different affinities for oxygen because of difference free energy to form oxides.
- Form trio oxides or more in the alloys.
- Disparity in acceptability dissolution between the oxides.

Alloys oxidation is so complication cooperation with pure metals because of [12 & 13]:

- Because metal ions are diverse then they possess different mobility in oxides phases.
- Metals in the alloys have different diffusion.
- Oxygen dissolution in alloy form secondary flat precipitation like interior oxides. Fig (2) show oxidation of pure metals and alloys.

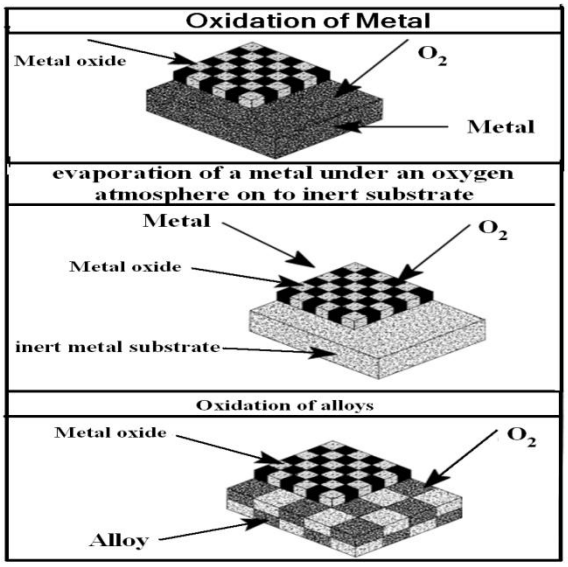

Fig. 2 Oxidation in pure metals & alloys [12]

Experimental , Germanium addition to Aluminum alloys in general has high affection to betterment alloy ductile and oxide plate even betterment oxidation resist at high temperature about (550 °C) , the oxide formation on alloys surface that container Germanium will stay right in all temperature (100 to 550) °C [13 & 14] .

3. Experimental:

a. Sample Preparation

Melting and Casting: after checking alloys constituents by a sensitive electric weighing scale a suitable quantity put in melting pot of silicon carbide in a furnace which corroboration at 700 °C, the melting alloys poured in cast mold , Figure (3)

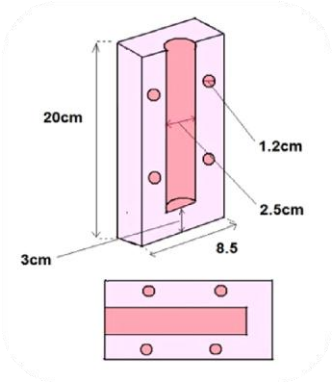

Fig.3 Sketch of cast mold.

then set aside to cool to laboratory temperature , the casting material then it was cut by cutting machine to a pieces of (2.75mm) thicknesses by using a cooling liquid , the alloys constitution were analyzed by Alloys Analyzer using X-Ray device , the results of analyses were given the Table (1) .

Table 1. Constituents the alloys which used in this experiment.

Sample	Al%	Ge%	Si%	Mg%
Alloy A	99.95	0.05	-	-
Alloy B	99.65	0.35	-	-
Alloy C	92.70	-	7	**0.3**

Rolling:

Through this operation different thicknesses were obtained (0.02 , 0.04 , 0.06 , 0.08 , 1) cm the alloys samples .

Cleaning, Grinding, and Polishing the samples :

The samples were cleaned by alcohol and by ultrasonic waves , and grinded by electric system for grinding and polishing to get a soft

Oxidation :

All samples oxidant by the electric furnace in to (0.5, 1, 1.5, 2, 2.5, 3, 3.5, 4) hours at the temperature (200, 300, 400) $^{\circ}$C.

Analysis the Oxidation on the Samples Surfaces:

To know the phases formation on each sample's surfaces after oxidized them at temperature under study , The X-Ray diffraction system were used with (Cu–Tube) and wavelength (λ=1.5406 A$^{\circ}$), by Bragg Law we determined interference distance (d) as follow in eq. (2):

$$2dsin\varphi = n\lambda \qquad \ldots\ldots\ldots (2)$$

After comparison the values with standard tables . The phases formation were selected on the surfaces of alloys .

b. Examination of Samples by x – rays

The (20 , 25 , 30 , 35) kV Mo - X-Ray Tube were used to measure surface , grinding papers were used also of (800 , 1000 , 1200 , 2000) micron , the samples then washed by purified water then by alcohol and dried by drying system , after that polishing by a special kind of polishing cloth and diamond paste with four stages (1 , 3/4 , 1/2 , 1/4) micron incrementally ,from soft to coarse then wash by purified water , alcohol and dried after each stage.

the attenuation coefficients , after measuring the average counts for each samples , theoretical values of attenuation coefficients determined by :

$$I = I_{\circ}\, e^{-\mu x} \qquad \ldots\ldots\ldots\ldots\ldots (3)$$

Such that $I_{\circ}/I$: absorption ratio .

μ : Attenuation coefficient

The experimental values of (μ_L) and (μ_m) determined by the slope of the curves to the logarithmic of absorption per thickness and equivalent thickness on succession for each sample .

4. The Calculations

A. we determined by weighting their masses and found their densities by using the eq.(4) :

$$\rho_{sample.} = \frac{m_{s.}}{V_{s.}} = \frac{m_{s.}}{\pi x r^2} \qquad \ldots\ldots\ldots (4)$$

Such that:

ρ_{sample} : represents the density by gm/cm^3 .

x : thickness of the sample in cm .

r : radius of the sample in cm .

m_s : mass of the sample in gm .
V_s : volume of the sample in cm^3 .

B. In the tables (2-4) experimental values were given for Linear and mass attenuation coefficients as well as mean free path and half thickness for alloys A, B & C, the slopes of the graphic Figures (7 to 14) represent the linear and mass attenuation coefficients.

Table 2 .The experimental results of linear and mass attenuation coefficients, mean free path and half thickness for alloy A oxidized at 400 ℃ which rolled to 0.06 cm.

U (kV)	$\mu_l = \frac{ln\frac{I_0}{I}}{X}$	$\mu_m = \frac{\mu_l}{\rho}$	$\lambda = \frac{1}{\mu}$		$X_{\frac{1}{2}} = \frac{0.693}{\mu}$	
			λ_l	λ_m	$X_{1/2_l}$	$X_{1/2_m}$
20	38.1375	14.16	0.0262	0.0706	0.0182	0.0489
25	37.6000	13.95	0.0266	0.0717	0.0184	0.0497
30	37.2625	13.84	0.0268	0.0723	0.0186	0.0501
35	36.8375	13.68	0.0271	0.0731	0.0188	0.0507

Table 3. The experimental results of linear and mass attenuation coefficients , mean free path and half thickness for alloy B oxidized at 400 ℃ which rolled to 0.06 cm.

U (kV)	$\mu_l = \frac{ln\frac{I_0}{I}}{X}$	$\mu_m = \frac{\mu_l}{\rho}$	$\lambda = \frac{1}{\mu}$		$X_{\frac{1}{2}} = \frac{0.693}{\mu}$	
			λ_l	λ_m	$X_{1/2_l}$	$X_{1/2_m}$
20	38.288	14.22	0.0261	0.0703	0.0185	0.0500
25	37.913	14.08	0.0264	0.0710	0.0188	0.0507
30	37.550	13.95	0.0266	0.0717	0.0191	0.0516
35	37.100	13.78	0.0270	0.0726	0.0194	0.0524

Table 4. The experimental results of linear and mass attenuation coefficients , mean free path and half thickness for alloy C oxidized at 400 ℃ which rolled to 0.06 cm.

U (kV)	$\mu_l = \frac{ln\frac{I_0}{I}}{X}$	$\mu_m = \frac{\mu_l}{\rho}$	$\lambda = \frac{1}{\mu}$		$X_{\frac{1}{2}} = \frac{0.693}{\mu}$	
			λ_l	λ_m	$X_{1/2_l}$	$X_{1/2_m}$
20	52.15	19.30	0.0192	0.0518	0.0133	0.0359
25	49.88	18.45	0.0200	0.0542	0.0139	0.0376
30	48.03	17.71	0.0208	0.0565	0.0144	0.0391
35	45.53	16.83	0.0220	0.0594	0.0152	0.0412

C. Effect of the oxidation:

To know the important of oxidation effects on attenuation coefficients of X-ray for alloys, it is necessary knowing oxidation circumstances from different oxidation times and temperatures . The Phases formation on the samples after tested them by X-ray diffraction shown in Figures (4 , 5 , 6) for example:

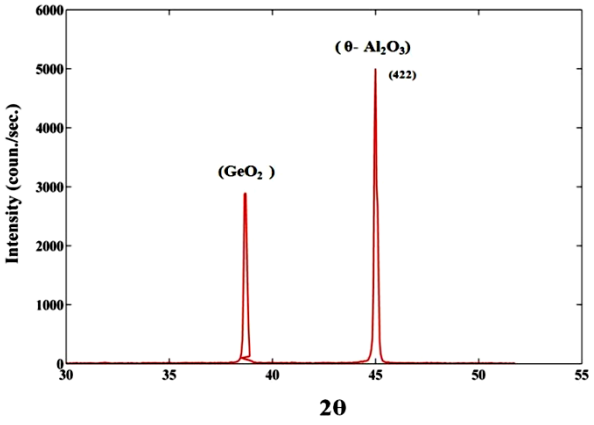

Fig.4 X-Ray diffraction pattern for oxidized Alloy A at temperature 400 °C which rolled to 0.06 cm

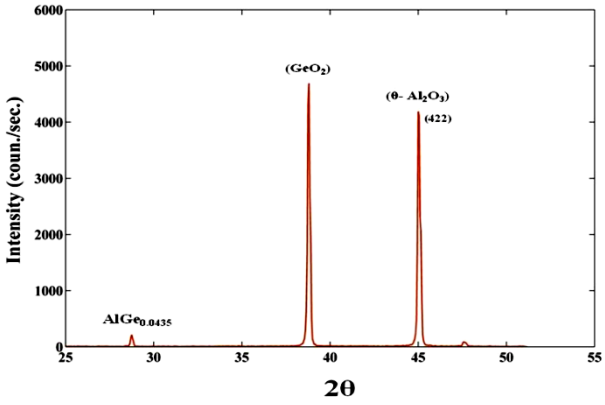

Fig.5 X-Ray diffraction pattern for oxidized Alloy B at temperature 400 °C which rolled to 0.06 cm.

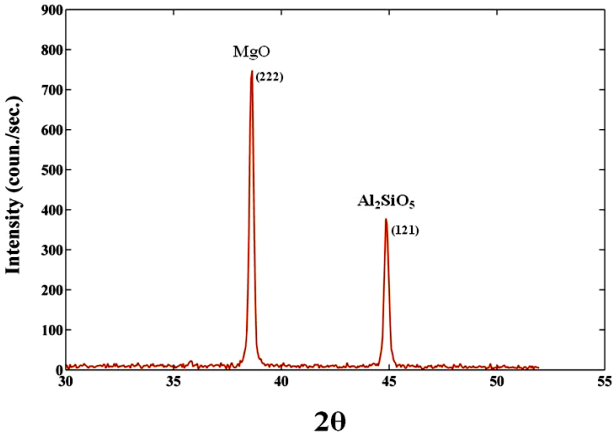

Fig.6 X-Ray diffraction pattern for oxidized Alloy C at temperature 400 °C which rolled to 0.06 cm.

D. Results and Discussion:

1. Figs. (7 , 8 , 9 , 10) shows the relation between logarithm of absorption with thickness for alloys A , B & C at temperature (400 ˚C) it is found an inverse relation for alloys A & B , this means that their absorption of X-ray decreased with increasing time , while the relation between logarithm of absorption with thickness for alloys C is linear this agrees with [15 - 17] , which due to the phases formation as shown in Figs. (4, 5, 6).
2. Figs. (11 , 12 , 13 , 14) shows the same result as in 1 .
3. Absorption Logarithm for alloy C oxidized at temperature (400 ˚C) after 4hr increased with ratio

(0.178%) compared with the same sample in the first half hour of oxidation at same temperature at 20kV , even the same sample oxidized at (400 ˚C) increased with ratio (0.097%) comparing with second alloy in [15] at room temperature at voltage 20kV .

4. The absorption decreases with increasing of voltage for alloys A , B & C .
5. Relation of absorption logarithm with thickness and equivalent thickness for alloys A , B & C that oxidized at temperature (200 , 300) ˚C were the same as in results (1) & (4) .
6. Attenuation coefficients of X-ray for these alloys oxidized at (200,300,400) ˚C have the same trend as in results (1) , (4) & (5) .
7. In Tables 2 to 4 we determined attenuation coefficients from the slope of the curves to the logarithm of absorption per thickness and equivalent thickness on succession for each sample .
8. In Tables 2 to 4 half thickness and mean free path had inverse relation with attenuation coefficients of x-ray .

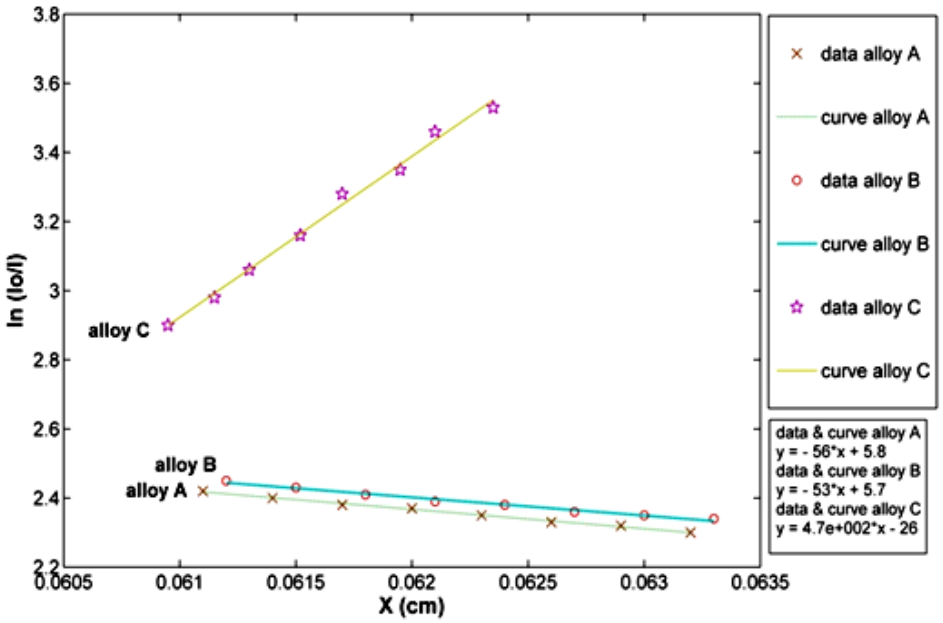

Fig.7 The relation between Logarithm of absorption with thickness for Oxidized alloys at 20kV.

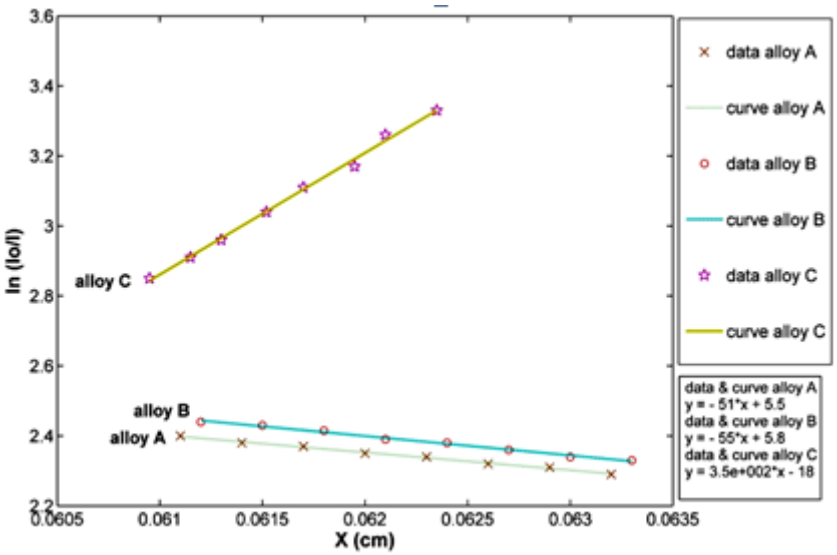

Fig.8 The relation between Logarithm of absorption with thickness for Oxidized alloys at 25kV.

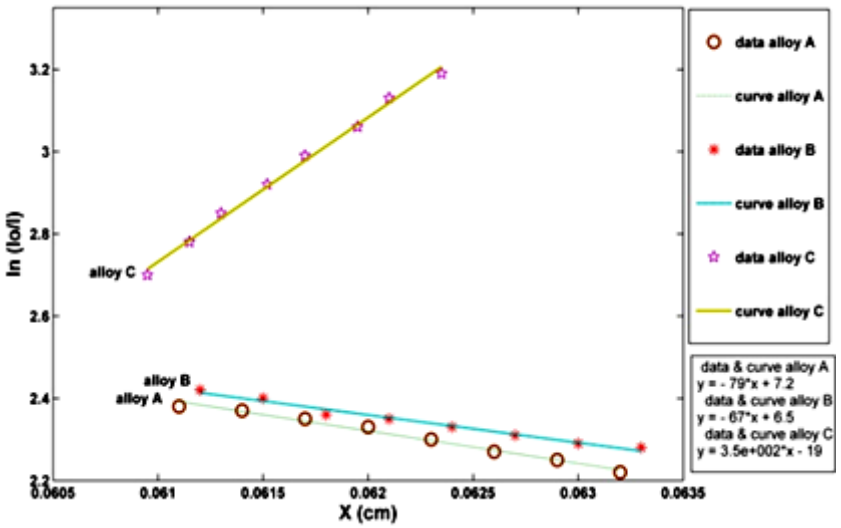

Fig.9 The relation between Logarithm of absorption with thickness for Oxidized alloys at 30kV .

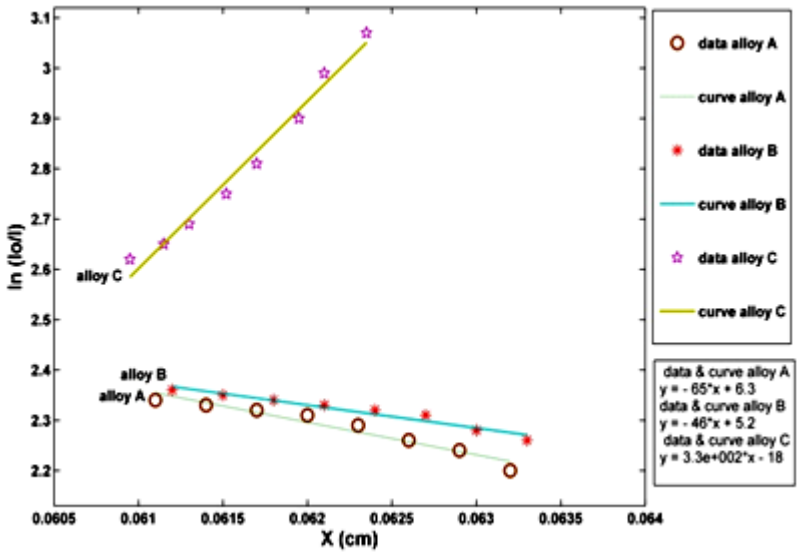

Fig.10 The relation between Logarithm of absorption with thickness for Oxidized alloys at 35kV

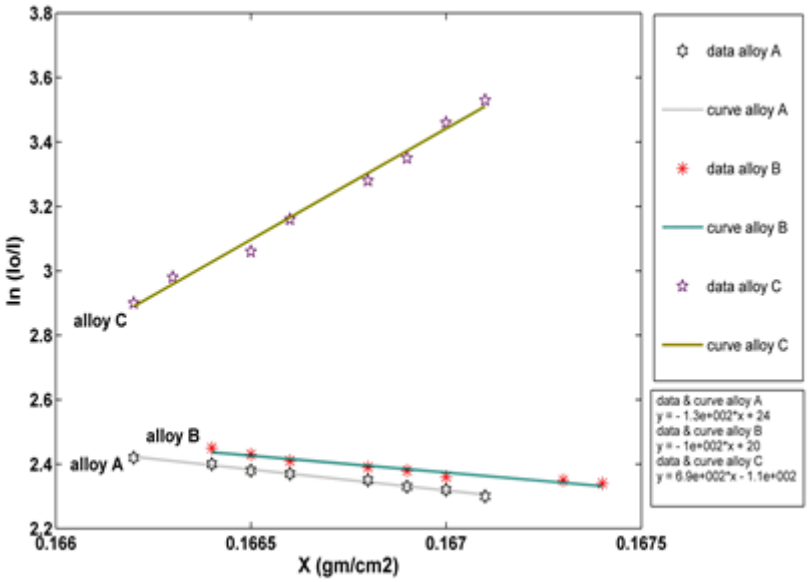

Fig.11The relation between Logarithm of absorption with Equivalent thickness for Oxidized alloys at 20kV .

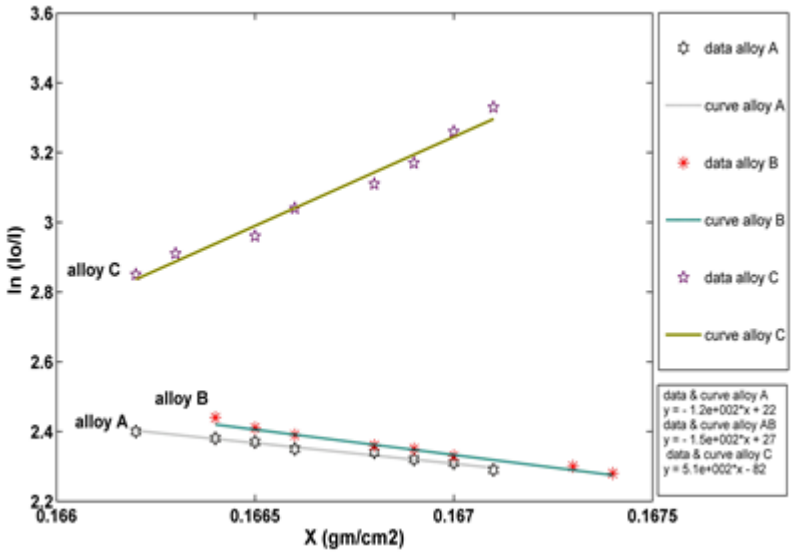

Fig.12 The relation between Logarithm of absorption with Equivalent thickness for Oxidized alloys at 25kV .

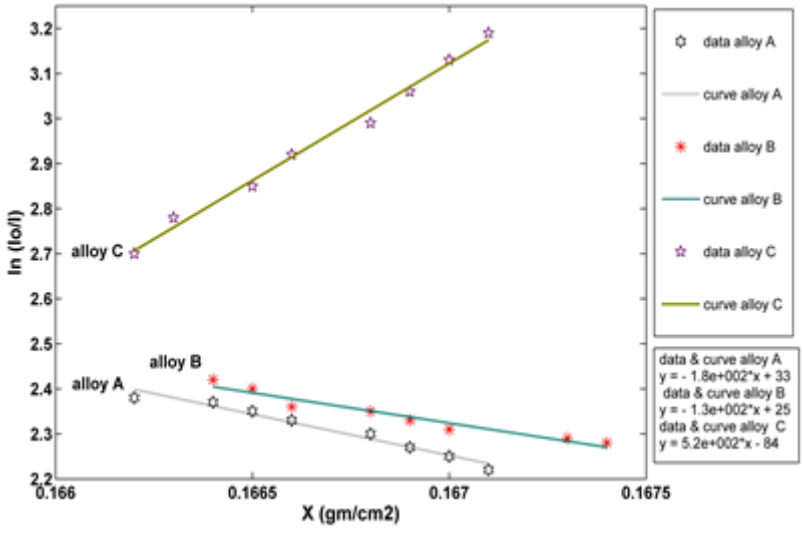

Fig.13 The relation between Logarithmic of absorption with Equivalent thickness for Oxidized alloys at 30kV.

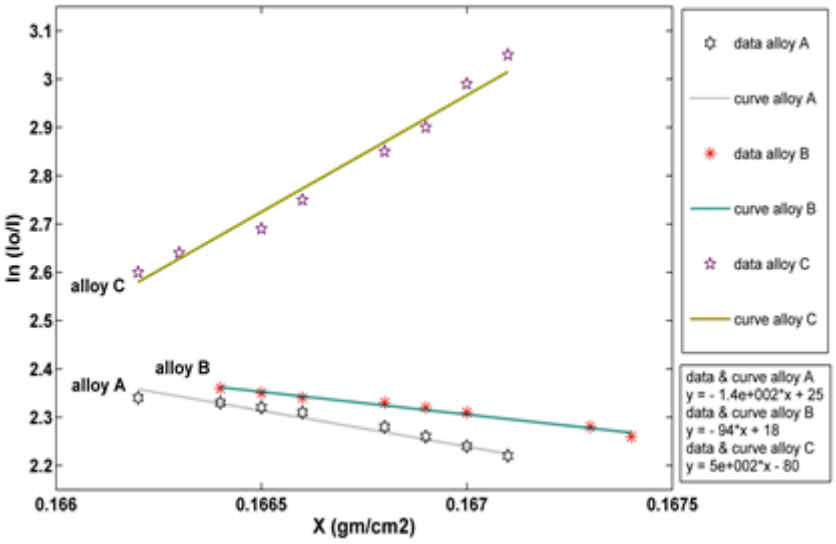

Fig.14. The relation between Logarithm of absorption with Equivalent thickness for Oxidized alloys at 35kV .

E. Conclusion:

1. Increasing of sample thickness hadn't any affection for alloys A & B as shown in the Figs. 7-10.
2. Trio alloy give best result comparing with double alloy even change alloys constituents.
3. Linear relations for (μ_L, μ_m) of X-Ray for alloy C , while it was inverse for alloys A and B .

$X_{1/2}$ and mean free path decrease for alloy C, while both of them increase for alloys A & B at different temperatures.

References:

1. James R. Connolly, "The Interaction of X-rays with Matter and Radiation Safety" , , for EPS400-001 , 2010 .
2. René Guinebretière , "X-ray Diffraction By Polycrystalline Material" , First published by ISTE Ltd in Great Britain and the United States , ISBN-13: 978-1-905209-21-7 , 2007
3. Gibilisco , Stan ''Physics Demystified'' 1st Ed. , U.S.A.2002 .
4. Podgorsak, E.B.'' Radiation Oncology Physics : A handbook for Teacher & Students'' International Atomic Energy Agency , Vienna , 2005 .
5. Hubbell, J.H., S.M. Seltzer '' Table of X-Ray Mass Attenuation Coefficients And Mass Energy – Absorption Coefficients'' National Institute of Standards And Technology , 2004
6. Wafa Altuieb Mohammad Mustafa ''Thickness Measurement Via X – Ray Radiation''Submitted in partial fulfillment of a postgraduate diploma at African Institute for Mathematical Sciences , Stellenbsch university , South Africa , 2010 .
7. Nielslen, J. A. ''Elements Of Modern X-ray Physics'', John Wiley & Sons , ltd , 2004
8. M. Blesa, P. Morando, A. Regazzoni , "Chemical Dissolution of Metal Oxides", CRC Press , Boca Raton, FL , 1993.
9. A.R. West , "Basic Solid State Chemistry", 2nd ed., Wiley, New York, 2000.
10. CRC Handbook of Chemistry and Physics , 72nd ed., CRC Press , Boca Raton, FL, 1991.
11. Hind A. Al-Abadleh, Vicki H. Grassian , "Oxide surfaces as environmental interfaces" , Elsevier Surface Science Reports , pp. 63–161 , Vol. 52 , 2003
12. Franchy, R. ''Growth of Thin , Crystalline Oxide , Nitride and Oxynitride Films on Metal and Metal Alloy Surfaces'' Surface Science Reports 38 pp.195-294 , Germany , 2000 .
13. Raed N. Razooqi , " affection of employment middle (Corrosion-Oxidation-Wear) on alloy properties with base (Aluminum – Lithium) , master a thesis , Application sciences department , Technology University, Baghdad , 1990 .
14. Jaafer T. Al Haidery , Muna K. Abbass " Affection some of alloyed elements on dead plate from Lithium in alloys with base Aluminum –

Lithium at its oxidation at different temperatures " Engineering and Technology Press , Vol.18 , No.1 , 1996 .

15. Farid M. Mohammed ,Raed N. Razooqi ,Safana M. Ismael ''The Effect Of Grain Size For Aluminum and Some Of Its Alloys On Attenuation Coefficients Of X-Ray'' Australian Journal of Applied Science, **(**under publication).
16. Farid M. Mohammed ,Raed N. Razooqi , Omar F. Abdullah''Determinations of the Relation Between The AttenuationCoefficients of X-Ray for Copper and Some of its Alloys With Grain Size'' European Journal of Scientific Research , ISSN 1450-216X Vol.45 No.2 , pp.176-189 , 2010.
17. Farid M. Mohammed ,Raed N. Razooqi , Mohsen H. Ali '' Modeling The Relationship Between Thickness and Hardness With Energy Attenuation of X-ray For Pure Aluminum ''Australian Journal of Basic and Applied Science , Vol.5 , No.10 , pp. 1268 -1272 , 2011 .

Study of Electron Momentum Distribution and Compton profiles of β-Mn

Farid M.Mohammad[1] and Abdul Hadi M.Ghaleb[2]

[1]Department of Physics, College of science, University of Tikreet, [2]Department of Physics, College of science, University of Kirkuk (abdlhadik@yahoo.com)

Abstract

Compton profile of transition metal (β-Mn) was calculated employing the renormalized-free-atom (RFA) and free electron models, choosing $3d^{6-x}$-$4s^{1-x}$ configuration, whereas (x=0 to 1 step 0.1). This result was compared with experiment values. It is seen that the RFA calculation in $3d^6 4s^1$ gives a better agreement with the experiment. This theoretical Compton profile data have been used to compute the cohesive energy of Manganese for the first time and compared it with available data.

دراسة توزيع الزخم الالكتروني وشكل منحني كومبتن في β−Mn

المستخلص

تم حساب شكل منحني كومبتن لمتعدد البلورات (β−Mn) والتي ينتمي الى سلسلة (3d) باستخدام النموذجين (اعادة معايرة الذرة الحرة والكترون الحر)، حيث تم اختيار عدد من الترتيبات الكترونية ($3d^{6-x}$ $4s^{1-x}$) اي (x=0,0.1,0.2,0.3,0.4,0.5,0.6,0.7,0.8,0.9,1). قورنت النتائج التي حصلنا عليها نظريا مع البيانات التجريبية السابقة والتي استخدمت فيها مصدر مشع Am^{241} بطاقة 60 KeV. لاحظنا افضل توافق جيد بين حسابتنا بواسطة استخدام نموذج(RFA)عند ترتيب الكتروني $3d^6$ $4s^1$. وكذلك ايضا حسبت طاقة التماسك في العنصر المنغيز وقورنت مع الحسابات المتوفرة.

1. Introduction

It is known that the Compton profile, J (P_z), can provide information about the projection of electronic momentum distribution on the scattering wave vector [1]. Within the impulse approximation, J (P_z) is given by:

$$J(P_z) = \iint \rho(\vec{P})\, dp_x dp_y \quad (1)$$

Where $p_x and p_y$ are the momentum components in $x and y$ directions while the z direction is parallel to the resultant of the incident and scattered wave vectors, $\rho(\vec{P})$ momentum density [2].

Mn belongs to the 3d transition metals and exists in many allotropic forms, most of which have complicated structures [3].In the last decade Compton scattering has been recognized as a powerful tool to study electron structure in light and medium transition metals [4-7], experimental results were predicted reasonably well at medium and high-momentum (p_z> 3.0 a.u) by the free atom profiles. In the low momentum region more refined calculation employing both the band structure as well as simple renormalized free atom (RFA) models can explain the Compton line shapes. Among 3d metals, very little work has been reported on Mn. The first Compton profile measurement on polycrystalline Mn and observed that the measured values were much flatter than the convoluted free atom values at low momenta[8].Compton profile were measured for α and β-Mn and determined the 4s band occupancies as 0.93 and 1.12 respectively[9].Their J(0) values in α and β-Phase different by about 2% and were both < 5 e/au, while a change of 2% in J(0) is rather large, their J(0) values are significantly lower than those observed for all other 3d- metals and thus do not follow the trend of constancy pointed out by [10].The electronic momentum distribution and Compton profiles of silver has been measured by [11].Also Study of electronic momentum distribution and Compton profiles of europium [12].

$3d^{5.6}4s^{1.4}$, $3d^{5.7}4s^{1.3}$) and after convolution electron configuration become ($3d^{5.8}4s^{1.2}$, $3d^{6}4s^{1}$, $3d^{5.7}4s^{1.3}$).Best agreement between our theoretical results and experimental [13] is found for ($3d^{6}4s^{1}$).In§2 we present the details of theoretical calculation .In§3and 4 described the result and discussion, conclusions. Objective of the study

is due to the shortage of refine calculation of electronic momentum density (β-Mn).

2. Calculation

A) Renormalized – free-atom (RFA) model:

The renormalized - atom approach was the firstly to be used by [14]. In the RFA model one starts with the free –atom wave function, truncates them at the Wigner-Sites (WS) Sphere and renormalizes the wave function to one within this Sphere to preserve charge neutrality .The effect of such renormalization in the case of (β-Mn) turned out to be the largest for 4s electron because only 38% of the wave function is contained in the WS Sphere. In contrast, this number is 96% for 3d wave function .Thus, only 4s electron were treated in the RFA scheme.

For bcc metals, the Compton profile $J_{4s}(p_z)$ for 4s electrons, can be written by as [15]:

$$J_{4s}(p_z) = 4\pi \sum_{n=0}^{\infty} |\Psi_0^c(K_n)|^2 \, G_n(p_z) \qquad (2)$$

Where K_n is a reciprocal lattice vector andp_z the projection of electron momentum along the scattering vector direction.

$\Psi_0^c(K_n)$ is the Fourier transform of the RFA wave function $\Phi_0^c(r)$.

(S_Electrons): The procedure for computing Compton profile is *already* published and here we rewrite this equation for the sake of completeness. Following [16] the momentum transform of a Bloch function (for the unhybridised outermost *electrons)* for the cubic structures is given by

$$\Psi_{\vec{K}}(\vec{P}) = N\delta(p - \vec{K}_1\vec{K}_n)\Psi_{\vec{K}}^c(\vec{p}) \qquad (3)$$

Here N is the total number of atoms, the transform $\Psi_{\vec{K}}^c(\vec{p})$ is defined as

$$\Psi_{\vec{K}}^c(\vec{p}) = (2\pi)^{-3/2} \int e^{-\overrightarrow{ip}.\vec{r}} \, \Psi_{\vec{K}}(\vec{r}) d\vec{r} \qquad (4)$$

Where the integration is over the Wigner-Seitz polyhedron. In the conventional cell approximation

$$\Psi_{\vec{K}}(\vec{r}) = e^{i\vec{K}.\vec{r}}\Psi_{\vec{K}=0}(\vec{r}) \quad (5)$$

When $\vec{K}_n = \vec{P} - \vec{K}$, then $\vec{K} = 0$

$$\Psi^c_{\vec{K}}(\vec{P}) = \Psi^c_0(\vec{K}_n) \quad (6)$$

For

$$K_n = 0\Psi^c_0(0) = (2\pi)^{\frac{1}{2}} \int_0^{r_0} dr\, r^2 \Phi^c_0(r) \quad (7)$$

And for $K_n \neq 0$

$$\Psi^c_0(K_n) = (\frac{2}{\pi})^{1/2} K_n^{-1} \int_0^{r_0} drr\sin(K_n r)\,[\Phi^c_0(r) - \Phi^c_0(r_0)] \quad (8)$$

The auxiliary function $G_n(P_z)$ in (1) is given as

For n=0

$$G_0(P_z) = \begin{cases} \frac{1}{2}(P_F^2 - P_Z^2)P_z \leq P_F \\ 0 \qquad otherwise \end{cases} \quad (9)$$

$$\text{For n}\neq 0 G_n(P_z) = \begin{cases} 0 & P_z > K_n + P_F \\ \tilde{G}_n(P_z) P_z \in (K_n - P_F, K_n + P_F) \\ \tilde{G}_n(K_n - P_F) P_Z < K_n - P_F \end{cases} \quad (10)$$

Where the auxiliary function $\tilde{G}_n(P_z)$ is defined as

$$\tilde{G}_n(P_z) = N_n \Big\{(P_F^2 - K_n^2)(K_n + P_F - P_z) - \frac{1}{3}[(K_n + P_F)^3 - P_z^3] + K_n[(K_n + P_F)^2 - P_z^2]\Big\} /4K_n \quad (11)$$

N_n is the number of points in the nth shell in the reciprocal space,as regards the wave function for 4s electrons, the free atom Hartree - Fock wave function was taken from tables of [17].The Compton profile $J_{4s}(P_z)$ was then calculated using equation (2) to (6) for several cases choosing various 3d-4s configuration. The values of the Compton profile of 3d electrons and other inner electrons were taken from [18]. All the theoretical Compton profiles were normalized to an area of 11.28 electrons. As

usual in all 15 shortest reciprocal lattice vectors were considered.

B) Free electron–based model profile:

In case of an isotropic momentum distribution, eq (1) reduces to the well-known form:

$$J_{4s}(p_z) = 2\pi \int_{p_z}^{\infty} dp\, \rho(\vec{p}) p \qquad (12)$$

If we consider the valence electrons in a metal as a non-interacting electron gas, then the momentum density by:

$$\rho(\vec{P}) = constant = \frac{n}{\frac{4}{3}\pi p_F^3} \qquad (13)$$

Where n is the number of free electrons per site and p_F is the Fermi momentum. Substitution of $\rho(p)$ from eq.(13) to eq.(12) gives

$$J_{4s}(p_z) = \frac{3n}{4p_F^3}(p_F^2 - p_z^2) \qquad for\ p_z \le p_F \qquad (14)$$

The free electron Compton profile is then an inverted parabola including discontinuities of the first derivative at $\pm p_F$ [1].Using eq.(14), we have also calculated the free electron Compton profile for 4s electron of Mn. To get a total profile in the momentum range 0 to +7 a.u.,the Compton profile for core electrons($1s^2$ to $3d^5$) were directly taken from the tables of Biggs et al [18].

C) Cohesive energy:

The cohesive energy E_{Coh} which is defined as the difference between the total ground –state energy of the solid and the energy of the individual isolated atoms can be calculated from Compton profile data [19] using following relation:

$$E_{Coh} = \int_0^{p_{max}} p_z^2 [J_s(p_z) - J_{FA}(p_z)] dp_z \qquad (15)$$

Where the $J_s(p_z)$ and $J_{FA}(p_z)$ refer to solid state and free atom profiles, respectively. In our calculation, p_{max} was taken as infinite. The values of $J_s(p_z)$ were taken from the present RFA calculation which represents the solid-state phase of Mn and those for $J_{FA}(p_z)$ from free atom Compton

profile tables[18].the contribution core electrons are same in the$J_s(p_z)$ and$J_{FA}(p_z)$ and hence cancel out in the difference seen in Eq(15) .

3. Results and Discussion

The results theoretical Compton profile for three different Configuration for β-Mn, namely ($3d^{5.8}4s^{1.2}$, $3d^{6}4s^{1}$, $3d^{5.7}4s^{1.3}$) and the free electron profile, all results compared with experimental data [13] given in table 1.In the low momentum region $p_z < 1.4$.It is seen that the experimental values higher than the theoretical (RFA) value but those for $p_z > 1.6$ the experiment values were found to be smaller than from theoretical. In momentum region $p_z > 3$ the experimental and the theoretical values using (RFA, FE and FA) models are nearly same because in this region the contribution is essentially due to inner core electrons. Moreover, these electrons remain nearly unaffected during the formation of solids and hence their Compton profiles can be expected to be described accurately by their atomic values. In order to investigate the effect of varying 3d-4s electron distribution, in Fig (1) we plot the various theoretical and experimental values. We observe that in the beginning from (p_z =0 to 0.4)au, the RFA value for($3d^{5.8}4s^{1.2}$,$3d^{5.7}4s^{1.3}$) are lower than $3d^{6}4s^{1}$ results but between (0.5 to 0.8)au, the trend is reversed and the $3d^{5.8}4s^{1.2}$,$3d^{5.7}4s^{1.3}$ values are higher than $3d^{6}4s^{1}$.Also in $p_z = 1\ to\ 3$ au, the $3d^{6}4s^{1}$ the larger from $3d^{5.8}4s^{1.2}$,$3d^{5.7}4s^{1.3}$,the latter in region$p_z > 3\ au,$ higher than from $3d^{6}4s^{1}$. From table (1) and Fig (1), it can see that the convoluted (free electron and free atom) model profile gives a very poor agreement with the experiment, which may be due to its unrealistic assumption.

Comparison between Free electron and Free atom, it is seen in low momentum Free electron ($3d^{5}4s^{2}$) higher than the Free atom ($3d^{5}4s^{2}$) but in part between p_z (0.3 and 0.8) the trends get reversed and the free electron values are somewhat larger than the free atom .At $p_z > 0.9au,$ both models values to become similar.

Figure (2) shows the difference between theoretical (after convolution) and experimental profiles in β-Mn. It can be seen in the low momentum that ΔJ($3d^{6}4s^{1}$-Expt) larger than fromΔJ ($3d^{5.8}4s^{1.2}$-Expt and $3d^{5.7}4s^{1.3}$-Expt), as well as the ΔJ ($3d^{5.8}4s^{1.2}$-Expt) and ($3d^{5.7}4s^{1.3}$-Expt) have similar values only in low momentum different, but (Free atom - Expt and Free Electron - Expt) are nearly the same where $p_z > 1\ au.$. Also in the high momentum transfer region(p_z >4

au), experimental values are very close to corresponding theoretical data .It is known that the contribution of valence electron is very small in this region and hence, most of the contribution may be due to the inner-core electrons. These inner-core electrons are reasonably described by the free-atom values. In order to determine the best configuration electrons, the total square deviation $\sum_0^{7\ a.u.}|\Delta J|^2$ was obtained for each cases .The values founded were (0.0.5393, 0.5416 and 0.5419) for ($3d^6 4s^1$,$3d^{5.8} 4s^{1.2}$,$3d^{5.7} 4s^{1.3}$) configuration respectively. Thus $3d^6 4s^1$seems to be the best configuration. From this we can observe by effect of convolution the theoretical values.

The purpose of the computation of cohesive energy was to see the applicability of the RFA scheme in reproducing the cohesive of transition metals. The value of calculated cohesive energy (with $p_{max} = 2\ au$). Table (2) show comparison between our theoretical by RFA model , experiment[13] and another data. A choice of low value ofp_{max} is justified because ,to a good approximation ,after this value the major contribution in the theoretical and experimental profile is expected only due to core electrons, which almost remain unaffected in formation of solids. This is evident from the core contribution plotted in Fig (2).

4. Conclusion

In this work compared has been compared theoretical values with experimental results [13].The RFA model shows good agreement with the experiment in the $3d^6 4s^1$ configuration, but Compton profiles value using free electron model higher those experimental. Evidently, there is a need for a relativistic band structure calculation to interpret the Compton profile data. In table (3) illustrate the comparison between theoretical results using (RFA)model with previous works [13,21] in the process transfer charge of shells(s,d).The cohesive energy of Manganese computed by (RFA) model and comparison with another results [13,20].

Table 1: Theoretical results compared with experimental value [13] for β-Mn. All the quantities in atomic. The profiles are normalized so that the integral from 0 to 7.0 au, is 11.28 electrons.

P_z(au)	J(P_z)(e/au)					
	Free electron ($3d^5 4s^2$)	Free atom ($3d^5 4s^2$)	Theory(RFA)			**Experiment [13]**
			Core + $3d^6 4s^1$	Core + $3d^{5.8} 4s^{1.2}$	Core + $3d^{5.7} 4s^{1.3}$	
0.0	5.737	7.1556	5.314	5.253	5.224	**5.371**
0.1	5.71	6.8496	5.279	5.223	5.194	**5.351**
0.2	5.634	6.1176	5.17	5.128	5.108	**5.283**
0.3	5.502	5.2856	5.002	4.981	4.969	**5.16**
0.4	5.314	4.6286	4.79	4.789	4.787	**5.01**
0.5	5.078	4.2084	4.55	4.568	4.576	**4.834**
0.6	4.778	3.9536	4.312	4.337	4.347	**4.629**
0.7	4.426	3.798	4.075	4.106	4.12	**4.416**
0.8	3.994	3.6596	3.875	3.896	3.905	**4.192**
1.0	3.429	3.4364	3.539	3.538	3.538	**3.73**
1.2	3.147	3.1548	3.26	3.247	3.24	**3.282**
1.4	2.837	2.839	2.973	2.962	2.955	**2.895**
1.6	2.518	2.5128	2.656	2.653	2.647	**2.565**
1.8	2.236	2.2242	2.333	2.331	2.328	**2.262**
2	1.964	1.949	2.035	2.025	2.029	**1.981**
3	1.078	1.064	1.111	1.11	1.107	**1.104**
4	0.701	0.692	0.714	0.725	0.715	**0.717**
5	0.514	0.508	0.509	0.512	0.515	**0.525**
6	0.392	0.388	0.378	0.384	0.388	**0.388**
7	0.301	0.298	0.194	0.195	0.195	**0.279**

Table 2: Cohesive energy of Manganese (E_{Coh}). 1 au, of Energy is equivalent to27.212 eV .

Reference	E_{Coh}**(in eV)**
Our theoretical(RFA)	8.04
Experiment[13]	8.24
Brooks and Johansson[20]	8.16

Table 3. Charge occupancies in β-Mn.

Reference	Q_{3d}	Q_{4s}
Das .G.P and Shhni .V.C.[21]	5.88	**1.12**
Ahuja.B.L.et al [13]	5.4	**1.6**
Present work	6	**1**

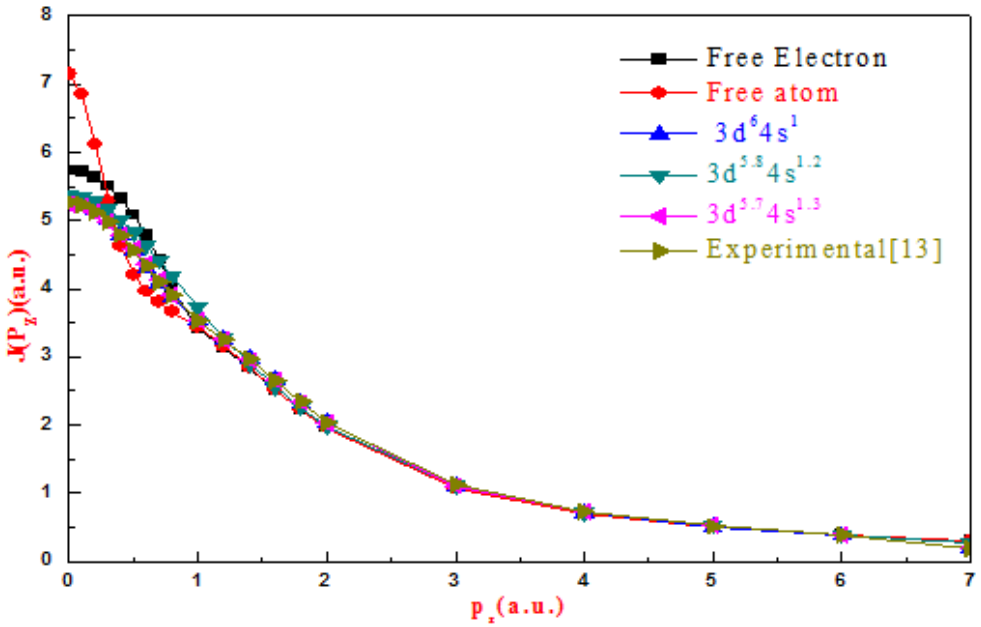

Fig(1). Comparison of theoretical results with experimental [13] Compton profiles for β-Mn.

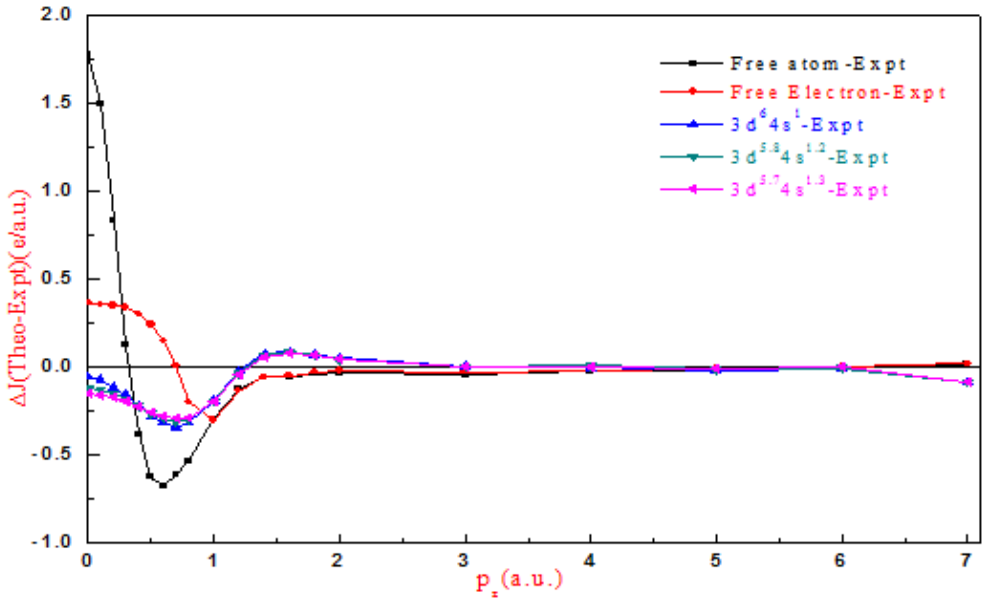

Fig (2). Difference between our theoretical and experimental [13] Compton profiles of β-Mn.

Reference

1. Cooper, M. J. **(1985).** Rep.Prog.Phys.48, 415.
2. Andrejczuk ,A. Reniewicz, H. Dobrzyuski, L . Zukowski, E. and Kaprzyk , S. **(2000)**.Phys.Status .Solid B217,903.
3. Pearson, W.B."A handbook of lattice spacing and structure of metals and alloys" **(1964)**,(New York: Pergamon press).
4. Paakkari,T.Manninen,S.andBerggren,K.F.**(1975)** Phys.Fenn.10207.
5. Beggren ,F.K. Manninen, S. Paakkari,T.Aikala,O and Mansikka K.**(1977)** Compton scattering(ed.)B.G. Williams(New York :McGraw Hill).
6. Sharma .B.K, Singh. H,Perkkiő .S,Paakkari.T and Mansika .K,**(1986)** Report Ser.Turku FTL-R109 Finland,(also 1987 Phys.Status Solidi B141 177).
7. Sharam.B.K,Gupta .A,Singh.H, Perkkiő.S,Kshirsagar.A and Kanhere.D.G.**(1988)** Phys .Rev B37 6821.
8. Gupta .A,Singh.H and Sharma .B.K,**(1988)**,Nucl,Solid state Phys.Symp C26 212.
9. Das .G.P and Sahni .V.C, **(1986)**,Pramana-J .Phys.27 585.
10. Gandhi.K.R and Singru .R.M, **(1981)** philos. Mag.43 999.
11. Thomas.V and Balakrishna.K.M**.(2008)**,Sci&Soc.6(1) 31-34.
12. Thomas.V and Balakrishna.K.M**.(2010)**,Eur.Phys.J.D-10.1140.
13. Gupta,A, Sharma ,B.K and Ahuja,B.L**,(1988)**, Pramana-J. Phys, Vol.31, No.3, pp.225-232.
14. Chodorow,M. **(1939),**Phys .Rev,55,675.
15. Berggren,K.F, Manninen,S and Paakkari,T. **(1973)**.Phys.Rev.B55 2516.
16. Berggren,K.F. **(1972)**, Phys.Rev.B6 2156-61.
17. Clementi ,E and Roetti, C .**(1974)** .Atomic Data and Nucl Data Tables 14 212.
18. Bigges,L.Mendelsohn,L.B and Mann,J.B.**(1975)**.At.DataNucl.Data Tables 16,201.

19. Holt ,R .S and Cooper, M.J.**(1980)"**The calculation of electronic energies from Compton Profiles". Philos.Mag.B 41 (2), 117-121.
20. Brooks, M.S. and Johansson, B. **(1983)**. J.Phys. F13, L197.
21. Das,G.P and Sahni ,V.C.**(1986)** Pramana-J. Phys. 27 585.

TTCM Burst-by-Burst Adaptive Wideband Coded Modulation in Rayleigh Channel

Hamid M. Farhan[1] , Mohammed Saeed Mohammed[1] and Ali Majeed[2]

[1] Assist. Lectural., College of Electrical and Electronic Techniques

[2] Assist. Lectural., College of Engineering, Al-Mustansiriya University

Abstract

The concept of wideband coded modulation has been in existence for many years. It was predominately utilized in many applications due to its inherent resistance to noise, including jamming and low probability of intercept. For this reason, it was the communication method of choice in various situations. The TTCM has been shown to be more efficient than TCM for transmissions over AWGN channels and narrowband fading channels. The multi-path channel model is characterized by its discretized symbol-spaced COST207 Typical Urban (TU) channel impulse response. The Rayleigh multipath channel is also discretized. Therefore, OTHMA can be applied as a multiple access scheme for low power, large scale, and low activity networks in UWB impulse radio communications. The performance of TTCM Burst-by-Burst Adaptive Wideband Coded Modulation system is tested in a Semi-realistic channel model that is based on an extensive set of outdoor channel measurements. Through semi-analytical evaluations of the bit error probability, we show that the TTCM Burst-by-Burst Adaptive Wideband Coded Modulation system is almost has good BER performance. Also, a comparison between the BER performances of many channels has been done.

Keywords: COST207, TTCM, Burst-by-Burst, Rayleigh

النظام المتكيف المشفر ذو الحزمة العريضه في قناة رايلي

المستلخص

لقد كان مفهوم تضمين ترميز النطاق العريض موجود لسنوات عديده. وقد استخدم في الغالب في كثير من التطبيقات بسبب المقاومة الكامنه للضوضاء، بما في ذلك التشويش واحتمال ضعيف للاعتراض. لهذا السبب كانت هي طريقة الاتصال التي يختارونها في مختلف الحالات. وقد تبين ان TTCM لتكون اكثر كفاءة من TCM التقليدي لنقل الحركة عبر قنوات AWGN وقنوات التلاشي الضيقة. وتتميز القناة ذات المسار المتعدد النمط التي لها Discretized رموز متعددة النموذجية في المناطق الحضرية COST207 استجابة نبضة قناة. كذلك قناة رالي المتعددة هي ايضا TU ولذلك يمكن تطبيق OTHMA كمشروع متعدد للحصول على الطاقة المنخفضة على نطاق واسع وشبكات انخفاض النشاط في مجال الاتصالات UWB. يتم اختبار اداء انفجار تلو انفجار Burst–by– Burst التكييف المتسع لنظام ترميز التحوير في نموذج قناة شبه واقعية تقوم على مجموعة واسعة من القياسات في قناة تعمل في الفضاء الحر من خلال تقييم شبه التحليل من احتمال الـ Bit الخطا. وتبين لنا الـ Burst–by–Burst باستخدام القناة رالي هو الافضل من حيث نتائج الاداء مقارنة مع قنوات عديده.

1. Introduction

The Trellis Coded Modulation (TCM), which is based on combining the functions of coding and modulation, is a bandwidth efficient scheme that has been widely recognized as an excellent error control technique suitable for applications in mobile communications. Turbo Trellis Coded Modulation (TTCM) is a more recent channel coding scheme that has a structure similar to that of the family of power efficient binary turbo codes, but employs TCM codes as component codes. The Rate 2/3 TTCM was to be 0.5 dB better in Signal-to-Noise Ratio (SNR) terms, than binary turbo codes over AWGN channels using 8-level Phase Shift Keying (8PSK) [1]. TTCM was also shown to outperform a similar-complexity TCM scheme in the context of Orthogonal Frequency Division Multiplexing (OFDM) transmission over various dispersive channels. In this latter context, the individual OFDM subcarriers experienced effectively narrowband fading and the TCM as well as TTCM complexity were rendered similar by adjusting the number of turbo iterations and code constraint

length. However, the above fixed mode transceiver failed to exploit the time varying nature of the mobile radio channel. By contrast, in BbB adaptive schemes 1671 a higher order modulation mode is employed, when the instantaneous estimated channel quality is high in order to increase the number of Bits Per Symbol (BPS) transmitted and conversely, a more robust lower order modulation mode is employed, when the instantaneous channel quality is low, in order to improve the mean Bit Error Rate (BER) performance. Un coded adaptive schemes and coded adaptive schemes have been investigated for narrowband fading channels. Finally, a turbo coded wideband adaptive scheme assisted by Decision Feedback Equalizer (DFE) was investigated in. In our practical approach the transmitter obtains the channel quality estimate generated by receiver B upon receiving the transmission of transmitter B. In other words, the modem mode required by receiver B is superimposed on the transmission burst of transmitter B. Hence a delay of one transmission burst duration s incurred. In the literature, adaptive coding for time-varying channels using outdated fading estimates has been investigated. Over wideband fading channels the DFE employed will eliminate most of the Inter-symbol Interference (ISI). Consequently, the Mean-Squared Error (MSE) at the output of the DFE can be calculated and used as the metric invoked to switch the modulation modes. This ensures that the performance is optimized by employing equalization and BbB adaptive TCM/TTCM jointly, in order to combat the signal power fluctuations of the wideband channel [1,2].

This paper is characterized as follows: In Section 2, the Multipath Rayleigh Fading Channel is previewed. In Section 3, the System Overview and Setup Parameters is presented. Section 4, the Performance of the Fixed Modem Modes is presented. In Section 5, the Performance of System with Rayleigh and COST 207 channels is presented. Section 6 presents the Performance of System with Rayleigh and AWGN channels. And finally, the conclusion points are given in Section 7.

2. Multipath Rayleigh Fading Channel

There are times when a mobile receiver is completely out of sight of the base station transmitter (i.e., there is no signal path traveling to the receiver via LOS). In this case, the received signals are made up of a

group of reflections from objects, and none of the reflected paths is any more dominant than the other ones. The different reflected signal paths arrive at slightly different times, with different amplitudes, and with different phases. It was verified, both theoretically and experimentally, that the envelope of a received carrier signal for a moving mobile is Rayleigh distributed. Therefore, this type of fading is called Rayleigh fading. The theoretical model makes use of the fact that there are many reflected signal paths from different directions (i.e., N signal paths). The composite received signal is:

$$r(t) = \sum_{n=1}^{N} R_n \cos\left(2\pi f t - 2\pi f_{D,n} t\right) \quad \ldots\ldots\ldots\ldots\ldots\ldots\ldots\ldots\ldots\ldots\ldots\ldots\ldots\ldots \quad (1)$$

Note that the received signal is made up of N reflected signals; each reflected path has an amplitude of R_n and f is the carrier frequency. The frequency shift of each reflected signal is due to the Doppler effect when the mobile user is in motion. If the signal is traveling parallel to the mobile's direction of motion, then the Doppler frequency shift $f_{D,n}$ is given by [3]:

$$f_{D,n} = \frac{v}{\lambda} \quad \ldots\ldots\ldots\ldots\ldots\ldots\ldots\ldots\ldots\ldots\ldots\ldots \quad (2)$$

where v is the velocity of the mobile.

Multipath fading is due to the constructive and destructive combination of randomly delayed, reflected, scattered, and diffracted signal components. This type of fading is relatively fast and is therefore responsible for the short-term signal variations. Depending on the nature of the radio propagation environment, there are different models describing the statistical behavior of the multipath fading envelope [4].

When the channel impulse response $c(\tau, t)$ at a delay τ and time instant t is modeled as a zero-mean complex-valued Gaussian distribution, the envelope $|c(\tau, t)|$ at that time instant t is known to be Rayleigh distributed. In this case the channel is said to be a Rayleigh fading channel. The Rayleigh

distribution has the probability density function (PDF) as [5]:

$$p(r) = \begin{cases} \frac{r}{\alpha^2}\exp\left(-\frac{r^2}{2\alpha^2}\right) & (0 \le r \le \infty) \\ 0 & (r < 0) \end{cases} \quad \ldots\ldots\ldots\ldots\ldots\ldots\ldots\ldots\ldots\ldots \quad (3)$$

where r is the envelope of the received signal and α^2 is the time average power of the received signal before envelope detection.

3. System Overview and Setup Parameters

The multi-path channel model is characterized by its discretized symbol-spaced Rayleigh channel impulse response. Each path is faded independently according to a Rayleigh distribution and the corresponding normalized Doppler frequency is 4.5, the system Baud rate is 5.3 MBd, the carrier frequency is 2.8 GHz and the vehicular speed is 100 km/h. The DFE incorporated 44 feed-forward taps and 9 feedback taps and the transmission burst structure used is shown in Figure (1). When considering a Time Division Multiple Access (TDMA)/Time Division Duplex (TDD) system of 16 slots per 4.615 TDMA frame, the transmission burst duration is 288 PS, as specified in the Pan-European FRAMES proposal. The following assumptions are assumed. Firstly, the equalizers capablling of estimating the Channel Impulse Response (CIR) perfectly from the equalizer training sequence of Figure (1).

Secondly, the CIR is time-invariant for the duration of a transmission burst, but varies from burst to burst according to the Doppler frequency, which corresponds to assuming that the CIR is slowly varying. The error propagation of the DFE will degrade the estimated performance, but the effect of error propagation is left for further study.

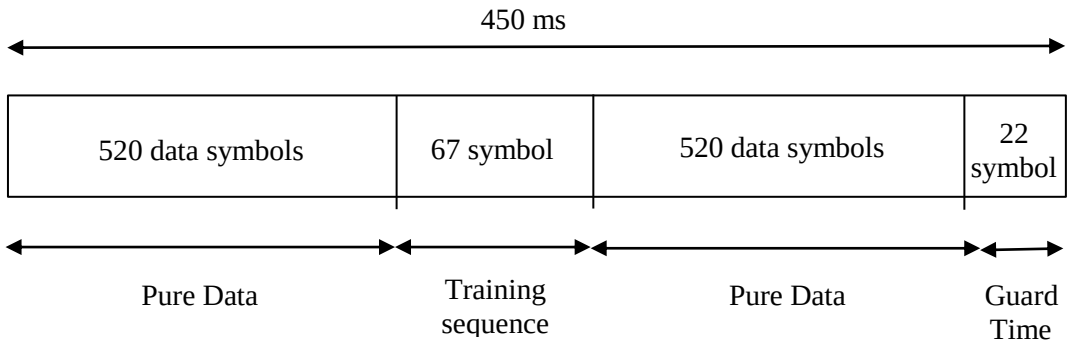

Figure (1). Transmission Data Burst.

At the receiver, the CIR is estimated, which is then used to calculate the DFE coefficients. Subsequently, the DFE is used to equalize the Inter-symbol Interference (ISI)-corrupted received signal. In addition, both the CIR estimate and the DFE feed-forward coefficients utilized to compute the SNR at the output of the DFE. More specifically, by assuming that the residual IS1 is near-Gaussian distributed and that the probability of decision feedback errors is negligible, the SNR at the output of the DFE, is calculated as:

$$\gamma_{dfe} = \frac{Wanted\ Signal\ Power}{Residual\ ISI\ Power + Effective\ Noise\ Power} \quad \ldots\ldots\ldots\ldots\ldots\ldots \quad (4)$$

$$\gamma_{dfe} = \frac{E\left[\left|s_k \sum_{m=0}^{N_f} C_m\, h_m\right|^2\right]}{\sum_{q=-(N_f-1)}^{-1} E\left[\left|\sum_{m=0}^{N_{f-1}} C_m\, h_m s_{k-q}\right|^2\right] + N_0 \sum_{m=0}^{N_f} |C_m|^2} \quad \ldots\ldots\ldots\ldots \quad (5)$$

where C, and h, denotes the DFE's feed-forward coefficients and the CIR, respectively. The transmitted signal is represented by s_k and N_0 denotes the noise spectral density.

The equalizer's SNR, γ_{dfe}, in Eq. 5, is then compared against a set of adaptive modem mode switching thresholds fn, and subsequently the appropriate modulation mode is selected. The modem mode required by receiver B is then fed-back to transmitter A. The modulation modes that are utilized in this scheme are, 8PSK, 16QAM and 256QAM. The simplified block diagram of the adaptive system is shown in Fig. (2) [6], where no channel interleaving is used. Transmitter A extracts the modulation mode required by receiver B from the reverse-link transmission burst in order to adjust the adaptive TCM/TTCM mode suitable for the channel. This incurs one TDMN/TDD frame delay between estimating the actual channel condition at receiver B and the selected modulation mode of transmitter A. Four encoders are invoked, each adding one parity bit to each information symbol, yielding the coding rate of 323 in conjunction with the TCM/TTCM mode of 114 for 8PSK, 335 for 16QAM and 760 for 256QAM. The design of TCM schemes for fading channels relies

on the time and space diversity provided by the associated coder.

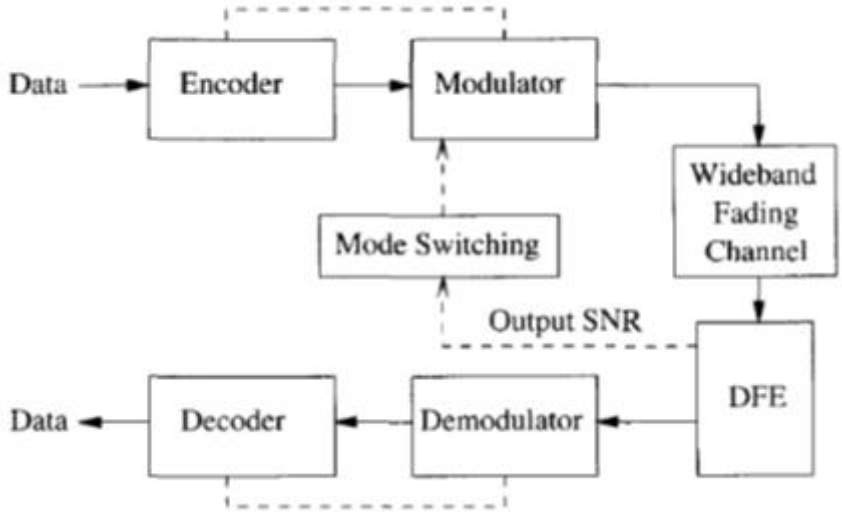

Figure (2). The burst-by-burst System without channel inter leaver.

4. Performance of the Fixed Modem Modes

In this section, the BER performance of the system with Rayleigh channel using fixed modem modes of 16QPSK, 64QAM and 256QAM are studied both with and without channel interleavers. These results are shown in Figure (3) for TCM. The random "CM symbol-interleaver memory was set to 684 symbols, where the corresponding number of bits was the number of data bits per symbol (BPS) x 775. A channel interleaver of 6 x 775 symbols was utilized, where the number of bits was (BPS + 1) x 4 x 775 bits, since one parity bit was added to each TCM/TTCM symbol. As shown in Figure (5), the BER performance of the channel-interleaved case is superior compared to that without channel interleaver in the case of 16QPSK.

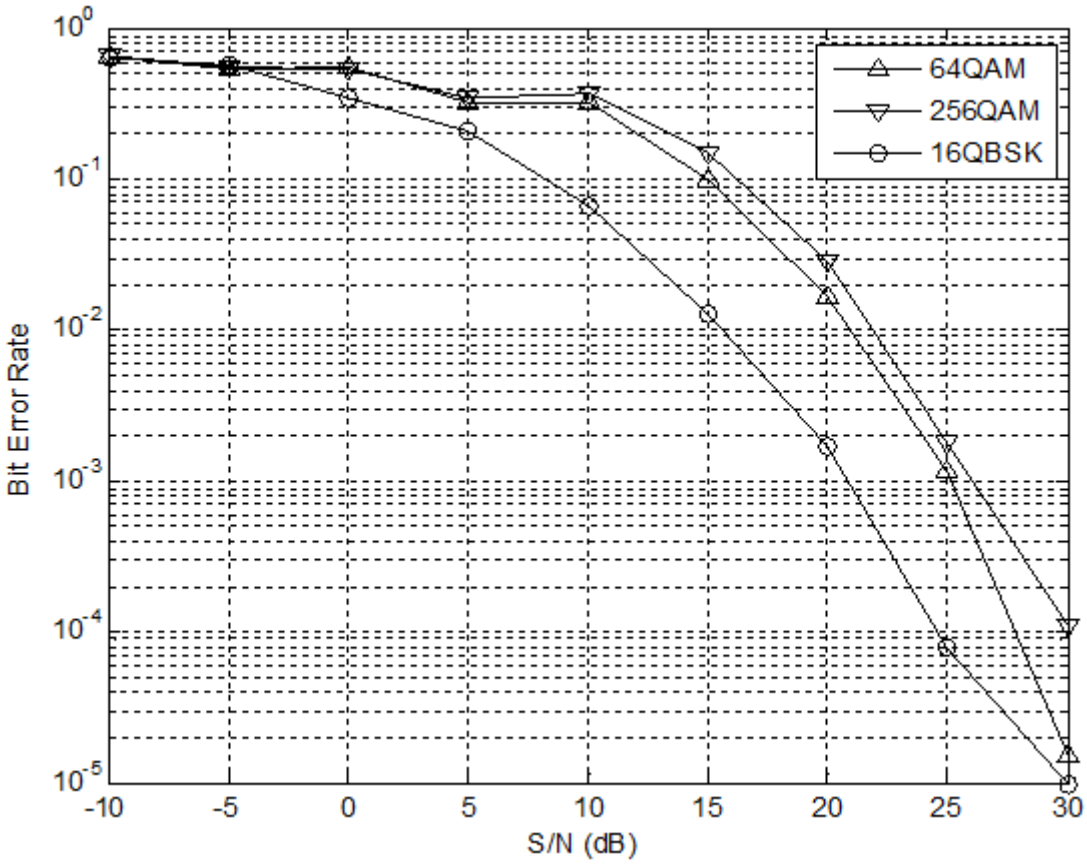

Figure (3). The BER performance for various modulation schemes.

The performance results is also shown in Table (1) for $= 10^{-4}$.

Table (1). The S/N ratio for various modulation schemes.

The modulation Scheme	S/N (dB)
64 QAM	25
256QAM	28
16QBSK	---

5. Performance of System with Rayleigh and COST 207 channels

The BER performance of the adaptive TTCM system using 4 iterations is shown in Figure (4) with Rayleigh and COST 207 [7] channels. In order to investigate the switching dynamic of the systems,

the mode switching together with the equalizer's output SNR is setup to 17 dB. As we notice from the figure, the BER performance of the system has a lower values with Rayleigh channel.

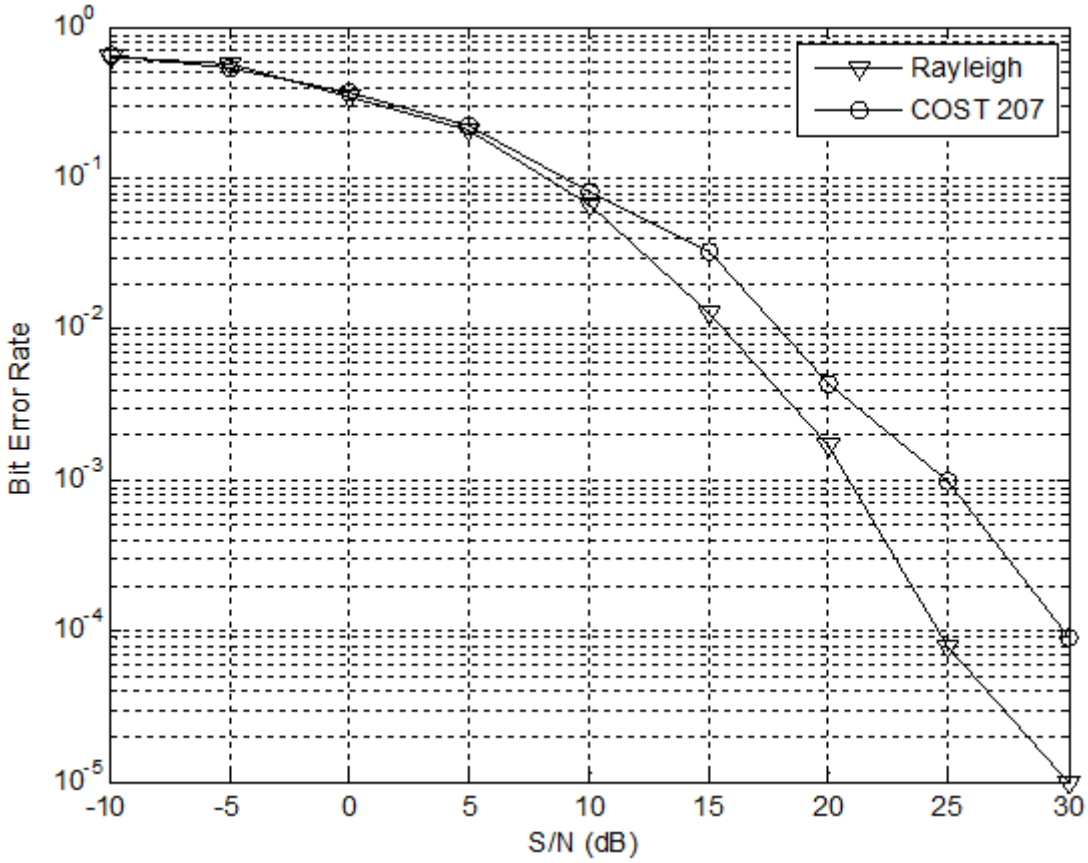

Figure (4). The System BER performance with Rayleigh and COST 207.

The performance results is also shown in Table (2) for $= 10^{-4}$.

Table (2). The S/N ratio for various channels.

The Channel Type	S/N (dB)
Rayleigh	24
COST 207	30

6. Performance of System with Rayleigh and AWGN channels

Again, the system performance is also tested in transmissions over AWGN channel and Rayleigh channels using 16QPSK scheme. Figure (5) shows the results. As we notice from the figure that the system BER with AWGN channel is

outperformed the system performance with Rayleigh channel.

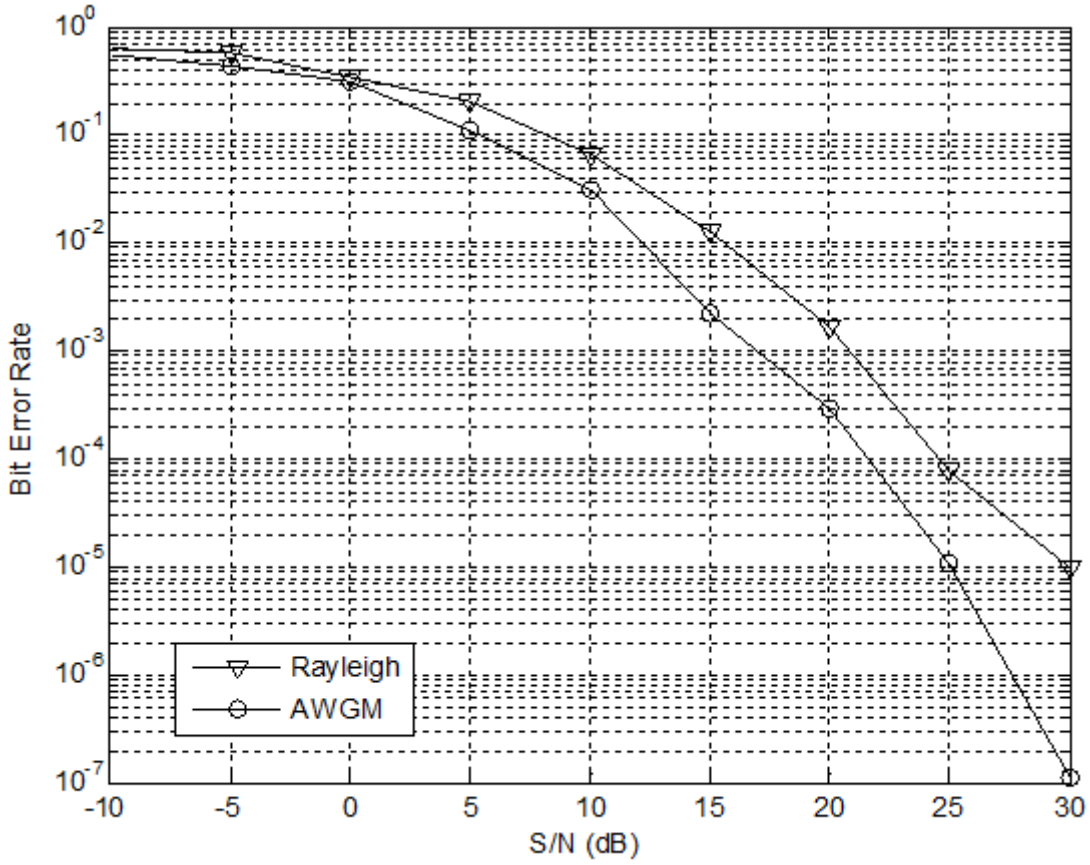

Figure (5): The System BER performance with Rayleigh and AWGN channels.

The performance results is also shown in Table (3) for $= 10^{-4}$.

Table (3). The S/N ratio for various chann*els*

The Channel Type	S/N (dB)
Rayleigh	24
AWGN	30

7. Conclusions

In the presented research, the TTCM Burst-by-Burst Adaptive Wideband Coded Modulation system tested in Rayleigh Channel.

Many important points can be noted during simulation and discussion of the results of the system with Rayleigh fading channel.

First, the system has gained a lower BER values by using 16QPSK modulation scheme. Second, the system is work better in Rayleigh multipath channel. Finally, a good performance is obtained with the AWGN channel.

8. References

1. Hanzo, L., C.H. Wong, M.S. Yee; " Adaptive Wireless Transceivers"; John Wiley & Sons Ltd; 2002.
2. Samuel C. Yang; "CDMA RF System Engineering"; Artech House; 1998.
3. Marvin K. Simon ; "Digital Communication over Fading Channels"; John Wiley & Sons, Inc.; 2000
4. Mohamed Ibnkahla; " Signal Processing for Mobile Communications"; CRC Press LLC; 2005.
5. Wong, C., T. Liew, and L. Hanzo; "Burst-by-burst turbo coded wodeband adaptive modulation; IEEE Journal on Selected Areas in Communications, vol. 18; July 2001.
6. "COST 207: Digital land mobile radio communications"; Office for Official Publications of the European Communities, 1989. Luxembourg.

Novel Technology for Image Steganography Based on Multi-level DWT and Block Permutation System

Hussam Abd Ali Darweesh

Department of Computer Technology Engineering, University of Madenat Al-Elem, Baghdad- Iraq (Email: hussamuot@ yahoo.com).

Abstract

This paper proposes a novel technology for image Cryptography, steganography system and embedded high capacity data at the same time. The proposed technologic first encrypted the information by using Zigzag Order Block Permutation (ZOBP), which divides the image into sub-block of size (8*8), then permutated the Blocks depend on Cipher Key. The permutation blocks pixels by zigzag order. The Encrypted information has been converted by Discrete Wavelet Transform (DWT) series of bits in order to increase the power coefficients. The secret information bits embedded into Binary of the cover image after converted by Multi-level DWT. The secret bits replace by bits in cover coefficients. The image results after Inverse Discrete Wavelet Transformation (IDWT) called stego-image. This embedded information casing statistically significant modification to the cover image. The simulation results calculate Peak Signal to Noise Ratio **(PSNR)**, and Correlation test **(Cor)** as parameters of robustness, and quality of reconstruct image. The proposed system hides high capacity of data depends on the level of DWT to cover image that hiding Capacity parameter calculated by Bit per Pixel **(BPP)**. The proposed method hidden high capacity information with most security and quilility system.

Keywords: Imgesteganography, Image Cryptography, Multi-level Discrete wavelet Transform, Zigzag order Block Permutation (ZOBP), Peak Signal to Noise Ratio (PSNR), Correlation test (Cor.), Bit per pixel (Bpp).

تصميم تقنية جديده لأخفاء الصور السرية باستخدام المويجة المتقطعة الرقمية المتعددة بعد تشفير الصورة بواسطة تضمين اجزاء صغيرة من الصورة

المستخلص

البحث المقدم يقترح نظاماً جديداً يقوم بتشفير وإخفاء المعلومات ذات السعة الكبيرة. يعمل النظام المقترح اولاً بتشفير الصورة السِرّية وذلك بتقسيمها الى اجزاء ذات حجم (8*8) وتضمن باستخدام طريقة الزيكزاك (zigzag order) وبعدها يضمن كل جزاء في الصورة المقطعة بالاعتماد على مفتاح سري (cipher key) لتوليد الصورة المشفرة (Encrypted Image). وتقوم عملية التشفير بتحويل الصورة المشفرة الى معاملاتِ Discrete Wavelet Transform (DWT) . وعن طريق زيادة طاقة المعاملات ثم تحولها الى متسلسلة من البت (stream of secret bits). ولكي نكمل عملية تشفير الصورة نقوم بتحويل صورة الغطاء(Cover Image) الى معاملات DWT ولعدة مرات (Multi-level). وبعدها نقوم بإخفاء المعلومات السرية (secret bits) داخل البت لصورة الغطاء وبعد الانتهاء من التحويل نعيد الصورة باستخدام Inverse Discrete Wavelet Transform لغرض توليد الصورة الحاملة stego-image. تتم المرحلة االاخيرة من العملية من خلال برنامج المحاكاةَ يقوم بالإضافة إلى برنامج الإخفاء بحساب نسبة طاقة الاشارة الى طاقة الضوضاء Peak Signal to Noise Ratio (PSNR) وعامل التقارب Correlation test (Cor) لحساب دقة الصورة المسترجعة بالمقارنة مع الصورة السرية الاصلية. تعتمد سعة الاخفاء للصورة السرية على عدد مرات اخذ Discrete Wavelet Transform لصورة الغطاء وكذلك يحسب نظام المحاكات عدد البت المخفية بالنسبة الى عدد وحدات الصورة (Pixels) في صورة الغطاء Bit per Pixel (Bpp) كعامل لسعة الاخفاء. وبهذه الطريقة تمكنا من أخفاء المعلومات ذات السعة الكبيرة وبكفاءة وأمنية عاليتين مقارنة مع طريقة الاخفاء بالبت الاخيرة (Least significant bit (LSB)) وطريقة المحولات (transformation methods).

1. INTRODUCTION

Data security is the methods to protecting data of computer and communication systems from unauthorized disclosure and modification [1]. Data in computer systems are in danger from many threats including indiscriminate searching, leakage, inference and accidental destruction [2].

Protecting security data is an important demand and there are two techniques available to transmit data using unprotected communication media [3]. First Cryptography can be defined more specifically as the area

within cryptology that is making communication unintelligible to all except the intended recipient or it may be defined as the science of hiding Enciphering the contents of secret message from an attacker [4]. The secret message is scrambled and can be reconstituted only by the holder of the key [5]. Second Steganography represents a class of process used to embed data into various forms of media such as image, audio or text with minimum amount of degradation to the cover image, so that the fact secret message is being transmitted is also a secret [6].

In cryptography, the structure of a message is changed to render it meaningless and unintelligible unless the decryption key is available, cryptography makes no attempt to disguise or hide then coded message [4]. Steganography does not alter the structure of the secret message, but hide it inside a cover [7]. The system has been proposed combines the techniques by encrypting message using cryptography and then hiding the encrypted message using Steganography. The resulting stego-image can be transmitted without revealing that secret information is being exchanged.

The challenge in information-hiding method can operate with either high payload capacity or high robustness to modification, but not both [8]. Robustness: The embedded data should be as immune as possible to modifications from intelligent attacks. Capacity: Ideally we want large capacity but would affect Imperceptibility and robustness. Security: the inability of adversary to detect hidden images accessible only to the authorized user [9].

Contribution of this paper as, is that the secret image has been embedded in the detailed bands of the Covert image. The two primary classes of digital image steganography are least significant bit (LSB) steganography and transform based steganography [10]. LSB steganography is more susceptible to image manipulation than transform based steganography [7]. Transform based steganography has the potential to achieve higher payload capacity than LSB steganography [11].

In this work the secret image is encrypted using Zigzag Block order ZOBP, increasing DWT power coefficients, then embedded the secret binary in binary cover image wavelet coefficients. This method results high quality and capacity embedded data and more security.

2. The PROPOSED CRYPTOGRAPHY SYSTEM

The proposed cryptography technique is shown in Fig.(1) and can explain by the following steps:

1. Divide the image into not join sub-image of size (128*128).
2. Divide every sub-image into not join sub-block of size (8*8).
3. Name every sub-block by sequence number start with one to up-left corner sub-block then increased the block numbers row by row.
4. Generate Cipher Key contain integer unrepeated numbers between (1 to number of sub-Blocks).

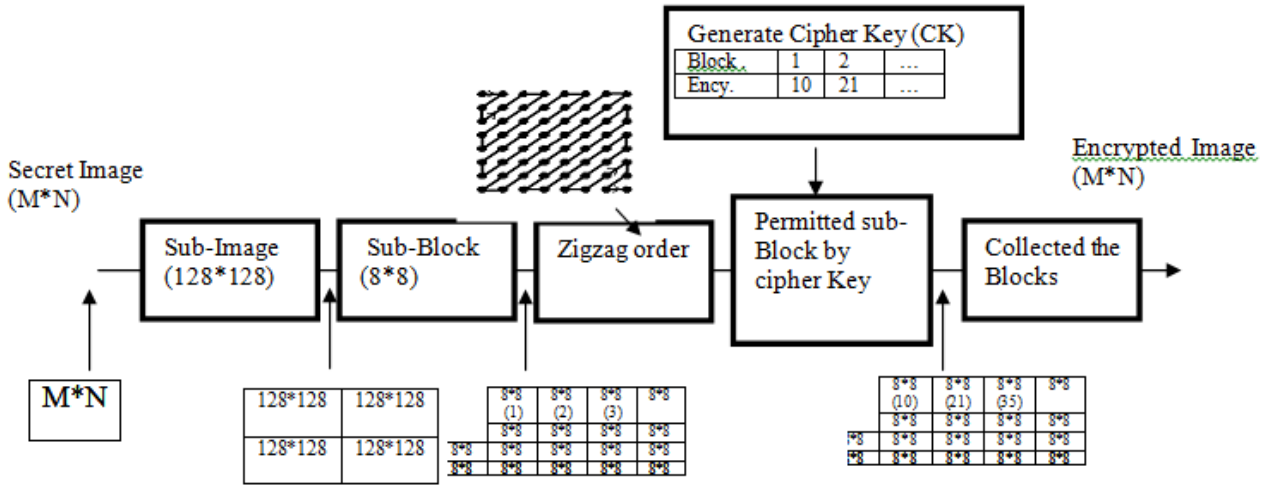

1- Every sub-block permuted by using Zigzag order as shown in Fig.(1) [12].
2- Permuted the sub-blocks depend on numbers in cipher Key as shown in Fig.(2).

The Encrypted and Decrypted system used the same cipher key to reconstructed image.

3. THE PROPOSED IMAGE STEGNOGRAPHY SYSTEM

I. Embedding of secret image

The embedding block diagram shown in Fig.(3) consist of the following steps:

1. The cover Gray-level image which have a flat histogram. This image is almost perfect distribution of pixel, which can hide the secret image in.

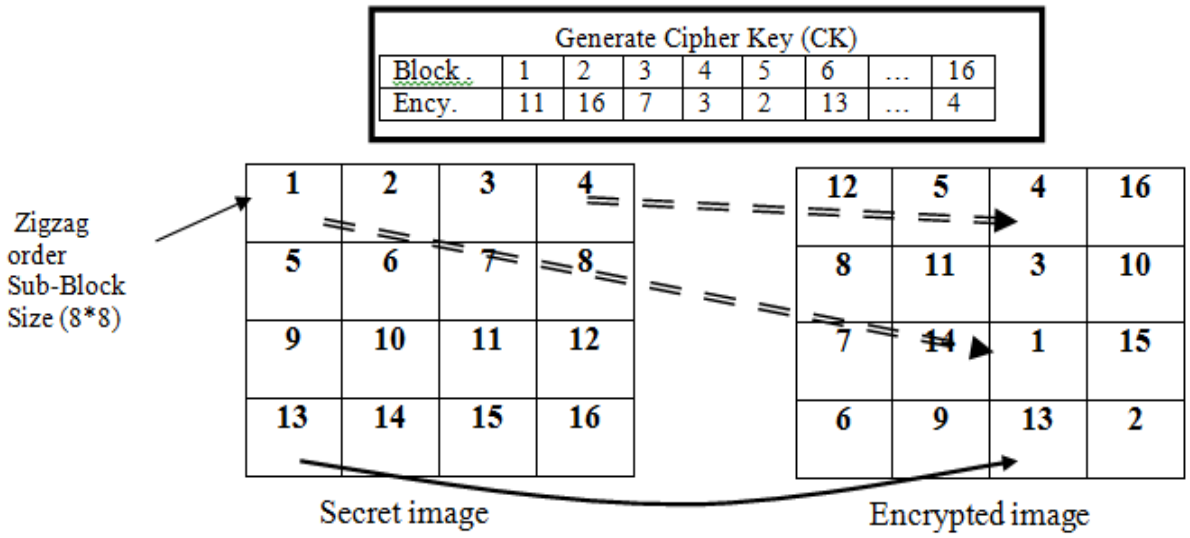

Fig. (2). Schematic of Encrypted System.

2. The DWT is considered to the cover image. The DWT2 divides the cover image into four quarters as shown in Fig.(4-a) [13] the upper-left (LL) is the cover image but with small scale. The three quarters (LH, HL, and HH) are the shadow of the cover image that the secret information will be embedded in these quarters, another DWT2 taken into LL of the first level to have second level DWT2 to increase the place of hiding data …atc as shown in Fig.(4-b). the vector **U** for n-level DWT2 are

$$\mathbf{U}=[LHn, HLn, HHn, \ldots, LH_1, HL_1, HH_1] \quad \ldots.(2)$$

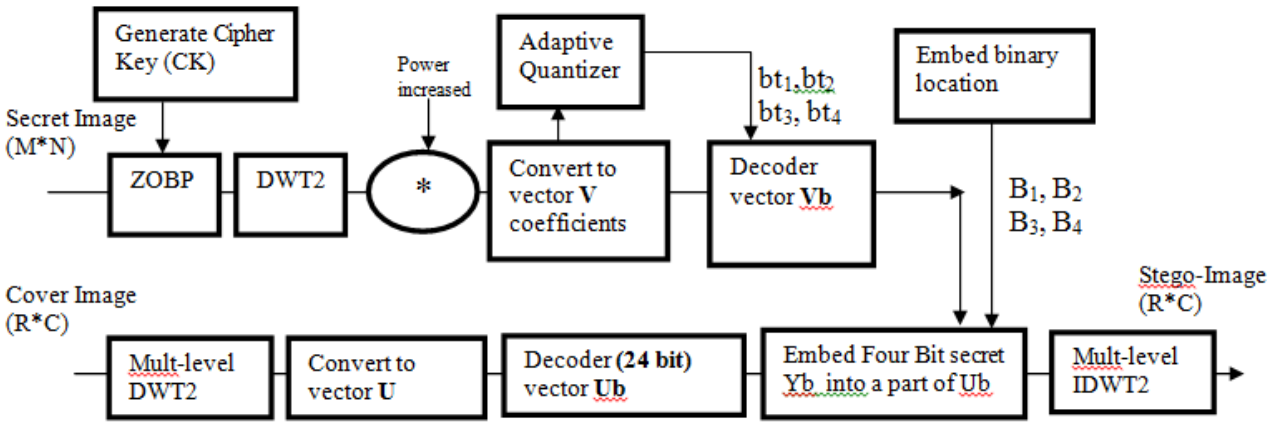

Fig. (3). Proposed Embedding System.

1. Re-arrange the cover coefficients as one dimension vector start from high level down to low-levels (expected the LL) as in eq.(2), then convert it by fixed decoder of 24 bit as shown in Fig.(5). The vector $\mathbf{U_b}$ are:

$$\mathbf{U}=[LHn*24, HLn*24, HHn*24 ,\ldots, LH_1*24, HL_1*24, HH_1*24] \quad \ldots (3)$$

2. The **secret image** transfer by DWT2 then increased the power of secret DWT coefficients by factor (Pinc), that result high equality to the reconstructed image.
3. Re-arrange the secret coefficients as one dimension vector as

$$\mathbf{V} = [LL, LH, HL, HH]. \quad \ldots.(4)$$

4. The number of bits for every part of Vector **V** decided by adaptive quantizer [13]. The part power is the more important parameter to decide number of bit, the analogy to digital converter shown in Fig.(1) design uniform fixed decoder for every part of secret coefficients this generate binary vector $\mathbf{V_b}$.

$$\mathbf{Vb} = [LL*bt1, LH*bt2, HL*bt3, HH*bt4] \quad \ldots..(5)$$

Where

bt1: number of bits to decode LL.

bt2: number of bits to decode LH.

bt3: number of bits to decode HL.

bt4: number of bits to decode HH.

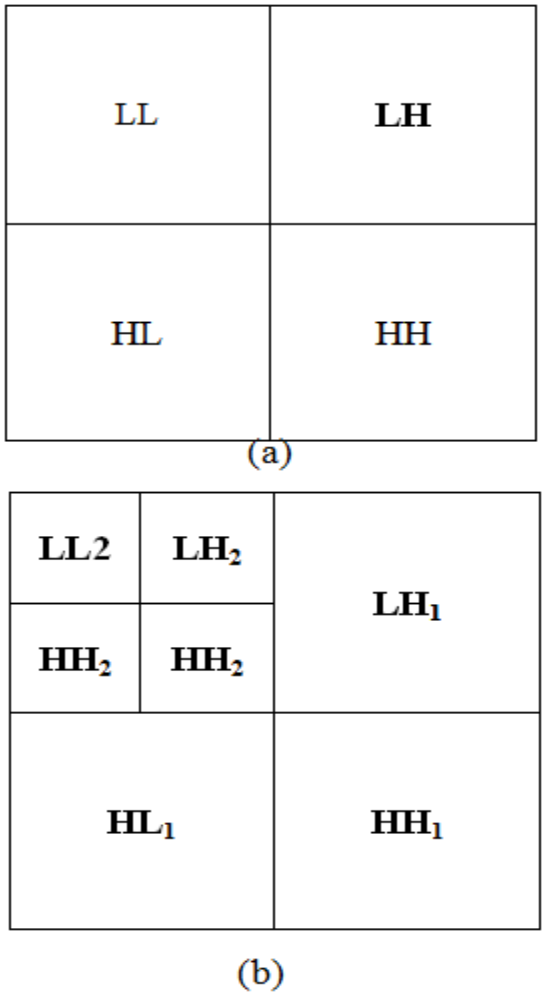

Fig.(4) Discrete Wavelet Transformation Decomposition [13]

(a) 1-level DWT (b) 2-level DWT .

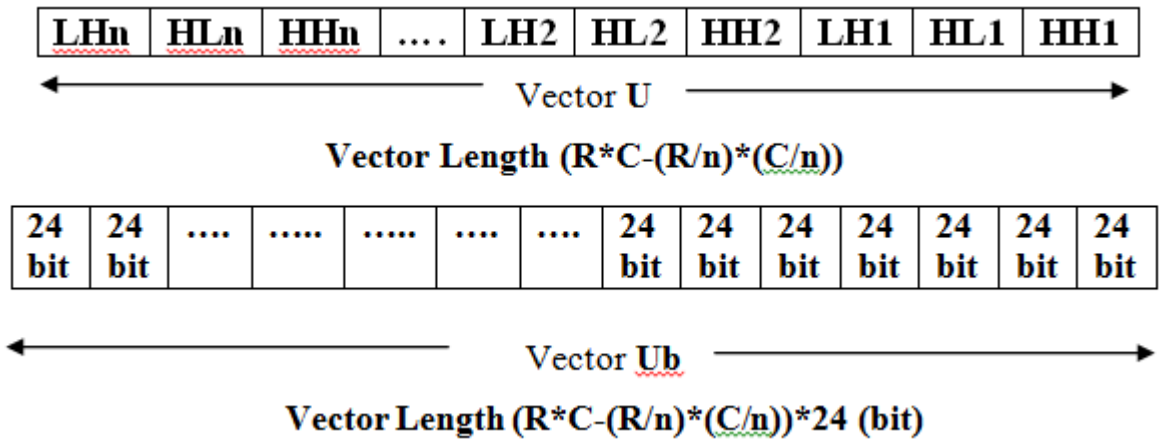

Fig.(5) Vector (U) Form n-level DWT2 Coefficients of Cover Image, and vector Ub (binary vector of cover image) .

3- Replacing every sequence four bits of the cover image, by the four sequence bits of the secret information.
4- The locations of embedded bits [B1, B2, B3, B4] can be generated randomly to increase degree of cipher.
5- The (n) -level IDWT2 to the cover coefficients generate stego-image.

II. Extraction of the secret Image

This process work powerfully to reconstruct secret image if same parameters of the embedded process received. The DWT of cover image levels (n), start location of embedded bit (Bi), number of bits that convert secret image DWT bands to Binary, power factor increasing of the secret image (P_{inc}), and Cipher key (CK).

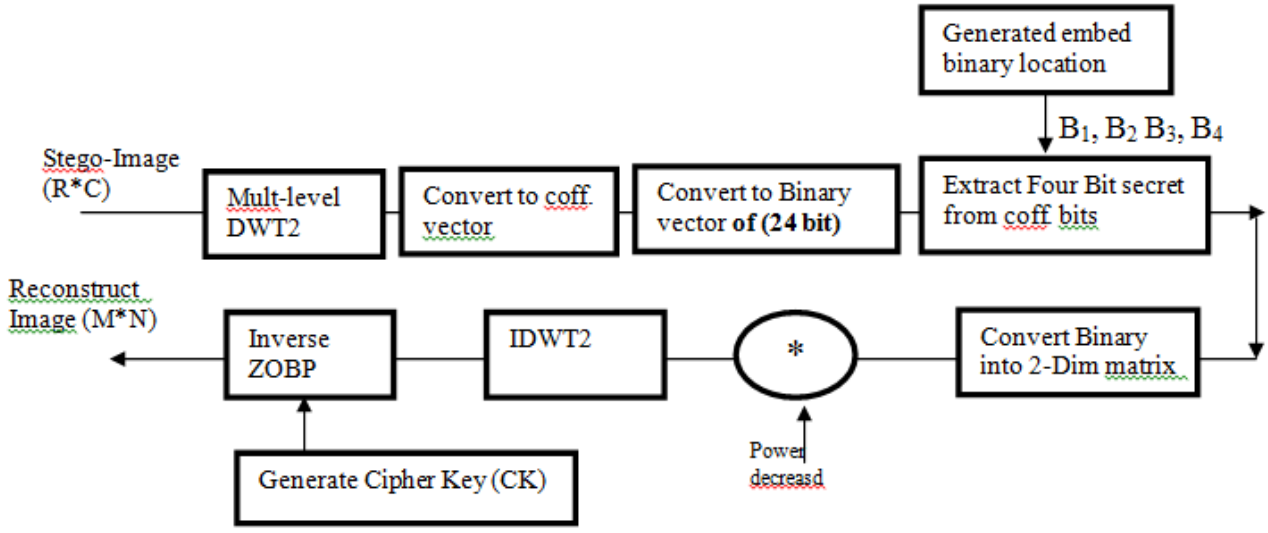

Fig.(6) Proposed Reconstructed System

The Reconstructed block diagram shown in Fig.(6) it consist of the following steps:

1- The received stego-image has been transformed by n level DWT2 transform.
2- re-arrange the DWT coefficients as shown in Fig.(5).
3- Extract the sequence four bits of location (B1, B2, B3, and B4) from cover image.
4- The Binary vector reconstruct convert to two dimension DWT coefficients
5- All coefficients divided by factor (P_{inc}).
6- IDWT2 to the reconstructed values.
7- Decrypted the image use the same cipher Key in the Encrypted process.
8- Reverse the Zigzag order to all blocks
9- Collect the sub-blocks, and sub images to generate reconstructed image.

4. FIDELITY CRITERIA

There are two types of image fidelity criteria namely, the objective and subjective criteria [11]. The first one depends on equations that are used to measure the amount of the error in the reconstructed image. While the second require the definition of qualitative scale to assess image quality and this scale can then be used by human test subjective to determine image fidelity [8].

I. The Similarity Test

Similarity test is the correlation between the two images, before and after process. When the two image are perceptually similar, then the correlation equals one. The correlation can be calculated as shown below [2]

$$Corr. = \frac{\sum_{i=1}^{M}\sum_{j=1}^{N}(X(i,j)-\overline{X})(Y(i,j)-\overline{Y})}{\sqrt{\left[\sum_{i=1}^{M}\sum_{j=1}^{N}(X(i,j)-\overline{X})^2\right]\left[\sum_{i=1}^{M}\sum_{j=1}^{N}(Y(i,j)-\overline{Y})^2\right]}} \quad ....(6)$$

where

*M and N:*height and width of the two images (because the two images must be of the same size).

i *and* j*: row and column numbers.*

X(i, j): the original image.

Y(i,j): modified image.

$\overline{X}$, $\overline{Y}$: Mean of original and modified image, respectively, and calculated by

$$\overline{X} = \frac{\sum_{i}^{M}\sum_{j}^{N}X(i,j)}{M \times N} \quad ..(7)$$

$$\overline{Y} = \frac{\sum_{i}^{M}\sum_{j}^{N}Y(i,j)}{M \times N} \quad ..(8)$$

II. Peak Signal to Noise Test (PSNR)

According to the human visual system, some amount of distortion between the original image and the modified one is allowed. Here the *PNSR* is employed to indicate the performance of the method. *PSNR* is usually measured in *db* as given in [10].

$$PSNR = 10\log_{10}\frac{(L-1)^2}{\frac{1}{M\times N}\sum_{i=1}^{M}\sum_{j=1}^{N}\left[Y(i,j)-X(i,j)\right]^2} \quad ..(9)$$

where:

L-1: maximum gray level (in Gray-level image equal to *L-1*=255).

The larger PSNR indicates the higher the image quality i.e. there is only little difference between the cover-image and the stego-image as a parameter of robustness, otherwise, the PSNR between secret image and reconstructed image as a parameter of equality. On the other hand, a smaller PSNR means there is huge distortion between the cover-image and the stego-image.

VI. Capacity Measure

The notion of capacity in data hiding indicates the maximum number of bits that can be hidden and successfully recovered by the steganographic system. Therefore the number of hidden bits varies depending on cover image size. To measure the hidden capacity bit per-pixel (BPP) is the factor of hidden capacity that given by [12]

$$BPP = \frac{Hidden\ Secret\ \ Image\ Bit}{Cover\ Image\ Pixel\ Size} \quad \ldots(11)$$

5. EXPERIMENTAL RESULTS

In this section, some experiments are carried out to prove the efficiency of the proposed system. The proposed technique has been simulated using the MATLAB-10 program platform. A set of 8-bit grayscale images of size 512 × 512 are used as the cover-image to form the stego-image. All results used power increased by ($P_{inc.}$=10).

The experiment results show that we can reconstruct the secret images from the stego-image without error matching image

(corr.=1 and PSNR= ∞) for hidden capacity less than 2.75 BPP.

Wherever, the different image between cover and stego-image gives the subjective criteria. The proposed system steps, shows in Fig. (7- a) is the original secret image (airplane (300*300)), Fig.(7-b) the Encrypted image by cipher Key using ZOBP method, Fig.(7-c) the DWT2 of the secret image, Fig.(7-d) the cover image (Lena), Fig.(7-e) the 2-level DWT2 to cover image, Fig(7-f) the 3-level DWT2 to cover image, Fig(7-g) the stego-image, Fig. (7-h) shows the differences image between cover image and stego-image image, and Fig.(7-i) decrypted reconstruct secret image.

The result for embedded the image airplane of size (300*300) in three different cover images (boys, City, and Flowers) the hidden capacity (3 Bpp), with 3-level DWT2 shown in Fig.(8). Fig.(9) shows the result for embedded the image MAP in the same three different cover images by used 3-level DWT2. The stego-images are the same as the cover images in visual. That shows the good transparency of the system.

The objective results shown in Table (1) corr., $PSNR_C$ (the PSNR between cover image and stego-image) for four different cover images, and $PSNR_S$ (the PSNR between secret image and reconstruct image) for two secret images. As shown in Table (1) for different secret image, the results have been recorded for 2-level and 3-level DWT2 to cover images. This result indicated the change in cover image don't gives high improved to $PSNR_C$ and don't effect at $PSNR_S$. The objective results gives little change when increased the DWT2 levels, whenever, that increase the hiding place and increased hidden data capacity as shown in Table (2). 3-level DWT2 gives improvement in the $PSNR_C$ and $PSNR_S$ compare with 2-level DWT2 and increasing the hidden data capacity.

The objective results obtain little change in $PSNR_C$ and $PSNR_S$ at hidden capacity less than 3.125 Bpp, when gives high drop in $PSNR_S$ in hidden capacity greater then 3.2 Bpp as shown in Table (2).

6. CONCLUSIONS

In this paper, a proposed Cryptography and steganography technique in DWT domain to improve security and quality of hiding data. According to the simulation results the stego-images of this method are almost identical to the original images. a proposed system also provides additional five layers of security by means of transformation (DWT and IDWT) of secret image, Multi-level DWT of

cover image, encoding of secret image, location of embed bits, and secret DWT power coefficients increase.

The demand of robustness in image Cryptography and steganography filed and quality of reconstructed secret image is requested as strongly as it is in LSB methods or transformation method. In our proposed system the BZOP methods, the embedding process is hidden under the transformation of both cover and secret images, increasing the secret coefficients power. These operations and encoding of secret image keep these images away from stealing, destroying from unintended users, hence the proposed method may be more robust against brute force attack. a proposed system has hidden data capacity greater than that in LSB methods or transformation method, with matching reconstructed secret images.

Table (1) The objective results of proposal system for different secret and cover images, hidden data capacity of 2.75 BPP.

2-level DWT2 Secret image airplane (300*300)				
Cover Image (512*512)	Corr.	$PSNR_C$ (dB)	Corr.	**PSNRS (dB)**
Lena	0.999999591	65.692	1	**320.6**
Boys	0.99999766	66.381	1	∞
City	0.99999616	66.315	1	∞
Flowers	0.99999722	66.044	1	∞
Secret image Map (300*300)				
Lena	0.9999966	66.494	1	∞
Boys	0.99999804	67.170	1	∞
City	0.99999671	67.021	1	∞
Flowers	0.99999766	66.792	1	∞
3-level DWT2 Secret image airplane (300*300)				
Cover Image (512*512)	Corr.	$PSNR_C$ (dB)	Corr.	**PSNRS (dB)**
Lena	0.99999596	67.742	1	**316.66**
Boys	0.999997679	66.413	1	∞
City	0.99999623	66.399	1	**316.66**
Flowers	0.99999724	66.0823	1	**316.68**

Secret image Map (300*300)				
Lena	0.99999666	66.576	1	**320.398**
Boys	0.99999808	67.247	1	**320.398**
City	0.99999675	65.042	1	∞
Flowers	**0.99999769**	**66.865**	**1**	**320.39**

(a)

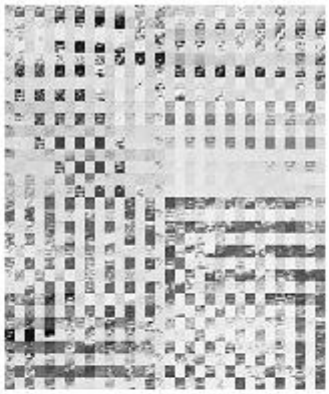

(b)

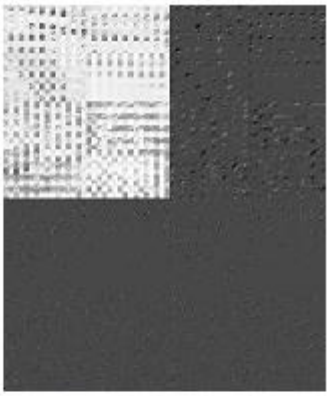

(c)

(d)

(e)

(f)

(g)

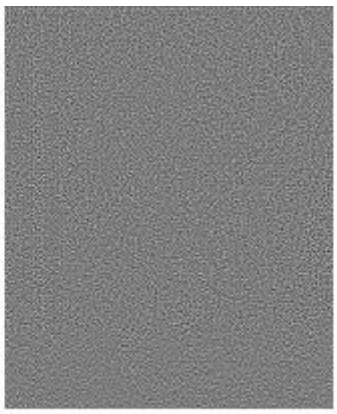

(h)

(i)

Fig.(7) Experimental Result for the Proposal technique. The Objective Result are Corr.=.99999718, $PSNR_C$ = 67.31 dB, $PSNR_S$= ∞ dB, and BPP = 2.75 bit/pixel

(a) Original secret image (airplane (300*300)), (b) Encrypted image by ZOBP (c) Wavelet 2-level for scaling secret image (d) Cover images (Lena (512*512)), (e) Wavelet 2-level to cover images, (f) Wavelet 3-level to cover images, (g) Stego-images, (h) Different between cover and stego-image, and cover image, (i) the Decrypted Reconstructed secret image.

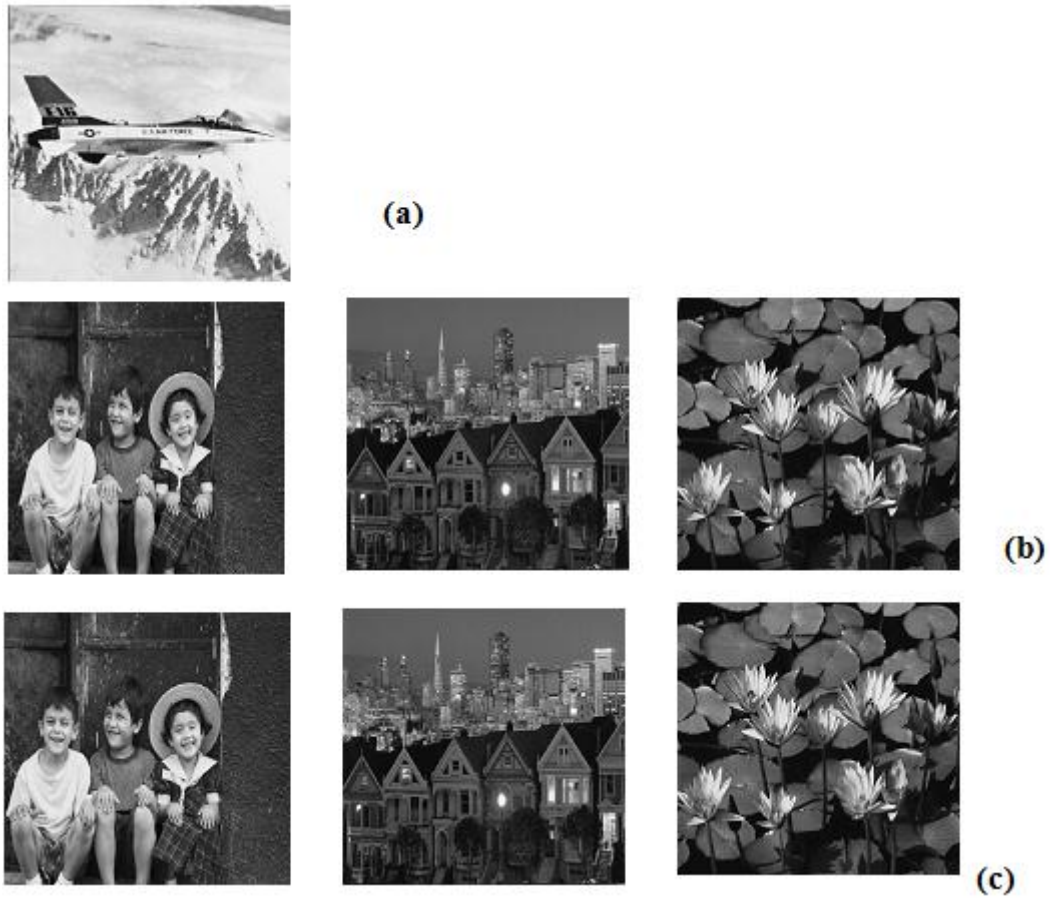

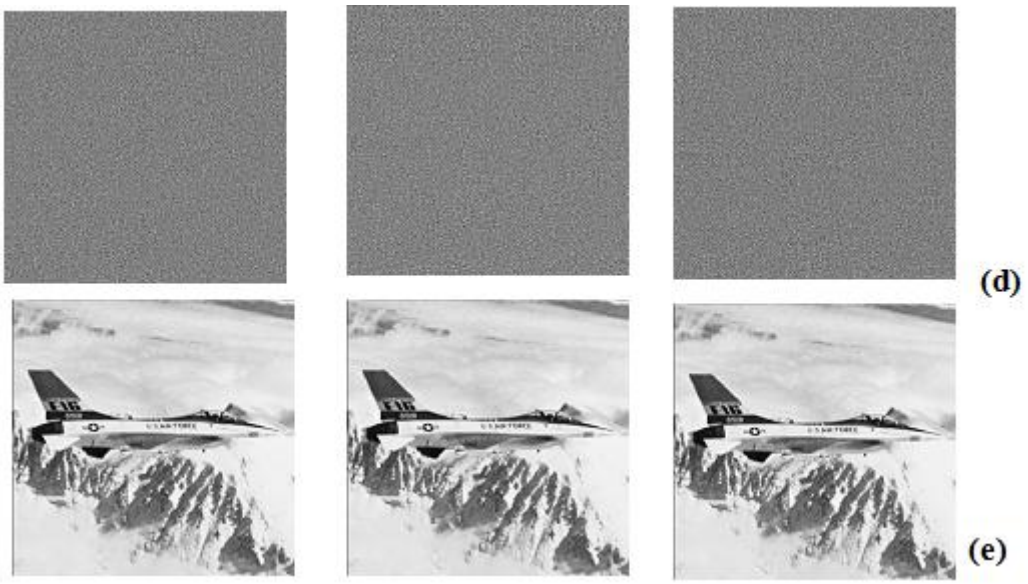

Fig.(8) Proposal System Experimental Results used Different Cover Image Hidden Capacity 2.75 BPP.

The reconstructed image matching to secret image (a) Original secret image (airplane (300*300)),

(b) Cover images (512*512), (c) Stego-images, (d) Difference between cover and stego-images,

(e) Reconstructed secret image.

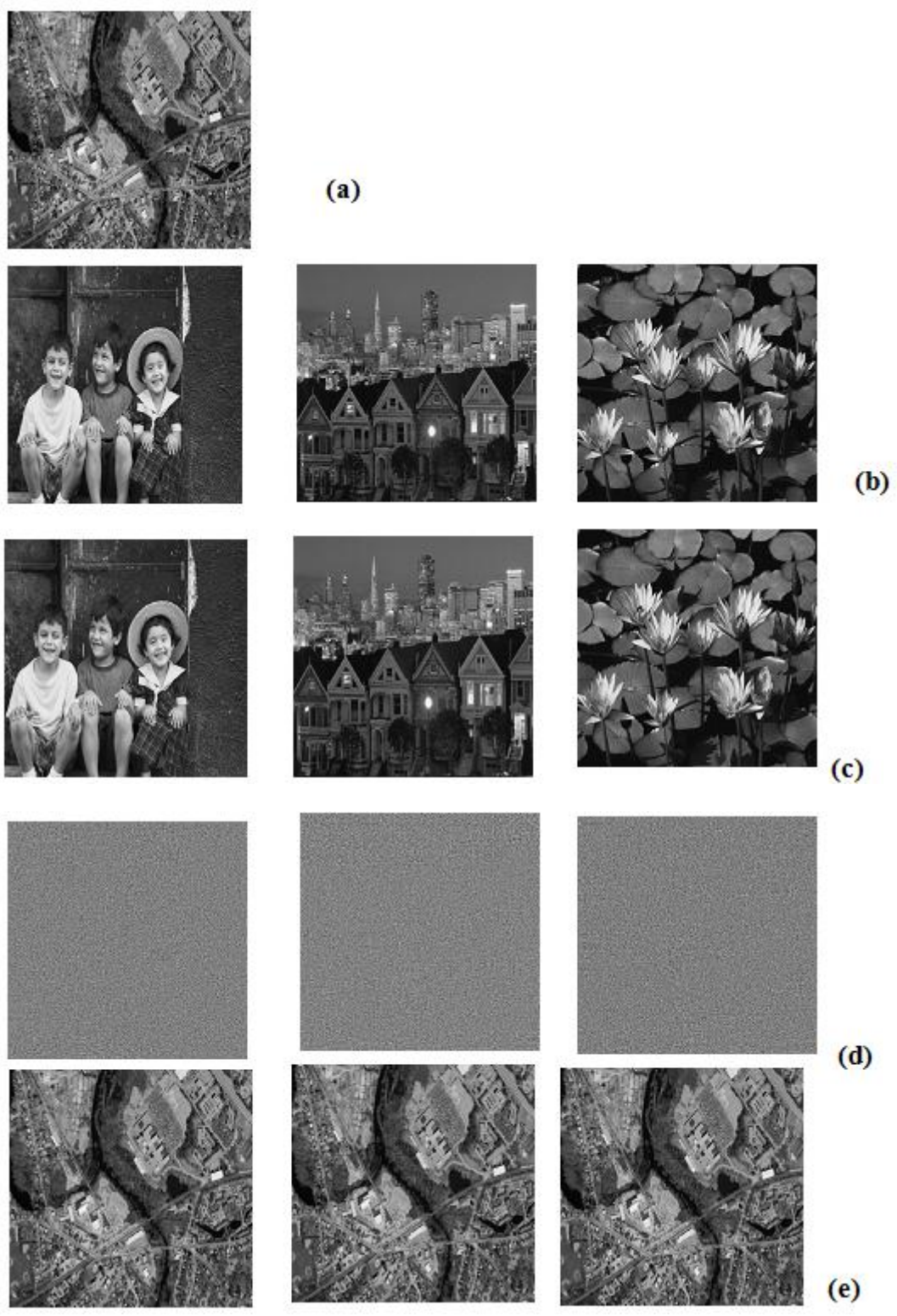

Fig.(9) Experimental Result for the Proposal System used Different Cover Image Hidden Capacity 2.75 BPP. (a) Original secret image (Map (300*300)), (b) Cover images (512*512), (c) Stego-images, (d) Difference between cover and stego-images,

(e) Reconstructed secret image.

REFERENCE

1. E. T. Lin and E. J. Delp***"R Review of Data Hiding in Digital Images"*** Purdue university, west Lafayehe, Indiana, 1999.
2. C. P. Pures., "***Security In Computing***", Prentice Hall, 2006.
3. W. Stallings "***Cryptography and Network Security Principles and Practices***", Fourth Edition, Prentice Hall, November, 2005.
4. A. Nag, S. Biswas, D. Sarkar, P.P. Sarkar, ***"A novel technique for image steganography based on Block-DCT and Huffman Encoding",*** International Journal of Computer Science and Information Technology, Volume 2, No. 3, pp. 103-112, June 2010.
5. M. S. Kasem., D. Muhammad., M. Kasem, and Khaled A., ***"Singular points detection using fingerprint orientation field reliability",***International Journal of Physical Sciences Vol. 5(4), pp. 352-357, April 2011.
6. S. Torres-Maya, M. Nakano-Miyatake and H. Perez-Meana, ***" An Image Steganography Systems Based on BPCS and IWT",***IEEE International Conference on Electronics, Communications and Computers, 2006.
7. R. C. Gonzalez and R. E. Woods ***" Digital Image Processing "***, Third Edition, Prentice Hall Upper Saddle River, New Jersey, 2008.
8. K. B. Raja, Vikas, V. KR, and L. M. Patnaik,***" High Capacity Lossless Secure Image Steganography using Wavelets"***, IEEE, 2006.
9. Y. Ying Chung, Y. Sun, ***"High Capacity Image Steganography System Using Wavelet Zerotree"***, Transations on Engineering, Computing and Technology, December 2004.
10. H. A. Darwessh., and A. Hussan, "***High Capacity Secret Image Steganography using DWT",***second conference university of Technology, April, pp 5-16, 2009.
11. C. Solomon, and T. Breckon, ***"Fundamentals of Digital Image Processing "***, John Wiley & Sons, Ltd 2011.
12. K. Mohemed., A. P. Kursem., and M. Solon, "***Image Denoising And Enhancement Using Multiwavelet With Hard Threshold In Digital Mammographic Images"***, International Arab Journal of E-Technology, Vol. 2, No. 1,pp 49- 56, January 2011.

13.P.-Yueh Chen and H.-Ju Lin ***" A DWT Based Approach for Image Steganography"*** International Journal of Applied Science and Engineering, 275-290, April 2006.

Flow Analysis of Third Order Fluid in a Helical Pipe with Circular Cross- Section

Wala'a AbdUl-Mageed Mahdi[1] and Ahmed M. Abdu l-Hadi[2]

[1]University College of Madinat al- Elem; [2]Dept. of Mathematics, College of Science, Baghdad University

Abstract

In this paper, we studied viscous non –Newtonian fluid of third order flowing in a helical pipe with circular cross-section under action of the pressure gradient. Particular consideration is given to fluid flow which can be represented by the equation of state of the form:

$$\mathbf{T}=\boldsymbol{\mu A_1}+\boldsymbol{\alpha_1 A_2}+\boldsymbol{\alpha_2 A_1^{\,2}}+\boldsymbol{\beta_1 A_3}+\boldsymbol{\beta_2}(\boldsymbol{A_1 A_2}+\boldsymbol{A_2 A_1})+\boldsymbol{\beta_3}(\boldsymbol{tr A_1^{\,2}})\boldsymbol{A_1}.$$

where $\alpha_i(\mathrm{i}=1,2), \beta_i(\mathrm{i}=1,2,3)$ are material moduli and A_i(i =1-3) are the first three Rivlin-Ericksen tenser. The cylindrical coordinates have been used to describe the fluid motion. It is found that motion equations are controlled by the dimensionless numbers namely Dean number L, non-Newtonian parameter β, and material moduli (γ_1, γ_3). The motion equations are solved analytically. The analytic solutions of the secondary velocity and the axial velocity are obtained. The effects of each of the dimensionless numbers upon the components of the secondary and the axial velocity are analyzed.

المستخلص

في هذا البحث درس جريان مائع لانيوتيني من الرتبة الثالثة في انبوب حلزوني ذو مقطع عرضي دائري تحت تأثيرالضغط. وبصورة خاصة يمكن ان يمثل ذلك المائع بمعادلة حالة من النوع

$$\mathbf{T}=\boldsymbol{\mu A_1}+\boldsymbol{\alpha_1 A_2}+\boldsymbol{\alpha_2 A_1^{\,2}}+\boldsymbol{\beta_1 A_3}+\boldsymbol{\beta_2}(\boldsymbol{A_1 A_2}+\boldsymbol{A_2 A_1})+\boldsymbol{\beta_3}(\boldsymbol{tr A_1^{\,2}})\boldsymbol{A_1}$$

استخدمت الاحداثيات المتعامدة لوصف حركة المائع. وجد أن معادلات الحركة مسيطرعليها باعداد لا بعدية وهي رقم دين معلمة لا نيوتينية وثوابت المائع. ان معادلات الحركة قد حلت تحليليا. حصلنا على التحليلية للجريان الثنائي والسرعة المحورية. وبالاضافة لذلك قمنا بدراسة تأثير الاعداد اللابعدية وتحليل مركبات الجريان الثنائي والسرعة المحوريه.

1. Introduction

The science of hydrodynamic is that branch of applied mathematics which deals with the behavior of fluids in motion. Fluid is that state of matter which capable of changing shape and is capable of flowing. Fluids may be classified as "Viscous" and "Perfect" according to whether the fluid capable of exerting shearing stress or not. Viscous fluid is called Newtonian if the relation between stress and rate of strain (state of equation) is linear, otherwise is called non-Newtonian fluid. The flow of Newtonian and non-Newtonian fluids has been the subject extensive theoretical studies till date. Dean [6] in 1927 was the first researcher who worked in flow analysis of Newtonian fluids in curved pipes. He introduced a toroidal coordinate system to show that the relation between pressure gradient and the rate of flow through a curved pipe with a circular cross-section of in compressible Newtonian is dependent on the curvature. In that paper he couldn't show this dependence but he did in his second paper [7]. He modified his analysis by including the higher order and he was able to show the rate of flow is straightly reduced by curvature. Jones [12] in 1969 made a theoretical analysis of the flow of an incompressible non-Newtonian viscous liquid in a curved by with circular cross-section. Keeping only the first order terms. He showed that the secondary motion consists of two symmetrical vortices and the distance of the stream line form the central plane decreases as the non-Newtonian parameter increases. Wang [17] in (1981) studied the flow of incompressible Newtonian fluid in a helical pipe with circular cross-section introduced non-orthogonal coordinates system to study the effect of torsion and the curvature. Employing a perturbation method and he found that the torsion has the first order effects on the secondary flow. In 1982 Germano [9] studied the same problem of Wang's but his solutions were obtained in an orthogonal coordinate system and he found the effects of torsion to be the second order. This results confirmed in his second paper in (1989) [10] in which he studied the effect of torsion in a helical pipe with an elliptical cross-section showing that there is unexpected form of the secondary where the walls act as sources and sinks. In 1990, Tuttle [15] solved the motion of the flow in pipes of elliptical cross-section and circular cross-section successively. Then he qualitatively stated that the order of torsion effect on the secondary flow dependent the frame of references of

the observer. Without any approximation in the governing equations. Chen and Jan in (1992) [5] studied the flow of Newtonian fluid in a helical pipe with circular cross-section in a non-orthogonal coordinates system. They obtained the solution by double series expansion method. But considering the series forms of dimensionless axial velocity and stream function used in their article return the method to have the same draw back as perturbation technique. Bolinder in (1996) [4] studied the first and higher order of effects of torsion on the flow in a helical duct with rectangular cross-section numerically and also introduced a method to obtain the Navier-Stocke equations in a helical coordinates system employing physical velocity components. In 2000. Hadi [1] studied the analysis of the flow of non-Newtonian fluid of a second order in helical pipes with ellipse cross-section and circular cross-section. In circular cross-section he showed that the secondary motion depended on two dimensionless parameters namely Dean and non-Newtonian parameter (β) also he studied the effects of torsion ($\lambda/\Re e$) β and Dean number on the secondary flow and axial velocity. Also, Zhang, Zhang, and Chen in 2000 [11] studied the viscous flow in annular pipes by a perturbation method . They found the secondary flow and the axial velocity are controlled by torsion, Dean number, and the radius of the cross section. Xue in 2002 [13] analyzed the laminar flow in helical circular pipes by using Galerkin method. His results indicate that Galerkin technique can effectively overcome the limitation of a small parameters for perturbation method finally this paper studies the flow of third order fluid in a helical pipe with circular cross-section founds the governing equations are controlled by dimensionless numbers namely Dean number(L), Reynoleds number($\Re e$), non-Newtonian parameter(β)and the material moduli (γ_1, γ_3) and studies the effects of (L,$\Re e, \beta, \gamma_1, \gamma_3$)on the secondary flow and the axial velocity.

2.Coordinates System

Let the position vector described by (Fig. 1)

$$R(s) = X(s)\,\mathbf{i} + Y(s)\,\mathbf{j} + Z(s)\,\mathbf{k} \qquad (1)$$

Where s is arc length along the pipe and i, j, k are units vector in the Cartesian direction. The **TNB**frame and Frenet formulas defined by:

$\mathbf{T}=\frac{d\boldsymbol{R}}{d\boldsymbol{s}}$, $\boldsymbol{N}=\frac{1}{\boldsymbol{k}}\frac{d\boldsymbol{T}}{d\boldsymbol{s}}$, $\boldsymbol{B}=\boldsymbol{T}\times\boldsymbol{N}$

$\frac{d\boldsymbol{N}}{d\boldsymbol{s}}=\tau\,\boldsymbol{B}-\kappa\,\boldsymbol{T}$, $\frac{d\boldsymbol{B}}{d\boldsymbol{s}}=-\tau\,\boldsymbol{N}$(2)

Here T, N, and B are the tangent normal and binormal vectors respectively, τ is the torsion and κ is the curvature[2]. To construct the orthogonal coordinate system(s, r ,θ) , let polar angle θ refers to a relation of the unit vector N* by the amount of $\emptyset + \emptyset_\circ$ and is given by:

$$\emptyset = -\int_{S_\circ}^{S} \tau(s)ds \qquad (3)$$

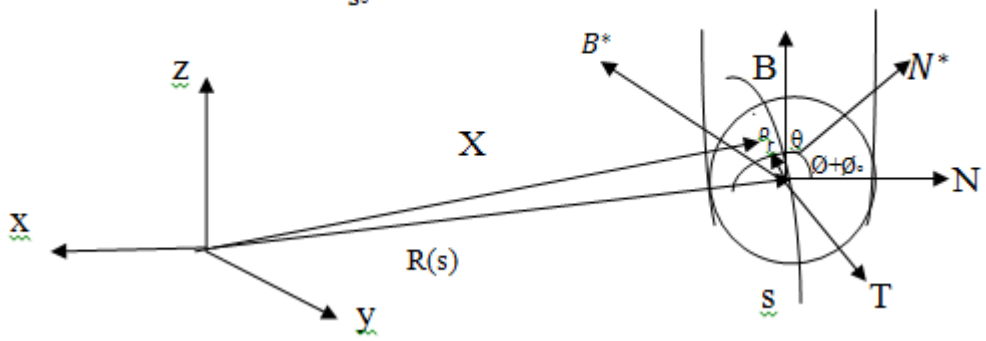

fig.(1) the coordinates system

3.Basic Equation

Consideration is given to a fluid characterized by a state equation of the form:

$$\mathbf{T}=\boldsymbol{\mu A_1}+\boldsymbol{\alpha_1 A_2}+\boldsymbol{\alpha_2 A_1^{\,2}}+\boldsymbol{\beta_1 A_3}+\boldsymbol{\beta_2}(\boldsymbol{A_1 A_2}+\boldsymbol{A_2 A_1})+\boldsymbol{\beta_3}(\boldsymbol{tr A_1^{\,2}})\boldsymbol{A_1}$$

(4)

$$A_1 = (\text{grad V}) + (\text{grad V})^T \qquad (5a)$$

$$A_n = \frac{dA_{n-1}}{dt} + A_{n-1}(\text{grad V}) + (\text{grad V})^T A_{n-1}, \qquad n > 1, \qquad (5b)$$

Where **V**the is the velocity vector grad the gradient operater μ is the viscosity,α_i(i = 1,2) , βi (i = 1,2,3)are material moduli, d/dt is the material derivative and A_i (i= 1,2,3) are the first Rivlin-Eriksen tensors.[8], thermodynamic of third grade fluid requires that

$\mu \geq 0$, $\alpha_1 \geq 0$, $|\alpha_1+\alpha_2| \leq \sqrt{24\mu\beta_3}$, (6) $\beta_1=\beta_2=0$, $\beta_3 \geq 0$

4.Governing Equations

We write down the motion and continuity equations in curvilinear coordinate for unsteady viscous fluid flow in helical pipe without imposing any of our restrictions,[3],[14].

The motion equations are in curvilinear coordinates are:-

$$\frac{\partial u}{\partial t}+\omega\, u\,\frac{\partial u}{\partial s}+v\,\frac{\partial u}{\partial r}+\frac{w}{r}\frac{\partial u}{\partial \theta}+\omega\, k\, u(v\sin(\theta+\emptyset)+w\cos(\theta+\emptyset))=-\omega\,\frac{\partial p}{\partial s}+\frac{1}{\rho}[\omega\,\frac{\partial T_{ss}}{\partial s}+\left(\frac{\partial}{\partial r}+\frac{1}{r}+2\omega\, k\sin(\theta+\emptyset)\right)T_{sr}+\left(\frac{1}{r}\frac{\partial}{\partial \theta}+2\omega\, k\cos(\theta+\emptyset)\right)T_{s\theta}\,(7)$$

$$\frac{\partial v}{\partial t}+\omega\, u\,\frac{\partial v}{\partial s}+v\,\frac{\partial v}{\partial r}+\omega\,\frac{\partial v}{\partial \theta}-\frac{w^2}{r^2}-\omega\, k\, u^2\sin(\theta+\emptyset)=-\frac{\partial p}{\partial r}+\frac{1}{\rho}\,[\left(\frac{\partial}{\partial r}+\frac{1}{r}+\omega\, k\sin(\theta+\emptyset)\right)T_{rr}+\left(\frac{1}{r}\frac{\partial}{\partial \theta}+2\omega\, k\cos(\theta+\emptyset)\right)T_{r\theta}+\omega\,\frac{\partial}{\partial s}T_{sr}-\frac{1}{r}T_{\theta\theta}-\omega\, k\sin(\theta+\emptyset)\,T_{ss}(8)$$

$$\frac{\partial w}{\partial t}+\omega u\frac{\partial w}{\partial s}+v\frac{\partial w}{\partial r}+\frac{w}{r}\frac{\partial w}{\partial \theta}-\frac{vw}{r}-\omega k u^2\cos(\theta+\emptyset)=-\frac{1}{r}\frac{\partial p}{\partial \theta}+\frac{1}{\rho}\left[\left(\frac{1}{r}\frac{\partial}{\partial \theta}+\omega k\cos(\theta+\emptyset)\right)T_{\theta\theta}+\omega\frac{\partial T_{\theta s}}{\partial s}+\left(\frac{\partial}{\partial \theta}+\frac{2}{r}+\omega k\cos(\theta+\emptyset)\right)T_{r\theta}-\omega k\cos(\theta+\emptyset)\,T_{ss}\right](9)$$

And $\omega\frac{\partial u}{\partial s}+\frac{\partial v}{\partial r}+\frac{v}{r}+\frac{1}{r}\frac{\partial w}{\partial \theta}+\omega k(v\sin(\theta+\emptyset)+w\cos(\theta+\emptyset))=0(10)$

where p is the kinematic pressure, u, v and w represent the velocity components in s, r, θ respectively, k is the curvature of the pipe, ρis the density and ωisdefinedas:

$$\omega=\frac{1}{1+krsin(\theta+\emptyset)}$$

Introduce the following new dimensionless variables to obtain the dimensionless equations.

$$\text{u}=U_{\circ}u_1,\quad v=\frac{\nu}{a}v_1,\quad w=\frac{\nu}{a}w_1,\quad s=as_1,\quad r=ar_1\,,$$

$$\lambda={}^{\tau}/_{k}\,,\qquad \varepsilon=ka\,,\qquad p=U_{\circ}{}^2p_1\,,\qquad \Re e=\frac{U_{\circ}a}{\nu}$$

Where a is the radius of the pipe,$U_{\circ}$isthemaximumvelocity in a straight pipe under the pressure gradient, ν is the viscosity and $p_1$is the pressure defined by:

$$p_1=p_{\circ}(s_1)+\varepsilon p_{11}(s_1,r_1)=-\frac{G}{\Re e}s_1+\varepsilon\, p_{11}(s_1,r_1)$$

Where G is the constant given by $[(\Re ea/\rho U_{\circ}{}^2)p^{**}],p^{**}$is the pressure gradient. For mathematical convenience, consideration is given to a helical pipe with constant curvature k and torsion τ .In this case it is possible to search helically symmetric solutions of the general equations, which is physically corresponding to a fully developed flow in a helical pipe and can be operated and setting all the resulting derivatives with respect to s equal zero except the pressure derivative the resulting of continuity and motion equations under these assumptions are:-

$$\frac{\partial(r_1 v_1)}{\partial r_1} + \frac{\partial}{\partial \theta_1}(w_1 - \varepsilon\lambda \Re e r_1 u_1) = 0 \qquad (11)$$

And the motion equations are:

$$\frac{\partial u}{\partial t} + v_1\frac{\partial u_1}{\partial r_1} + \frac{w_1}{r_1}\frac{\partial u_1}{\partial \theta_1} - \varepsilon\lambda\Re e u_1\frac{\partial u_1}{\partial \theta_1} = -G + [\left(\frac{\partial}{\partial r_1} + \frac{1}{r_1}\right)\left(\frac{\partial u_1}{\partial r_1}\right) + \left(\frac{1}{r_1}\frac{\partial}{\partial \theta_1}\right)\left(\frac{1}{r_1}\frac{\partial u_1}{\partial \theta_1}\right)] +$$
$$\beta[\left(\frac{\partial}{\partial r_1} + \frac{1}{r_1}\right)\left(2\frac{\partial u_1}{\partial r_1}\frac{\partial v_1}{\partial r_1} + \frac{1}{r_1}\frac{\partial u_1}{\partial \theta_1}\frac{\partial w_1}{\partial r_1} - \frac{w_1}{{r_1}^2}\frac{\partial u_1}{\theta_1} + \frac{1}{{r_1}^2}\frac{u_1}{\partial \theta_1}\frac{\partial v_1}{\partial \theta_1}\right)\left(\frac{1}{r_1}\frac{\partial}{\partial \theta_1}\right)\left(\frac{\partial u_1}{\partial r_1}\frac{\partial w_1}{\partial r_1} - \frac{w_1}{r_1}\frac{\partial u_1}{\partial r_1} +$$
$$\frac{1}{r_1}\frac{\partial u_1}{\partial r_1}\frac{\partial v_1}{\partial \theta_1} + \frac{2}{{r_1}^2}\frac{\partial u_1}{\partial \theta_1}\frac{\partial w_1}{\partial \theta_1} + 2\frac{v_1}{r_1}\frac{\partial u_1}{\partial \theta_1}\right)] + \gamma_1[\left(\frac{\partial}{\partial r_1} + \frac{1}{r_1}\right)\left(\frac{\partial^2 u_1}{\partial r_1 t_1} + \frac{\partial u_1}{\partial r_1}\frac{\partial v_1}{\partial r_1} + \frac{1}{r_1}\frac{\partial u_1}{\partial \theta_1}\frac{\partial w_1}{\partial r_1}\right) +$$
$$\left(\frac{1}{r_1}\frac{\partial}{\partial \theta_1}\right)\left(\frac{1}{r_1}\frac{\partial^2 u_1}{\partial \theta_1 t_1} + \frac{2}{{r_1}^2}\frac{\partial u_1}{\partial \theta_1}\frac{\partial w_1}{\partial \theta_1} + 2\frac{v_1}{r_1}\frac{\partial u_1}{\partial \theta_1}\right)] + \gamma_2[\left(\frac{\partial}{\partial r_1} + \frac{1}{r_1}\right)(4\frac{\partial u_1}{\partial r_1}\left(\frac{\partial v_1}{\partial r_1}\right)^2 + 2\frac{\partial u_1}{\partial r_1}\left(\frac{\partial w_1}{\partial r_1}\right)^2 +$$
$$\frac{2}{{r_1}^2}\frac{\partial u_1}{\partial \theta_1}\left(\frac{\partial v_1}{\partial \theta_1}\right)^2 + 2\frac{{w_1}^2}{{r_1}^2}\frac{\partial u_1}{\partial r_1} - \frac{4}{r_1}\frac{\partial u_1}{\partial r_1}\frac{\partial w_1}{\partial r_1}\frac{\partial v_1}{\partial \theta_1} - 4\frac{w_1}{r_1}\frac{\partial u_1}{\partial r_1} - 4\frac{w_1}{{r_1}^2}\frac{\partial u_1}{\partial r_1}\frac{\partial v_1}{\partial \theta_1} + \frac{4}{{r_1}^2}\frac{\partial u_1}{\partial r_1}\left(\frac{\partial w_1}{\partial \theta_1}\right)^2 +$$
$$8\frac{v_1}{{r_1}^2}\frac{\partial u_1}{\partial r_1}\frac{\partial w_1}{\partial \theta_1} + 4\frac{{v_1}^2}{{r_1}^2}\frac{\partial u_1}{\partial r_1} + \left(\frac{1}{r_1}\frac{\partial}{\partial \theta_1}\right)(4\frac{\partial u_1}{\partial \theta_1}\left(\frac{\partial v_1}{\partial r_1}\right)^2 + \frac{2}{{r_1}^2}\frac{\partial u_1}{\partial \theta_1}\left(\frac{\partial w_1}{\partial r_1}\right)^2 + \frac{2}{{r_1}^2}\frac{\partial u_1}{\partial \theta_1}\left(\frac{\partial v_1}{\partial \theta_1}\right)^2 + 2\frac{{w_1}^2}{{r_1}^3}\frac{\partial u_1}{\partial \theta_1} -$$
$$\frac{4}{{r_1}^2}\frac{\partial u_1}{\partial \theta_1}\frac{\partial v_1}{\partial \theta_1}\frac{\partial w_1}{\partial r_1} - 4\frac{w_1}{{r_1}^2}\frac{\partial u_1}{\partial \theta_1}\frac{\partial w_1}{\partial r_1} - \frac{4}{{r_1}^3}\frac{\partial u_1}{\partial \theta_1}\frac{\partial v_1}{\partial \theta_1} + \frac{4}{{r_1}^3}\frac{\partial u_1}{\partial \theta_1}\left(\frac{\partial w_1}{\partial \theta_1}\right)^2 + 8\frac{v_1}{{r_1}^3}\frac{\partial u_1}{\partial \theta_1}\frac{\partial w_1}{\partial \theta_1} + 4\frac{{v_1}^2}{{r_1}^3}\frac{\partial u_1}{\partial \theta_1}] +$$
$$\gamma_3[\left(\frac{\partial}{\partial r_1} + \frac{1}{r_1}\right)(2\left(\frac{\partial u_1}{\partial r_1}\right)^3 + \frac{2}{{r_1}^2}\frac{\partial u_1}{\partial r_1}\left(\frac{\partial u_1}{\partial \theta_1}\right)^2) + \left(\frac{1}{r_1}\frac{\partial}{\partial \theta_1}\right)(\frac{2}{r_1}\frac{\partial u_1}{\partial \theta_1}\left(\frac{\partial u_1}{\partial r_1}\right)^2 + \frac{2}{r^3}\left(\frac{\partial u_1}{\partial \theta_1}\right)^3)] \qquad (12a)$$

$$\frac{\partial v_1}{\partial t_1} + v_1\frac{\partial v_1}{\partial r_1} + \frac{w_1}{r_1}\frac{\partial v_1}{\partial \theta_1} - \frac{{w_1}^2}{r_1} - \varepsilon\Re e^2 {u_1}^2 sin\theta_1 - \varepsilon\Re e u_1\frac{\partial v_1}{\partial \theta_1} = -\varepsilon\Re e^2\frac{\partial P_{11}}{\partial r_1} + [\left(\frac{\partial}{\partial r_1} + \frac{1}{r_1}\right)\left(2\frac{\partial v_1}{\partial r_1}\right)$$
$$+ \left(\frac{1}{r_1}\frac{\partial}{\partial \theta_1}\right)\left(\frac{\partial w_1}{\partial r_1} - \frac{w_1}{r_1} + \frac{1}{r_1}\frac{\partial v_1}{\partial \theta_1}\right) - \frac{1}{r_1}\left(\frac{2}{r_1}\frac{\partial w_1}{\partial \theta_1} + 2\frac{v_1}{r_1}\right)] + \beta[(\frac{\partial}{\partial r_1} + \frac{1}{r_1})(4(\frac{\partial v_1}{\partial r_1})^2 + (\frac{\partial w_1}{\partial r_1})^2 + \frac{w_1}{{r_1}^2} +$$
$$(\frac{\partial v_1}{\partial \theta_1})^2 - 2\frac{w_1}{r_1}\frac{\partial w_1}{\partial r_1} + \frac{2}{r_1}\frac{\partial w_1}{\partial r_1}\frac{\partial v_1}{\partial \theta_1} - 2\frac{w_1}{{r_1}^2}\frac{\partial v_1}{\partial \theta_1}) + \frac{1}{r_1}\frac{\partial}{\theta_1}(2\frac{\partial v_1}{\partial r_1}\frac{\partial w_1}{\partial r_1} - 2\frac{w_1}{r_1}\frac{\partial v_1}{\partial r_1} + \frac{2}{r_1}\frac{\partial v_1}{\partial r_1}\frac{\partial v_1}{\partial \theta_1} + \frac{2}{r_1}\frac{\partial w_1}{\partial r_1}\frac{\partial w_1}{\partial \theta_1} +$$
$$2\frac{v_1}{r_1}\frac{\partial w_1}{\partial r_1} - 2\frac{w_1}{{r_1}^2}\frac{\partial w_1}{\partial \theta_1} - 2\frac{v_1 w_1}{{r_1}^2} + \frac{2}{{r_1}^2}\frac{\partial v_1}{\partial \theta_1}\frac{\partial w_1}{\partial \theta_1} + 2\frac{v_1}{{r_1}^2}\frac{\partial v_1}{\partial \theta_1}) - \frac{1}{r_1}((\frac{\partial w_1}{\partial r_1})^2 + \frac{{w_1}^2}{{r_1}^2} + \frac{1}{{r_1}^2}(\frac{\partial v_1}{\partial \theta_1})^2 -$$
$$2\frac{w_1}{r_1}\frac{\partial w_1}{\partial r_1} + \frac{2}{r_1}\frac{\partial w_1}{\partial r_1}\frac{\partial v_1}{\partial \theta_1} - \frac{w_1}{{r_1}^2}\frac{\partial v_1}{\partial \theta_1} + \frac{4}{{r_1}^2}(\frac{\partial w_1}{\partial \theta_1})^2 + 4\frac{{v_1}^2}{{r_1}^2} + 8\frac{v_1}{{r_1}^2}\frac{\partial w_1}{\partial \theta_1})] + \gamma_1[(\frac{\partial}{\partial r_1} + \frac{1}{r_1})(2\frac{\partial^2 v_1}{\partial r_1 \partial t_1} +$$
$$4(\frac{\partial v_1}{\partial r_1})^2 + 2(\frac{\partial w_1}{\partial r_1})^2 + \frac{2}{r_1}\frac{\partial w_1}{\partial r_1}\frac{\partial v_1}{\partial \theta_1} - 2\frac{w_1}{r_1}\frac{\partial w_1}{\partial r_1}) + (\frac{1}{r_1}\frac{\partial}{\partial \theta_1})(\frac{\partial^2 w_1}{\partial r_1 \partial t_1} + \frac{1}{r_1}\frac{\partial^2 v_1}{\partial \theta_1 \partial t_1} - \frac{1}{r_1}\frac{\partial w_1}{\partial t_1} + \frac{3}{r_1}\frac{\partial v_1}{\partial r_1}\frac{\partial v_1}{\partial \theta_1} -$$
$$3\frac{w_1}{r_1}\frac{\partial v_1}{\partial r_1} + \frac{\partial v_1}{\partial r_1}\frac{\partial w_1}{\partial r_1} + \frac{3}{r_1}\frac{\partial w_1}{\partial r_1}\frac{\partial w_1}{\partial \theta_1} + 3\frac{v_1}{r_1}\frac{\partial w_1}{\partial r_1} + \frac{2}{{r_1}^2}\frac{\partial v_1}{\partial \theta_1}\frac{\partial w_1}{\partial \theta_1} + 2\frac{v_1}{{r_1}^2}\frac{\partial v_1}{\partial \theta_1} + 2\frac{w_1}{{r_1}^2}\frac{\partial w_1}{\partial \theta_1} - 2\frac{v_1 w_1}{{r_1}^2}) -$$

$$2\frac{w_1}{r_1}\frac{\partial w_1}{\partial r_1}+\frac{2}{r_1}\frac{\partial w_1}{\partial r_1}\frac{\partial v_1}{\partial \theta_1}-2\frac{w_1}{r_1^2}\frac{\partial v_1}{\partial \theta_1}+\frac{4}{r_1^2}(\frac{\partial w_1}{\partial \theta_1})^2+4\frac{v_1^2}{r_1^2}+8\frac{v_1}{r_1^2}\frac{\partial w_1}{\partial \theta_1})]+\gamma_1[(\frac{\partial}{\partial r_1}+\frac{1}{r_1})(2\frac{\partial^2 v_1}{\partial r_1 \partial t_1}+$$
$$4(\frac{\partial v_1}{\partial r_1})^2+2(\frac{\partial w_1}{\partial r_1})^2+\frac{2}{r_1}\frac{\partial w_1}{\partial r_1}\frac{\partial v_1}{\partial \theta_1}-2\frac{w_1}{r_1}\frac{\partial w_1}{\partial r_1})+(\frac{1}{r_1}\frac{\partial}{\partial \theta_1})(\frac{\partial^2 w_1}{\partial r_1 \partial t_1}+\frac{1}{r_1}\frac{\partial^2 v_1}{\partial \theta_1 \partial t_1}-\frac{1}{r_1}\frac{\partial w_1}{\partial t_1}+\frac{3}{r_1}\frac{\partial v_1}{\partial r_1}\frac{\partial v_1}{\partial \theta_1}-$$
$$3\frac{w_1}{r_1}\frac{\partial v_1}{\partial r_1}+\frac{\partial v_1}{\partial r_1}\frac{\partial w_1}{\partial r_1}+\frac{3}{r_1}\frac{\partial w_1}{\partial r_1}\frac{\partial w_1}{\partial \theta_1}+3\frac{v_1}{r_1}\frac{\partial w_1}{\partial r_1}+\frac{2}{r_1^2}\frac{\partial v_1}{\partial \theta_1}\frac{\partial w_1}{\partial \theta_1}+2\frac{v_1}{r_1^2}\frac{\partial v_1}{\partial \theta_1}+2\frac{w_1}{r_1^2}\frac{\partial w_1}{\partial \theta_1}-2\frac{v_1 w_1}{r_1^2})-$$
$$\frac{1}{r_1}(\frac{2}{r_1}\frac{\partial^2 w_1}{\partial \theta_1 \partial t_1}+\frac{2}{r_1}\frac{\partial v_1}{\partial t_1}+\frac{2}{r_1^2}(\frac{\partial v_1}{\partial \theta_1})^2+\frac{2}{r_1}\frac{\partial v_1}{\partial \theta_1}\frac{\partial w_1}{\partial r_1}-4\frac{w_1}{r_1^2}\frac{\partial v_1}{\partial \theta_1}+2\frac{w_1^2}{r_1^2}-2\frac{w_1}{r_1}\frac{\partial w_1}{\partial r_1}+\frac{4}{r_1^2}(\frac{\partial w_1}{\partial \theta_1})^2+$$
$$8\frac{v_1}{r_1^2}\frac{\partial w_1}{\partial \theta_1}+4\frac{v_1^2}{r_1^2})]+\gamma_2[(\frac{\partial}{\partial r_1}+\frac{1}{r_1})(4\frac{\partial v_1}{\partial r_1}(\frac{\partial w_1}{\partial \theta_1})^2+\frac{4}{r_1^2}\frac{\partial v_1}{\partial r_1}(\frac{\partial v_1}{\partial \theta_1})^2+4\frac{w_1^2}{r_1^2}\frac{\partial v_1}{\partial r_1}+\frac{8}{r_1}\frac{\partial v_1}{\partial r_1}\frac{\partial w_1}{\partial r_1}\frac{\partial \gamma_2 v_1}{\partial \theta_1}-$$
$$8\frac{w_1}{r_1}\frac{\partial v_1}{\partial r_1}\frac{\partial w_1}{\partial r_1}-8\frac{w_1}{r_1^2}\frac{\partial v_1}{\partial r_1}\frac{\partial v_1}{\partial \theta_1}+\frac{8}{r_1^2}\frac{\partial v_1}{\partial r_1}(\frac{\partial w_1}{\partial \theta_1})^2+16\frac{v_1}{r_1^2}\frac{\partial v_1}{\partial r_1}\frac{\partial w_1}{\partial \theta_1}+8(\frac{\partial v_1}{\partial r_1})^3+8\frac{v_1^2}{r_1^2}\frac{\partial v_1}{\partial r_1})$$
$$+(\frac{1}{r_1}\frac{\partial}{\partial \theta_1})(\frac{4}{r_1}\frac{\partial v_1}{\partial \theta_1}(\frac{\partial v_1}{\partial r_1})^2+4\frac{\partial w_1}{\partial r_1}(\frac{\partial v_1}{\partial r_1})^2-\frac{w_1}{r_1}(\frac{\partial v_1}{\partial r_1})^2+\frac{2}{r_1^3}(\frac{\partial v_1}{\partial \theta_1})^3+\frac{6}{r_1^2}(\frac{\partial v_1}{\partial \theta_1})^2\frac{\partial w_1}{\partial r_1}-6\frac{w_1}{r_1^2}(\frac{\partial v_1}{\partial \theta_1})^2+$$
$$\frac{6}{r_1}\frac{\partial v_1}{\partial \theta_1}(\frac{\partial w_1}{\partial r_1})^2-12\frac{w_1}{r_1^2}\frac{\partial v_1}{\partial \theta_1}\frac{\partial w_1}{\partial r_1}-6\frac{w_1}{r_1^2}(\frac{\partial v_1}{\partial \theta_1})^2+4\frac{w_1^2}{r_1^2}\frac{\partial w_1}{\partial r_1}-4\frac{w_1^2}{r_1^2}\frac{\partial v_1}{\partial \theta_1}+2(\frac{\partial w_1}{\partial r_1})^3+\frac{4}{r_1^3}\frac{\partial v_1}{\partial \theta_1}(\frac{\partial w_1}{\partial \theta_1})^2-$$
$$2\frac{w_1^3}{r_1^3}+\frac{4}{r_1^2}\frac{\partial w_1}{\partial r_1}(\frac{\partial w_1}{\partial \theta_1})^2-4\frac{w_1}{r_1^3}(\frac{\partial w_1}{\partial \theta_1})^2+8\frac{v_1}{r_1^3}\frac{\partial v_1}{\partial \theta_1}\frac{\partial w_1}{\partial \theta_1}+8\frac{v_1}{r_1^2}\frac{\partial w_1}{\partial r_1}\frac{\partial w_1}{\partial \theta_1}-8\frac{v_1 w_1}{r_1^3}\frac{\partial w_1}{\partial \theta_1}+4\frac{v_1^2}{r_1^2}\frac{\partial v_1}{\partial \theta_1}+$$
$$4\frac{v_1^2}{r_1^2}\frac{\partial w_1}{\partial r_1}-4\frac{v_1^2 w_1}{r_1^3})-\frac{1}{r_1}(\frac{8}{r_1}(\frac{\partial v_1}{\partial r_1})^2\frac{\partial w_1}{\partial \theta_1}+8\frac{v_1}{r_1}(\frac{\partial v_1}{\partial r_1})^2+\frac{4}{r_1}(\frac{\partial w_1}{\partial r_1})^2\frac{\partial w_1}{\partial \theta_1}+4\frac{v_1}{r_1}(\frac{\partial w_1}{\partial r_1})^2+$$
$$\frac{4}{r_1^3}(\frac{\partial v_1}{\partial \theta_1})^2\frac{\partial w_1}{\partial \theta_1}+4\frac{v_1}{r_1^2}(\frac{\partial v_1}{\partial \theta_1})^2+2\frac{w_1^2}{r_1^3}\frac{\partial w_1}{\partial \theta_1}+2\frac{v_1 w_1^2}{r_1^3}-8\frac{w_1}{r_1^2}\frac{\partial w_1}{\partial r_1}\frac{\partial w_1}{\partial \theta_1}-8\frac{v_1 w_1}{r_1^2}\frac{\partial w_1}{\partial r_1}+$$
$$\frac{8}{r_1^2}\frac{\partial w_1}{\partial r_1}\frac{\partial v_1}{\partial \theta_1}\frac{\partial w_1}{\partial \theta_1}+8\frac{v_1}{r_1^2}\frac{\partial w_1}{\partial r_1}\frac{\partial v_1}{\partial \theta_1}-8\frac{w_1}{r_1^3}\frac{\partial v_1}{\partial \theta_1}\frac{\partial w_1}{\partial \theta_1}-8\frac{v_1 w_1}{r_1^3}\frac{\partial v_1}{\partial \theta_1}+\frac{8}{r_1^3}(\frac{\partial w_1}{\partial \theta_1})^3+24\frac{v_1^2}{r_1^3}\frac{\partial w_1}{\partial \theta_1}+$$
$$16\frac{v_1}{r_1^3}(\frac{\partial w_1}{\partial \theta_1})^2+8\frac{v_1^3}{r_1^3})]+\gamma_3[(\frac{\partial}{\partial r_1}+\frac{1}{r_1})(4\frac{\partial v_1}{\partial r_1}(\frac{\partial u_1}{\partial r_1})^2+\frac{4}{r_1^2}\frac{\partial v_1}{\partial r_1}(\frac{\partial u_1}{\partial \theta_1})^2)+(\frac{1}{r_1}\frac{\partial}{\partial \theta_1})(\frac{2}{r_1}\frac{\partial v_1}{\partial \theta_1}(\frac{\partial u_1}{\partial r_1})^2+$$
$$2\frac{\partial w_1}{\partial r_1}(\frac{\partial u_1}{\partial r_1})^2+\frac{2}{r_1^3}\frac{\partial v_1}{\partial \theta_1}(\frac{\partial u_1}{\partial \theta_1})^2+\frac{2}{r_1^2}\frac{\partial w_1}{\partial r_1}(\frac{\partial u_1}{\partial \theta_1})^2-2\frac{w_1}{r_1}(\frac{\partial u_1}{\partial r_1})^2-2\frac{w_1}{r_1}(\frac{\partial u_1}{\partial \theta_1})^2)-\frac{1}{r_1}(\frac{4}{r_1}\frac{\partial w_1}{\partial \theta_1}(\frac{\partial u_1}{\partial r_1})^2+$$
$$4\frac{v_1}{r_1}(\frac{\partial u_1}{\partial r_1})^2+\frac{4}{r_1^3}\frac{\partial w_1}{\partial \theta_1}(\frac{\partial u_1}{\partial \theta_1})^2+4\frac{v_1}{r_1^3}(\frac{\partial u_1}{\partial \theta_1})^2]+\gamma_4[(\frac{\partial}{\partial r_1}+\frac{1}{r_1})(2(\frac{\partial u_1}{\partial r_1})^2+\frac{2}{r_1}\frac{\partial u_1}{\partial r_1}\frac{\partial u_1}{\partial \theta_1})+$$
$$(\frac{1}{r_1}\frac{\partial}{\partial \theta_1})(\frac{1}{r_1^2}(\frac{\partial u_1}{\partial \theta_1})^2+\frac{1}{r_1}\frac{\partial u_1}{\partial r_1}\frac{\partial u_1}{\partial \theta_1})-\frac{1}{r_1^3}(\frac{\partial u_1}{\partial \theta_1})^2] \qquad (12b)$$

$$\frac{\partial w_1}{\partial t_1}+v_1\frac{\partial w_1}{\partial r_1}+\frac{w_1}{r_1}\frac{\partial w_1}{\partial \theta_1}+\frac{v_1 w_1}{r_1}-\varepsilon \Re e^2 u_1{}^2 Cos\theta_1-\varepsilon\lambda \Re e u_1\frac{\partial w_1}{\partial \theta_1}=$$
$$-\frac{1}{r_1}\varepsilon \Re e^2\frac{\partial P_{11}}{\partial \theta_1}+\left[\left(\frac{1}{r_1}\frac{\partial}{\partial \theta_1}\right)\left(\frac{2}{r_1}\frac{\partial w_1}{\partial \theta_1}+2\frac{v_1}{r_1}\right)+\left(\frac{\partial}{\partial r_1}+\frac{2}{r_1}\right)\left(\frac{\partial w_1}{\partial r_1}-\frac{w_1}{r_1}+\frac{1}{r_1}\frac{\partial v_1}{\partial \theta_1}\right)\right]+$$
$$\beta[(\frac{1}{r_1}\frac{\partial}{\partial \theta_1})((\frac{\partial w_1}{\partial r_1})^2+\frac{w_1^2}{r_1^2}+\frac{1}{r_1^2}(\frac{\partial v_1}{\partial \theta_1})^2-2\frac{w_1}{r_1}\frac{\partial w_1}{\partial r_1}+\frac{2}{r_1}\frac{\partial w_1}{\partial r_1}\frac{\partial v_1}{\partial \theta_1}-2\frac{w_1}{r_1^2}\frac{\partial v_1}{\partial \theta_1}+\frac{4}{r_1^2}(\frac{\partial w_1}{\partial \theta_1})^2+4\frac{v_1^2}{r_1^2}+$$
$$8\frac{v_1}{r_1^2}\frac{\partial w_1}{\partial \theta_1})+\left(\frac{\partial}{\partial r_1}+\frac{2}{r_1}\right)\left(2\frac{\partial v_1}{\partial r_1}\frac{\partial w_1}{\partial r_1}-2\frac{w_1}{r_1}\frac{\partial v_1}{\partial r_1}+\frac{2}{r_1}\frac{\partial v_1}{\partial r_1}\frac{\partial v_1}{\partial \theta_1}+\frac{2}{r_1}\frac{\partial w_1}{\partial r_1}\frac{\partial w_1}{\partial \theta_1}+2\frac{v_1}{r_1}\frac{\partial w_1}{\partial r_1}-2\frac{w_1}{r_1^2}\frac{\partial w_1}{\partial \theta_1}-\right.$$
$$\left.2\frac{v_1 w_1}{r_1^2}+\frac{2}{r_1^2}\frac{\partial v_1}{\partial \theta_1}\frac{\partial w_1}{\partial \theta_1}+2\frac{v_1}{r_1^2}\frac{\partial v_1}{\partial \theta_1}\right)]+\gamma_1[(\frac{1}{r_1}\frac{\partial}{\partial \theta_1})(\frac{2}{r_1}\frac{\partial^2 w_1}{\partial \theta_1 \partial t_1}+\frac{2}{r_1}\frac{\partial v_1}{\partial t_1}+\frac{2}{r_1^2}(\frac{\partial v_1}{\partial \theta_1})^2+2\frac{w_1^2}{r_1^2}+$$
$$\frac{2}{r_1}\frac{\partial w_1}{\partial r_1}\frac{\partial v_1}{\partial \theta_1}-4\frac{w_1}{r_1^2}\frac{\partial v_1}{\partial \theta_1}-2\frac{w_1}{r_1}\frac{\partial w_1}{\partial r_1}+\frac{4}{r_1^2}(\frac{\partial w_1}{\partial \theta_1})^2+4\frac{v_1^2}{r_1^2}+8\frac{v_1}{r_1^2}\frac{\partial w_1}{\partial \theta_1})+\left(\frac{\partial}{\partial r_1}+\frac{2}{r_1}\right)\left(\frac{\partial^2 w_1}{\partial r_1 \partial t_1}+\right.$$
$$\left.\frac{1}{r_1}\frac{\partial^2 v_1}{\partial \theta_1 \partial t_1}-\frac{1}{r_1}\frac{\partial w_1}{\partial t_1}+\frac{3}{r_1}\frac{\partial v_1}{\partial r_1}\frac{\partial v_1}{\partial \theta_1}-3\frac{w_1}{r_1}\frac{\partial v_1}{\partial r_1}+\frac{\partial v_1}{\partial r_1}\frac{\partial w_1}{\partial r_1}+\frac{2}{r_1^2}\frac{\partial v_1}{\partial \theta_1}\frac{\partial w_1}{\partial \theta_1}+2\frac{v_1}{r_1^2}\frac{\partial v_1}{\partial \theta_1}-2\frac{w_1}{r_1^2}\frac{\partial w_1}{\partial \theta_1}-2\frac{v_1 w_1}{r_1^2}+\right.$$
$$\left.\frac{3}{r_1}\frac{\partial w_1}{\partial r_1}\frac{\partial w_1}{\partial \theta_1}+3\frac{v_1}{r_1}\frac{\partial w_1}{\partial r_1}\right)]+\gamma_2[(\frac{1}{r_1}\frac{\partial}{\partial \theta_1})(\frac{8}{r_1}\frac{\partial w_1}{\partial \theta_1}(\frac{\partial v_1}{\partial r_1})^2+8\frac{v_1}{r_1}(\frac{\partial w_1}{\partial r_1})^2+\frac{4}{r_1}\frac{\partial w_1}{\partial \theta_1}(\frac{\partial w_1}{\partial r_1})^2+4\frac{v_1}{r_1}(\frac{\partial w_1}{\partial r_1})^2+$$

$$\frac{4}{r_1^3}\frac{\partial w_1}{\partial\theta_1}\left(\frac{\partial v_1}{\partial\theta_1}\right)^2+4\frac{v_1}{r_1^3}\left(\frac{\partial v_1}{\partial\theta_1}\right)^2+4\frac{w_1^2}{r_1^3}\frac{\partial w_1}{\partial\theta_1}+4\frac{v_1w_1^2}{r_1^3}+\frac{8}{r_1^2}\frac{\partial w_1}{\partial r_1}\frac{\partial v_1}{\partial\theta_1}\frac{\partial w_1}{\partial\theta_1}+8\frac{v_1}{r_1^2}\frac{\partial w_1}{\partial r_1}\frac{\partial v_1}{\partial\theta_1}-$$
$$8\frac{w_1}{r_1^2}\frac{\partial v_1}{\partial\theta_1}\frac{\partial w_1}{\partial\theta_1}-8\frac{v_1w_1}{r_1^2}\frac{\partial v_1}{\partial\theta_1}-8\frac{w_1}{r_1^2}\frac{\partial w_1}{\partial r_1}\frac{\partial w_1}{\partial\theta_1}-8\frac{v_1w_1}{r_1^2}\frac{\partial w_1}{\partial r_1}+\frac{8}{r_1^3}\left(\frac{\partial w_1}{\partial\theta_1}\right)^2+24\frac{v_1}{r_1^3}\left(\frac{\partial w_1}{\partial\theta_1}\right)^2+24\frac{v_1^2}{r_1^3}\frac{\partial w_1}{\partial\theta_1}+$$
$$8\frac{v_1^3}{r_1^3}\Big)+\Big(\frac{\partial}{r_1}+\frac{2}{r_1}\Big)\Big(4\frac{\partial w_1}{\partial r_1}\left(\frac{\partial v_1}{\partial r_1}\right)^2+\frac{4}{r_1}\frac{\partial v_1}{\partial\theta_1}\left(\frac{\partial v_1}{\partial r_1}\right)^2-4\frac{w_1}{r_1}\left(\frac{\partial v_1}{\partial r_1}\right)^2+\frac{6}{r_1^2}\frac{\partial w_1}{\partial r_1}\left(\frac{\partial v_1}{\partial\theta_1}\right)^2-\frac{2}{r_1^3}\left(\frac{\partial v_1}{\partial\theta_1}\right)^2-$$
$$2\left(\frac{\partial w_1}{\partial r_1}\right)^3-2\frac{w_1^3}{r_1^3}-6\frac{w_1}{r_1^3}\left(\frac{\partial v_1}{\partial\theta_1}\right)^2+\frac{6}{r_1}\left(\frac{\partial w_1}{\partial r_1}\right)^2\frac{\partial v_1}{\partial\theta_1}-6\frac{w_1}{r_1}\left(\frac{\partial w_1}{\partial r_1}\right)^2-12\frac{w_1}{r_1^2}\frac{\partial w_1}{\partial\theta_1}\frac{\partial v_1}{\partial\theta_1}-4\frac{w_1^2}{r_1^3}\frac{\partial v_1}{\partial\theta_1}-$$
$$4\frac{w_1^2}{r_1^2}\frac{\partial w_1}{\partial r_1}+\frac{4}{r_1^2}\frac{\partial w_1}{\partial r_1}\left(\frac{\partial w_1}{\partial\theta_1}\right)^2+\frac{4}{r_1^3}\frac{\partial v_1}{\partial\theta_1}\left(\frac{\partial w_1}{\partial\theta_1}\right)^2-4\frac{w_1}{r_1^2}\left(\frac{\partial w_1}{\partial\theta_1}\right)^2+8\frac{v_1}{r_1^2}\frac{\partial w_1}{\partial r_1}\frac{\partial w_1}{\partial\theta_1}+8\frac{v_1}{r_1^3}\frac{\partial v_1}{\partial\theta_1}\frac{\partial w_1}{\partial\theta_1}-$$
$$8\frac{v_1w_1}{r_1^2}+4\frac{v_1^2}{r_1^2}\frac{\partial w_1}{\partial r_1}+4\frac{v_1^2}{r_1^2}\frac{\partial v_1}{\partial\theta_1}-4\frac{v_1^2w_1}{r_1^3}\Big)\Big]+\gamma_3\Big[\Big(\frac{1}{r_1}\frac{\partial}{\partial\theta_1}\Big)\Big(\frac{4}{r_1}\frac{\partial w_1}{\partial\theta_1}\left(\frac{\partial u_1}{\partial r_1}\right)^2+4\frac{v_1}{r_1}\left(\frac{\partial u_1}{\partial r_1}\right)^2+$$
$$\frac{4}{r_1^2}\frac{\partial w_1}{\partial\theta_1}\left(\frac{\partial u_1}{\partial\theta_1}\right)^2+4\frac{v_1}{r_1^2}\left(\frac{\partial u_1}{\partial\theta_1}\right)^2+\Big(\frac{\partial}{\partial r_1}+\frac{2}{r_1}\Big)\Big(2\frac{4}{r_1}\frac{\partial w_1}{\partial r_1}\left(\frac{\partial u_1}{\partial r_1}\right)^2+\frac{2}{r_1}\frac{\partial v_1}{\partial\theta_1}\left(\frac{\partial u_1}{\partial r_1}\right)^2-2\frac{w_1}{r_1}\left(\frac{\partial u_1}{\partial r_1}\right)^2+$$
$$\frac{2}{r_1^2}\frac{\partial w_1}{\partial r_1}\left(\frac{\partial u_1}{\partial\theta_1}\right)^2+\frac{2}{r_1^3}\frac{\partial v_1}{\partial\theta_1}\left(\frac{\partial u_1}{\partial\theta_1}\right)^2-2\frac{w_1}{r_1^3}\left(\frac{\partial u_1}{\partial\theta_1}\right)^2\Big)\Big]+\gamma_4\Big[\Big(\frac{1}{r_1}\frac{\partial}{\partial\theta_1}\Big)\Big(\frac{2}{r_1^2}\left(\frac{\partial u_1}{\partial\theta_1}\right)^2+\Big(\frac{\partial}{\partial r_1}+\frac{2}{r_1}\Big)\Big(\frac{\partial u_1}{\partial r_1}\frac{\partial u_1}{\partial\theta_1}\Big)\Big]$$
(12c)

The above equations are controlled by the following dimensionless numbers: $\beta=\alpha_2/\rho\,a^2$, $\gamma_1=\alpha_1/\rho a^2$, $\gamma_2=\beta_3\nu/\rho a^4$, $\gamma_3=\beta_3 u_\circ^2/\rho a^2\nu$,

and $\gamma_4=\alpha_1 u_\circ^2/\rho\,\nu^2$.

5.The Flow of fluid in Circular Cross-Section

In equations (12a),(12b)and (12c) we set

$$\mathrm{v}=\frac{-1}{r}\frac{\partial\Psi}{\partial\theta},\ \mathrm{w}=\frac{\partial\Psi}{\partial r}+\frac{\lambda}{2\Re e}Lru \quad (13a)$$

$$\frac{\partial u}{\partial t}=0,\frac{\partial u}{\partial t}=0 \text{and}\frac{\partial\Psi}{\partial t}=0 \quad (13b)$$

to gives the steady flow of third order fluid in a helical pipe with circular cross-section.

Where$\Psi$is the pseudo − stream functionand $\mathrm{L}=2\varepsilon\Re$eis Dean number.

$$\nabla^2u+G=\frac{1}{r}\left(-\frac{\partial u}{\partial r}\frac{\partial\Psi}{\partial\theta}\right)-\beta\left[\frac{2}{r^3}\frac{\partial^2u}{\partial r^2}\frac{\partial\Psi}{\partial\theta}-\frac{2}{r}\frac{\partial^2u}{\partial r^2}\frac{\partial^2\Psi}{\partial r\,\partial\theta}-\frac{2}{r^3}\frac{\partial u}{\partial r}\frac{\partial\Psi}{\partial\theta}+\frac{1}{r^2}\frac{\partial u}{\partial r}\frac{\partial^2\Psi}{\partial r\,\partial\theta}-\right.$$
$$\left.\frac{1}{r}\frac{\partial u}{\partial r}\frac{\partial^3\Psi}{\partial r^2\,\partial\theta}-\frac{1}{r^3}\frac{\partial u}{\partial r}\frac{\partial^3\Psi}{\partial\theta^3}\right]+\gamma_1\left[\frac{-1}{r^3}\frac{\partial u}{\partial r}\frac{\partial\Psi}{\partial\theta}+\frac{1}{r^2}\frac{\partial^2u}{\partial r^2}\frac{\partial\Psi}{\partial\theta}+\frac{1}{r^2}\frac{\partial^2u}{\partial r^2}\frac{\partial^2\Psi}{\partial r\,\partial\theta}-\right.$$
$$\left.\frac{1}{r}\frac{\partial^2u}{\partial r^2}\frac{\partial^2\Psi}{\partial r\,\partial\theta}-\frac{1}{r}\frac{\partial u}{\partial r}\frac{\partial^3\Psi}{\partial r^2\partial\theta}\right]+2\gamma_3\left[\frac{1}{r^2}\left(\frac{\partial u}{\partial r}\right)^2\left(r\frac{\partial u}{\partial r}+3r^2\frac{\partial^2u}{\partial r^2}\right)\right]$$
(14)

and

$$\nabla^4\Psi = \frac{1}{r}\left(\frac{\partial\Psi}{\partial r}\frac{\partial}{\partial\theta} - \frac{\partial\Psi}{\partial\theta}\frac{\partial}{\partial r}\right)\nabla^2\Psi + Lu\left(-Cos\theta\frac{\partial u}{\partial r}\right) + 2GL\frac{\lambda}{\Re e} + \gamma_1[\frac{30}{r^6}\frac{\partial\Psi}{\partial\theta}\frac{\partial^2\Psi}{\partial\theta^2} + \frac{8}{r^5}\frac{\partial\Psi}{\partial\theta}\frac{\partial^2\Psi}{\partial\theta^2} - \frac{4}{r^4}\frac{\partial\Psi}{\partial\theta}\frac{\partial^2\Psi}{\partial\theta^2} - \frac{13}{r^5}\frac{\partial^2\Psi}{\partial\theta^2}\frac{\partial^3\Psi}{\partial\theta^3} - \frac{1}{r^5}\frac{\partial\Psi}{\partial\theta}\frac{\partial^4\Psi}{\partial\theta^4} + \frac{20}{r^5}\frac{\partial\Psi}{\partial r}\frac{\partial\Psi}{\partial\theta} - \frac{3}{r^3}\frac{\partial\Psi}{\partial r}\frac{\partial\Psi}{\partial\theta} + \frac{3}{r^4}\frac{\partial\Psi}{\partial r}\frac{\partial^3\Psi}{\partial\theta^3} - \frac{30}{r^5}\frac{\partial^2\Psi}{\partial r\partial\theta}\frac{\partial^2\Psi}{\partial\theta^2} - \frac{6}{r^4}\frac{\partial^2\Psi}{\partial r\partial\theta}\frac{\partial^2\Psi}{\partial\theta^2} + \frac{4}{r^3}\frac{\partial^2\Psi}{\partial r\partial\theta}\frac{\partial^2\Psi}{\partial\theta^2} + \frac{1}{r^4}\frac{\partial^2\Psi}{\partial r\partial\theta}\frac{\partial^2\Psi}{\partial\theta^2} - \frac{20}{r^4}\frac{\partial^2\Psi}{\partial r\partial\theta}\frac{\partial\Psi}{\partial\theta} + \frac{8}{r^3}\frac{\partial\Psi}{\partial r}\frac{\partial^2\Psi}{\partial r\partial\theta} + \frac{3}{r^2}\frac{\partial\Psi}{\partial r}\frac{\partial^2\Psi}{\partial r\partial\theta} + \frac{10}{r^5}\frac{\partial^3\Psi}{\partial r\partial\theta^2}\frac{\partial\Psi}{\partial\theta} - \frac{9}{r^4}\frac{\partial^3\Psi}{\partial r\partial\theta^2}\frac{\partial\Psi}{\partial\theta} + \frac{1}{r^3}\frac{\partial^3\Psi}{\partial r\partial\theta^2}\frac{\partial\Psi}{\partial\theta} - \frac{2}{r^4}\frac{\partial^3\Psi}{\partial r\partial\theta^2}\frac{\partial^3\Psi}{\partial\theta^3} + \frac{10}{r^4}\frac{\partial^2\Psi}{\partial r\partial\theta}\frac{\partial^3\Psi}{\partial r\partial\theta^2} + \frac{9}{r^3}\frac{\partial^2\Psi}{\partial r\partial\theta}\frac{\partial^3\Psi}{\partial r\partial\theta^2} - \frac{1}{r^2}\frac{\partial^2\Psi}{\partial r\partial\theta}\frac{\partial^3\Psi}{\partial r\partial\theta^2} - \frac{3}{r^4}\frac{\partial^4\Psi}{\partial r\partial\theta^3}\frac{\partial^2\Psi}{\partial\theta^2} - \frac{1}{r^3}\frac{\partial\Psi}{\partial r}\frac{\partial^4\Psi}{\partial r\partial\theta^3} + \frac{16}{r^4}\frac{\partial^2\Psi}{\partial r^2}\frac{\partial\Psi}{\partial\theta} - \frac{3}{r^2}\frac{\partial^2\Psi}{\partial r^2}\frac{\partial\Psi}{\partial\theta} - \frac{6}{r^2}\frac{\partial^2\Psi}{\partial r^2}\frac{\partial^2\Psi}{\partial r\partial\theta} - \frac{16}{r^3}\frac{\partial^2\Psi}{\partial r^2}\frac{\partial^2\Psi}{\partial r\partial\theta} - \frac{6}{r^3}\frac{\partial^2\Psi}{\partial r^2}\frac{\partial^3\Psi}{\partial\theta^3} + \frac{3}{r}\frac{\partial^2\Psi}{\partial r^2}\frac{\partial^2\Psi}{\partial r\partial\theta} + \frac{2}{r^2}\frac{\partial^2\Psi}{\partial r^2}\frac{\partial^4\Psi}{\partial r\partial\theta^3} + \frac{9}{r^4}\frac{\partial^3\Psi}{\partial r^2\partial\theta}\frac{\partial^2\Psi}{\partial\theta^2} - \frac{8}{r^3}\frac{\partial^3\Psi}{\partial r^2\partial\theta}\frac{\partial^2\Psi}{\partial\theta^2} - \frac{1}{r^2}\frac{\partial^3\Psi}{\partial r^2\partial\theta}\frac{\partial^2\Psi}{\partial\theta^2} + \frac{7}{r^3}\frac{\partial\Psi}{\partial r}\frac{\partial^3\Psi}{\partial r^2\partial\theta} - \frac{6}{r}\frac{\partial\Psi}{\partial r}\frac{\partial^3\Psi}{\partial r^2\partial\theta} - \frac{1}{r}\frac{\partial\Psi}{\partial r}\frac{\partial^3\Psi}{\partial r^2\partial\theta} - \frac{2}{r^3}\frac{\partial^3\Psi}{\partial r\partial\theta^2}\frac{\partial^3\Psi}{\partial r^2\partial\theta} + \frac{4}{r^2}\frac{\partial^3\Psi}{\partial r\partial\theta^2}\frac{\partial^3\Psi}{\partial r^2\partial\theta} + \frac{8}{r^2}\frac{\partial^2\Psi}{\partial r^2}\frac{\partial^3\Psi}{\partial r^2\partial\theta} + \frac{4}{r}\frac{\partial^2\Psi}{\partial r^2}\frac{\partial^3\Psi}{\partial r^2\partial\theta} + 2\frac{\partial^2\Psi}{\partial r^2}\frac{\partial^3\Psi}{\partial r^2\partial\theta} + \frac{1}{r^4}\frac{\partial^4\Psi}{\partial r^2\partial\theta^2}\frac{\partial\Psi}{\partial\theta} - \frac{2}{r^3}\frac{\partial^4\Psi}{\partial r^2\partial\theta^2}\frac{\partial\Psi}{\partial\theta} - \frac{1}{r^3}\frac{\partial^2\Psi}{\partial r\partial\theta}\frac{\partial^4\Psi}{\partial r^2\partial\theta^2} + \frac{2}{r^2}\frac{\partial^2\Psi}{\partial r\partial\theta}\frac{\partial^4\Psi}{\partial r^2\partial\theta^2} - \frac{11}{r^3}\frac{\partial^3\Psi}{\partial r^3}\frac{\partial\Psi}{\partial\theta} - \frac{2}{r}\frac{\partial^2\Psi}{\partial r\partial\theta}\frac{\partial^3\Psi}{\partial r^3} + \frac{11}{r^2}\frac{\partial^2\Psi}{\partial r\partial\theta}\frac{\partial^3\Psi}{\partial r^3} - 2\frac{\partial^2\Psi}{\partial r\partial\theta}\frac{\partial^3\Psi}{\partial r^3} - \frac{4}{r}\frac{\partial^3\Psi}{\partial r^2\partial\theta}\frac{\partial^3\Psi}{\partial r^3} + 4\frac{\partial^3\Psi}{\partial r^2\partial\theta}\frac{\partial^3\Psi}{\partial r^3} - \frac{1}{r^3}\frac{\partial^2\Psi}{\partial\theta^2}\frac{\partial^4\Psi}{\partial r^3\partial\theta} - \frac{1}{r}\frac{\partial\Psi}{\partial r}\frac{\partial^4\Psi}{\partial r^3\partial\theta} - \frac{2}{r}\frac{\partial^2\Psi}{\partial r^2}\frac{\partial^4\Psi}{\partial r^3\partial\theta} + 4\frac{\partial^2\Psi}{\partial r^2}\frac{\partial^4\Psi}{\partial r^3\partial\theta} + \frac{2}{r^2}\frac{\partial^4\Psi}{\partial r^4}\frac{\partial\Psi}{\partial\theta} - \frac{2}{r}\frac{\partial^4\Psi}{\partial r^4}\frac{\partial^2\Psi}{\partial r\partial\theta} + L\frac{\lambda}{\Re e}(-\frac{3}{r^3}\frac{\partial u}{\partial r}\frac{\partial\Psi}{\partial\theta} + \frac{1}{2r}\frac{\partial u}{\partial r}\frac{\partial\Psi}{\partial\theta} - \frac{3}{r^2}\frac{\partial u}{\partial r}\frac{\partial^3\Psi}{\partial\theta^3} - \frac{3}{r^2}\frac{\partial u}{\partial r}\frac{\partial^2\Psi}{\partial r\partial\theta} - \frac{1}{2}\frac{\partial u}{\partial r}\frac{\partial^2\Psi}{\partial r\partial\theta} + \frac{1}{r}\frac{\partial u}{\partial r}\frac{\partial^3\Psi}{\partial r\partial\theta^2} - \frac{5}{2r^2}\frac{\partial^2 u}{\partial r^2}\frac{\partial\Psi}{\partial\theta} + \frac{\partial^2 u}{\partial r^2}\frac{\partial\Psi}{\partial\theta} + \frac{5}{2r}\frac{\partial^2 u}{\partial r^2}\frac{\partial^2\Psi}{\partial r\partial\theta} - r\frac{\partial^2 u}{\partial r^2}\frac{\partial^2\Psi}{\partial r\partial\theta} + 6\frac{\partial u}{\partial r}\frac{\partial^3\Psi}{\partial r^2\partial\theta} - r\frac{\partial u}{\partial r}\frac{\partial^3\Psi}{\partial r^2\partial\theta} + 2\frac{\partial^2 u}{\partial r^2}\frac{\partial^3\Psi}{\partial r^2\partial\theta} + 2r\frac{\partial^2 u}{\partial r^2}\frac{\partial^3\Psi}{\partial r^2\partial\theta} + \frac{1}{r}\frac{\partial^3 u}{\partial r^3}\frac{\partial\Psi}{\partial\theta} - \frac{\partial^3 u}{\partial r^3}\frac{\partial^2\Psi}{\partial r\partial\theta} - \frac{\partial u}{\partial r}\frac{\partial^4\Psi}{\partial r^3\partial\theta} + 2r\frac{\partial u}{\partial r}\frac{\partial^4\Psi}{\partial r^3\partial\theta} - (r^3-6)\frac{3}{r^3}u\frac{\partial\Psi}{\partial\theta} - \frac{18}{r^3}u\frac{\partial^2\Psi}{\partial r\partial\theta} + \frac{1}{r^2}u\frac{\partial^2\Psi}{\partial r\partial\theta} + \frac{3}{r}u\frac{\partial^2\Psi}{\partial r\partial\theta} + \frac{15}{r^2}u\frac{\partial^3\Psi}{\partial r^2\partial\theta} - \frac{3}{2r^5}u\frac{\partial^3\Psi}{\partial r^3} - \frac{3}{r}u\frac{\partial^2\Psi}{\partial r\partial\theta} + \frac{1}{2r^2}u\frac{\partial^3\Psi}{\partial r^2\partial\theta} - \frac{1}{r}u\frac{\partial^3\Psi}{\partial r^2\partial\theta} - \frac{3}{2}u\frac{\partial^3\Psi}{\partial r^2\partial\theta} - \frac{3}{2r}u\frac{\partial^4\Psi}{\partial r^2\partial\theta^2} - 2u\frac{\partial^4\Psi}{\partial r^2\partial\theta^2})] + \gamma_3[\frac{-2}{r^4}(\frac{\partial u}{\partial r})^2\frac{\partial^4\Psi}{\partial\theta^4} - \frac{4}{r^3}(\frac{\partial u}{\partial r})^2\frac{\partial\Psi}{\partial r} - \frac{\partial u}{\partial r}\frac{\partial^2 u}{\partial r^2}\frac{\partial^3\Psi}{\partial r\partial\theta^2} + \frac{4}{r}(\frac{\partial^2 u}{\partial r^2})^2\frac{\partial\Psi}{\partial r} + \frac{4}{r^2}(\frac{\partial u}{\partial r})^2\frac{\partial^2\Psi}{\partial r^2} - 4(\frac{\partial^2 u}{\partial r^2})^2\frac{\partial^2\Psi}{\partial r^2} - \frac{1}{r^2}(\frac{\partial u}{\partial r})^2\frac{\partial^4\Psi}{\partial r^2\partial\theta^2} + \frac{4}{r}\frac{\partial u}{\partial r}\frac{\partial^3 u}{\partial r^3}\frac{\partial\Psi}{\partial r} - 4\frac{\partial u}{\partial r}\frac{\partial^3 u}{\partial r^3}\frac{\partial^2\Psi}{\partial r^2} - \frac{6}{r^4}(\frac{\partial u}{\partial r})^2\frac{\partial^2\Psi}{\partial\theta^2} - \frac{2}{r^2}(\frac{\partial^2 u}{\partial r^2})^2\frac{\partial^2\Psi}{\partial\theta^2} + \frac{2}{r^3}\frac{\partial u}{\partial r}\frac{\partial^2 u}{\partial r^2}\frac{\partial^2\Psi}{\partial\theta^2} + \frac{2}{r^2}\frac{\partial u}{\partial r}\frac{\partial^3 u}{\partial r^3}\frac{\partial^2\Psi}{\partial\theta^2} - \frac{2}{r}(\frac{\partial u}{\partial r})^2\frac{\partial^3\Psi}{\partial r^3} - 8\frac{\partial u}{\partial r}\frac{\partial^2 u}{\partial r^2}\frac{\partial^3\Psi}{\partial r^3} - 2(\frac{\partial u}{\partial r})^2\frac{\partial^4\Psi}{\partial r^4} - L\frac{\lambda}{\Re e}(12(\frac{\partial u}{\partial r})^2\frac{\partial^2 u}{\partial r^2} + 6r\frac{\partial u}{\partial r}(\frac{\partial^2 u}{\partial r^2})^2 + 3\frac{\partial u}{\partial r}\frac{\partial^3 u}{\partial r^3})] \tag{15}$$

6. The Solution

we are going to solve the equations (14) and (15). We start by the successive approximation for u and Ψ. This method equivalent to expand u and Ψ in secondary power of Dean number .In this way we obtain recursive relations. These equations are solved analytically.

This equation in polar coordinates is

$$r^2 = 1 \quad \text{or} \quad 1 - r^2 = 0 \tag{16}$$

Where r is the radius of the cross section and the non slip conditions are

$$u = \Psi = \frac{\partial \Psi}{\partial r} = 0 \qquad atr = 1 \qquad (17)$$

The solution of equations (14) and (15) subject to associate boundary conditions are $\Psi(\mathrm{r},\theta, L, \lambda/\Re e\,, \gamma_1, \gamma_3), u(\mathrm{r},\theta, L, \lambda/\Re e\,, \gamma_1, \gamma_3)$.The prime parameter Dean number L, and the successive approximation method is adopted. This method equivalent to expand Ψand u in a secondary power of Dean number L.

$$\Psi = L\Psi_1 + L^2\Psi_2$$

$$u = u_\circ + Lu_1 \tag{18}$$

$$u_\circ = 1 - r^2 + 4\gamma_3(1 - r^4)$$

(19)

Provided G = 4, and if we set $\gamma_3 = 0$ we will obtain the solution in a case of a straight pipe (Dean, [6]).

$$\Psi_1 = \{\frac{1}{144}\left(r - \frac{9}{4}r^3 + \frac{3}{2}r^5 - \frac{1}{4}r^7\right) + \gamma_3[\frac{1}{69120}(1859\,r - 4707\,r^3 + 3870r^5 - 1055\,r^7 + 33\,r^9)] +$$
$$\gamma_3{}^2[\left(\frac{-114717\,r}{512000} +$$
$$\frac{1}{27648000}(6346285\,r^3 + 338900\,r^5 + 659750r^7 - 5900750\,r^9 + 1699533\,r^{11})\right)] +$$
$$\gamma_3{}^3[-\frac{13441590109\,r}{13934592000} + \frac{1}{69672960000}(77681344479\,r^3 + 5827344600\,r^5 + 26411464625\,r^7 -$$
$$37061159625\,r^9 - 13580472150\,r^{11} + 7929428616\,r^{13})]\}cos\theta + \frac{\lambda}{\Re e}[\frac{1}{8}\left(1 - r^2\right)^2 +$$

$$\gamma_3\left(\frac{1}{2}-\frac{3}{4}r^2+\frac{1}{4}r^6\right)+{\gamma_3}^2\left(\frac{3589}{490}-\frac{5086}{525}r^2-\frac{576}{1225}r^7+\frac{17}{6}r^8\right)+{\gamma_3}^3\left(\frac{1744}{315}-\frac{332}{49}r^2-\frac{512}{441}r^9+\frac{12}{5}r^{10}\right)+{\gamma_3}^4\left(128-\frac{768}{5}r^2+\frac{128}{5}r^{12}\right)\Big] \qquad (20)$$

Now if we set $\gamma_3 = 0$, in to equation (20) will describe the flow of non Newtonian fluid of second order, [1].

$$u_1=\{\frac{2413}{3572100}-\frac{r^8}{648}+\frac{r^5}{800}-\frac{r^7}{2352}+\frac{r^9}{23328}+\beta\left[\frac{493}{44100}-\frac{r^8}{36}+\frac{r^5}{50}-\frac{r^7}{294}\right]+[-\frac{1}{140}+\frac{r^3}{48}-\frac{r^5}{60}+\frac{r^7}{336}]\gamma_1+\gamma_3[\frac{596675249}{51866892000}-\frac{1859r^3}{311040}-\frac{679r^5}{32000}+\frac{2281r^7}{94080}-\frac{37691r^9}{3919104}+\frac{4447r^{11}}{4181760}+\beta\left[\frac{864641}{4082400}-\frac{523r^3}{4320}-\frac{181r^5}{400}+\frac{2263r^7}{5040}-\frac{7123r^9}{81648}\right]+\left[-\frac{2171}{18144}+\frac{523r^3}{5760}+\frac{149r^5}{480}-\frac{2861r^7}{8064}+\frac{949r^9}{12960}\right]\gamma_1]+{\gamma_3}^2[-\frac{245107349704291}{16392632256000000}+\frac{13441590109r^3}{62705664000}-\frac{9250236533r^5}{290304000000}-\frac{r^6}{9}-\frac{35359529r^7}{58060800}+\frac{9r^8}{16}+\frac{12038419643r^9}{22574039040}-\frac{9r^{10}}{20}-\frac{216172771r^{11}}{1021870080}+\frac{7r^{12}}{90}+\frac{314836117r^{13}}{6853017600}-\frac{586000193r^{15}}{108864000000}+\beta\left[-\frac{93018484869529}{32056703078400}+\frac{25893781493r^3}{13063680000}+\frac{265327r^5}{345600}-2r^6-\frac{48870443r^7}{5806080}+9r^8+\frac{1489056343r^9}{156764160}-\frac{18r^{10}}{5}-\frac{428326027r^{11}}{78059520}+\frac{563339753r^{13}}{486720000}\right]+\left[\frac{26410449711223063}{11219846077440000}+\frac{114717r^2}{64000}-\frac{39769949813r^3}{17418240000}-\frac{1269257r^4}{921600}+\frac{30381317r^5}{51840000}+\frac{59413r^6}{62208}+\frac{2017171643r^7}{325140480}-\frac{1677353r^8}{221184}-\frac{2316781123r^9}{313528320}+\frac{144563r^{10}}{38400}+\frac{530731199r^{11}}{133816320}-\frac{2077207r^{12}}{13824000}-\frac{5714525549r^{13}}{6814080000}\right]\gamma_1]+{\gamma_3}^3[(\frac{314779477711671019}{531978483156120000}+\frac{13441590109r^5}{3628800000}-\frac{517390257329r^7}{177811200000}-\frac{14r^8}{3}-\frac{561033997r^9}{41990400}+\frac{558r^{10}}{25}+\frac{12110038331r^{11}}{903260160}-\frac{123r^{12}}{7}-\frac{1085929391r^{13}}{196245504}+\frac{136r^{14}}{45}+\frac{2259476969r^{15}}{2021760000}-\frac{5256329023r^{17}}{43696800000}+\beta\left[-\frac{107925190514441563}{1252214964000000}+\frac{25893781493r^5}{648000000}-\frac{543323r^7}{22680}-84r^8-\frac{1142220467r^9}{5598720}+\frac{8928r^{10}}{25}+\frac{5344760417r^{11}}{21954240}-\frac{984r^{12}}{7}-\frac{57395600747r^{13}}{449729280}+\frac{440595703r^{15}}{17062500}\right]+\left[\frac{1025744282912993}{11925856800000}+\frac{344151r^4}{16000}-\frac{36300907733r^5}{907200000}-\frac{1269257r^6}{57600}+\frac{86046059r^7}{2268000}+\frac{183829r^8}{3456}+\frac{375438079r^9}{2612736}-\frac{689365r^{10}}{2304}-\frac{8258830571r^{11}}{43908480}+\frac{259763r^{12}}{1920}+\frac{2006612321r^{13}}{21415680}-\frac{2077207r^{14}}{672000}-\frac{4643819759r^{15}}{245700000}\right]\gamma_1]\}\sin\theta$$

(21)

and

$$\Psi_2 = \{\left[-\frac{916757r}{311662391040}+\frac{r^2}{62208}-\frac{49661063r^8}{2574483912000}+\frac{2413r^5}{685843200}+\frac{1009r^6}{174182400}-\frac{3103r^8}{762048000}+\frac{1849r^{10}}{1738598400}-\frac{19687r^{12}}{129459762432}+\frac{461r^{14}}{83264163840}\right]+\beta\left[\frac{401957r}{5708102400}-\frac{10703611r^3}{63567504000}+\frac{493r^5}{8467200}+\frac{r^6}{9450}-\frac{43r^8}{496125}+\frac{172r^{10}}{7640325}-\frac{4r^{12}}{2081079}\right]+\gamma_1\left[\frac{1640486561477r}{5744561191649280}-\frac{r^2}{864}+\frac{30576305891r^3}{14878428364800}-\frac{509r^4}{311040}-\frac{5309r^5}{23224320}+\frac{15101r^6}{14515200}+\frac{8579r^7}{127401984}-\frac{28879r^8}{50803200}-\frac{1457r^9}{159252480}+\frac{133829r^{10}}{754427520}-\frac{293r^{11}}{530841600}-\frac{2815r^{12}}{105380352}+\frac{23r^{13}}{139345920}+\frac{361r^{14}}{256988160}+\frac{11r^{15}}{1783627776}\right]+\gamma_3\left[\left[-\frac{30710795212666169r}{4383602838332669952000}+\frac{3455881r^2}{14332723200}-\frac{57990708218181 77r^3}{15770418374430720000}+\frac{r^4}{34992}+\frac{610015499r^5}{9958443264000}+\frac{1787591r^6}{33443020800}+\frac{299921r^7}{10973491200}-\frac{1263171557r^8}{92177326080000}-\frac{15131r^9}{557383680}-\frac{3247622827r^{10}}{260730150912000}+\frac{271057r^{11}}{15676416000}+\frac{516169243r^{12}}{112983065395200}-\frac{43409r^{13}}{7315660800}-\frac{261282706801r^{14}}{473926298311065600}+\frac{4157r^{15}}{4096770048}-\frac{39908417r^{16}}{1437267566592000}-\frac{797r^{17}}{12039487488}-\frac{121r^{18}}{285769728000}\right]+\beta\left[\frac{6990572977307r}{3926946127104000}-\frac{6625672667 69r^3}{164766970368000}+\frac{r^4}{1944}+\frac{883541r^5}{783820800}+\frac{379r^6}{453600}+\frac{196043r^7}{406425600}-\frac{54091r^8}{166698000}-\frac{1343r^9}{2903040}-\frac{1495481r^{10}}{6601240800}+\frac{73453r^{11}}{290304000}+\frac{778727r^{12}}{7224317100}-\frac{6217r^{13}}{101606400}-\frac{158491r^{14}}{15937281360}+\frac{629r^{15}}{113799168}\right]+\gamma_1\left[-\frac{2123558539838419r}{457769719959552000}+\frac{8341r^2}{737280}-\frac{14338861175753r^3}{1300799737036800}+\frac{267779r^4}{37324800}-\frac{8408119r^5}{4459069440}-\frac{15433417r^6}{3483648000}+\frac{7743539r^7}{1981808640}+\frac{18106811r^8}{7315660800}-\frac{64119517r^9}{19110297600}-\frac{3620083r^{10}}{5912248320}+\frac{19031893r^{11}}{15925248000}+\frac{476527r^{12}}{13699445760}-\frac{2114813r^{13}}{13377208320}+\frac{2999443r^{14}}{1295220326400}+\frac{212185r^{15}}{149824733184}+\frac{583r^{16}}{10998374400}+\frac{121r^{17}}{53508833280}\right]\Bigg\}\sin\theta\cos\theta+\frac{\lambda}{\Re e}\{\left[\frac{44442527r}{1393459200}-\frac{7r^2}{864}-\frac{713129r^3}{11612160}+\frac{43r^4}{17280}+\frac{4757r^5}{110592}+\frac{223r^6}{201600}-\frac{3163r^7}{442368}-\frac{157r^8}{51840}+\frac{3103r^9}{4423680}+\frac{115r^{10}}{217728}-\frac{433r^{11}}{11059200}+\frac{r^{13}}{7741440}\right]\gamma_1+\gamma_3\left[-\frac{5279r}{6220800}+\frac{2981r^3}{2419200}-\frac{r^5}{3456}+\frac{r^7}{2560}-\frac{109r^9}{179200}+\frac{481r^{11}}{3628800}-\frac{r^{13}}{108864}+\beta\left[\frac{79r}{1120}-\frac{1109r^3}{6720}+\frac{29r^5}{240}-\frac{193r^7}{6720}+\frac{r^9}{420}\right]+\left[-\frac{89253672928451r}{920602755072000}+\frac{2915r^2}{82944}+\frac{3971662847r^3}{24908083200}-\frac{3689r^4}{1036800}-\frac{593701r^5}{6635520}-\frac{115601r^6}{8064000}-\frac{298819r^7}{26542080}+\frac{643709r^8}{60963840}+\frac{561731r^9}{53084160}+\frac{15271r^{10}}{6531840}-\frac{1015021r^{11}}{66355200}-\frac{232279r^{12}}{217451520}+\frac{45769r^{13}}{464486400}\right]\gamma_1\}\sin\theta \tag{22}$$

7. Results & Discussion

In this section we study the effects of the parameters L, β, γ_1, γ_3, and $\frac{\lambda}{\Re e}$ upon the components of the secondary flow and the axial velocity. Since the pseudo stream- function, for duct with non zero torsion dose not represent the secondary flow as described by v and w, therefore vector plots are employed to present the secondary flow.

7.1. The Secondary Flow Motion

A helical pipe characterized by non zero torsion. We have more than 40 cases to a certain how the parameters L, $\frac{\lambda}{\Re e}\beta, \gamma_1, \gamma_3$ effects on the secondary flow in helical and straight pipes.In equation (21) , if $\beta = 0, \gamma_1 = 0, \gamma_3 = 0$, we recover the first order results in L of Gremano, [9]for Newtonian flow in a helical pipe with an elliptical cross- section, and if $\gamma_1 = 0, \gamma_3 = 0$ in that equation we recover the flow of non Newtonian fluid of second order.

Figure (2) shows the effects of a material moduli γ_3 on the secondary flow. For $\lambda/\Re e = 0.01$, $\beta = 0.5$, $\gamma_1 = 1$, and $\gamma_3$increases from 0.01 to 1 we observed:-

- There is new secondary flow which increases when $\gamma_3$increased.
- There is a shifting toward the left side of cross- section. That is means the intensity of flow in the right side is increased and consequently begins to push the main flow to the left, figure (3).
- When γ_3=0.07, there is a secondary flow which near the center of the cross- section, figure (4).
- When γ_3=1, the effect of this disappears, figure (5).
    - When$\gamma_1 = 0, \gamma_3 = 0$, $\beta = 0$,and torsion equal zero ,the flow is in a straight pipe.

Figure(6)illustrates the effects of $\gamma_1$on the secondary flow. Here $\Re e = 2$, $\beta = 0$, $\gamma_3 = 0$ and $\gamma_1$varies from 0.1 to 4.

- The effects of $\gamma_1$appear when $\gamma_1$is greater than 1, figure (7).
- When $\gamma_1$increases there is new secondary flow, figure (8).
- The intensity of fluid which is found in the lower part and near the center of cross-section is stronger that is the secondary flow of fluid in the upper part is weaker ,figure (9).

Figure (10) shows the effects of β upon the secondary flow, we noted

- That the parameter βinfluouns the secondary velocity of fluid when it is very large since, it is product by small values.
- There is a displacement to the towardupper part of the cross-section .That is due to the increasing in the intensity of fluid the lower part of cross- section, figure(11).
- There is new secondary flow in the lower part of cross section, figure (12).

Figure (13) explains the effects of $\lambda/\Re e$ on the secondary flow.

These effects are:-

- There is a displacement to the left toward of cross- section, There is a small secondary flow near the center the cross-section.

The intensity of fluid in the lower part and near of the center cross- section increases.

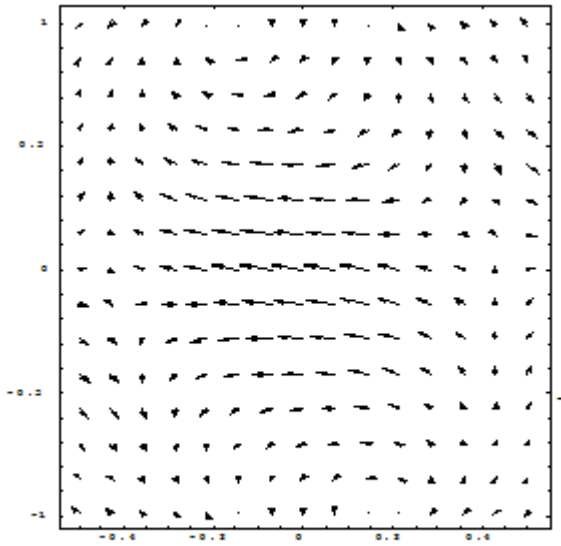

Figure (2), β=0.5, γ1=0,γ 3=0,λ=0

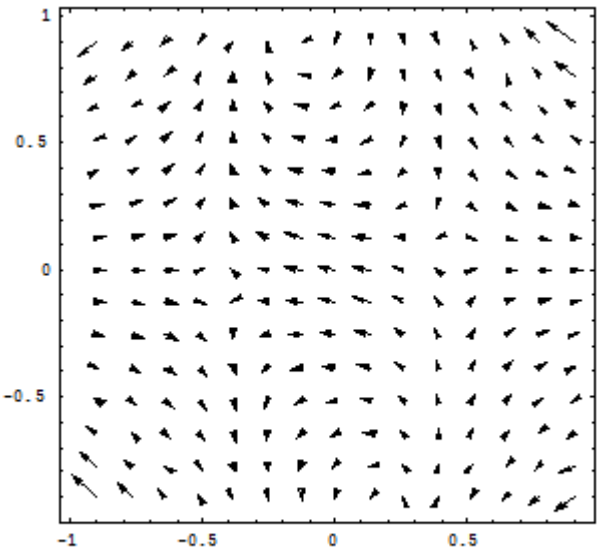

Figure (3), β=0.5, γ1=1,γ3=0.01,λ=2

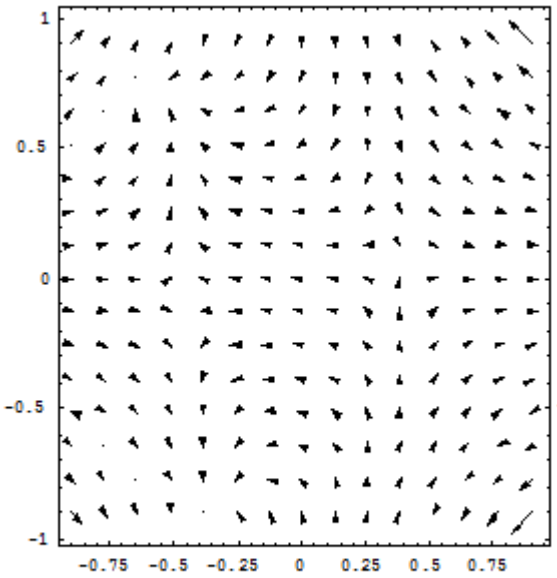

Figure (4), β =0.5, γ1=1,γ3=0.07,λ=0.2

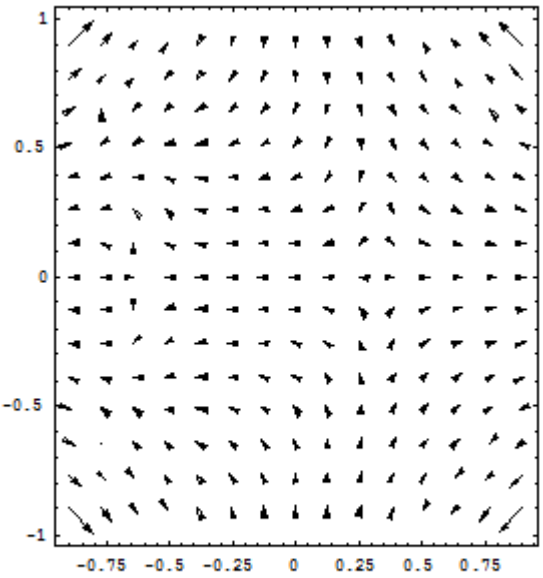

Figure (5), β=0.5, γ1=1, γ3=1,λ=0.2

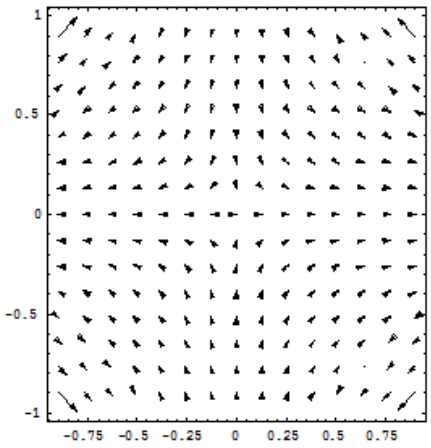

Figure (6), β=0, γ1=1, γ3=0,λ=0.2

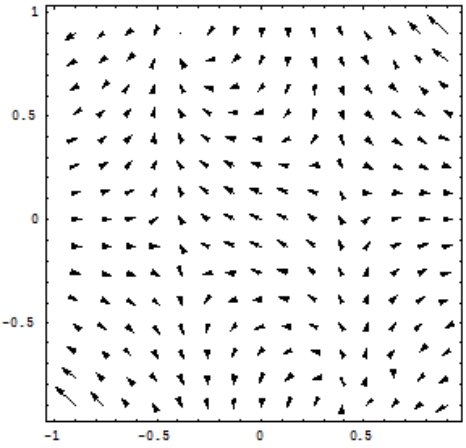

Figure (7) β=0, γ1=2 γ3=0,λ=0.

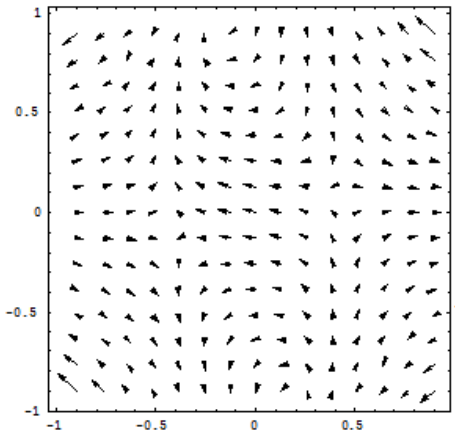

Figure (8) β=1.4, γ1=0, γ3=0,λ=0.2

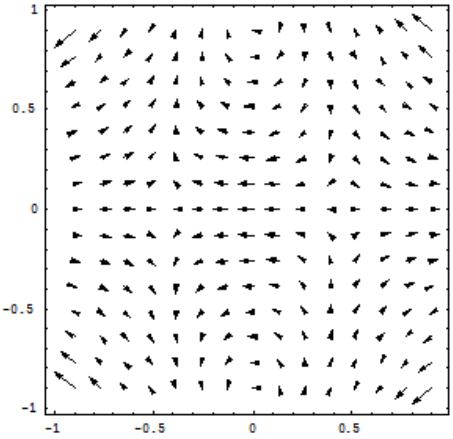

Figure (9), β=0.5, γ1=1, γ3=1,λ=0.2

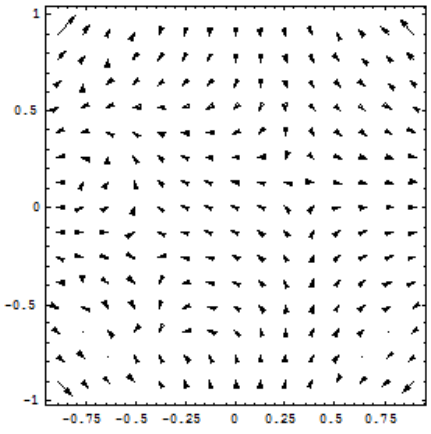

Figure (10) β=0.5, γ1=1, γ3=0.01,ℜe=4

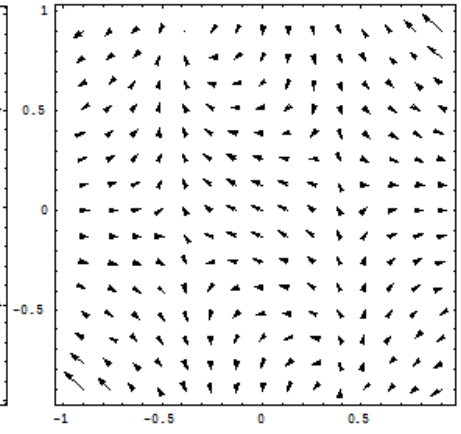

Figure (11) β=1.4, γ1=2, γ3=0,λ=0.2

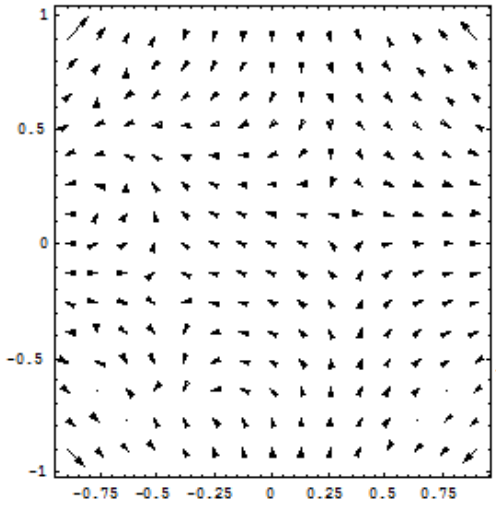

Figure (12) β=0.5, γ1=1, γ3=0.01,ℜe=4

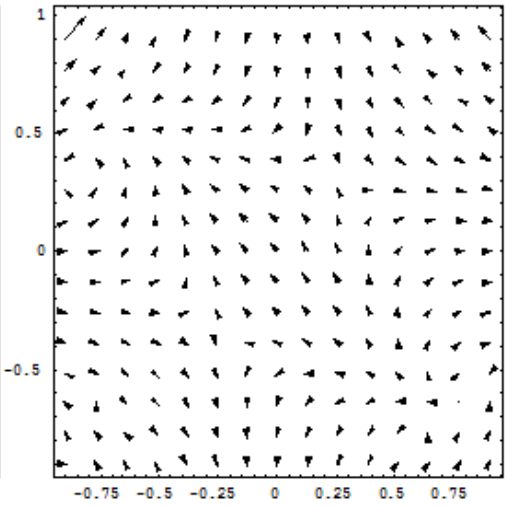

Figure (13) β=0, γ1=0, γ3=0,ℜe=10

7.2. The Axial Flow

In this we analyze the axial flow by studies the effects of γ_1, γ_3 and β.If $\beta = 0, \gamma_1 = 0, \gamma_3 = 0,$ in equation(19)we go to the flow in a straight pipe, figure (14)

Figure (15) shows the effects of γ_3.For L=80, $\beta = 0.01$, $\gamma_1 = 1$, as $\gamma_3$increases from 0.01 to 2.

- Thereis a displacement toward upper part of the pipe. That is the velocity of fluid in the lower part of the pipe is stronger, figure (16).
- When γ_3= 1, in which there a continuous a displacement and a stagnation region short to appear in the middle of the pipe, figure (17).
- In addition there are two vortexes in the upper and lower part of the pipe.

Figure (18) gives the axial flow under the effects of γ_1, as increases from 0.1 to 3.

- Thereis a displacement toward the upper wall of the pipe, figure (19).
- There is a stagnation region in the middle of pipe, figure (20).
- When γ_1=1.5, the stream lines becomes thicker near the stagnation region, figure (21).

Figure (22) expresses the effects of β, as it varies from 0.01 to 1.5.

- Thereis a displacement toward the upper wall of the pipe . That is the axial velocity in the lower part of pipe is stronger then it pushes the fluid to the upper part of pipe, figure (23).
- There is a stagnation region in a center plane of pipe, figure (24).

For $\beta = 1.7$, we note that there is a displacement toward the lower wall of the pipe, and the intensity of the fluid in the upper part of cross- section becomes stronger.

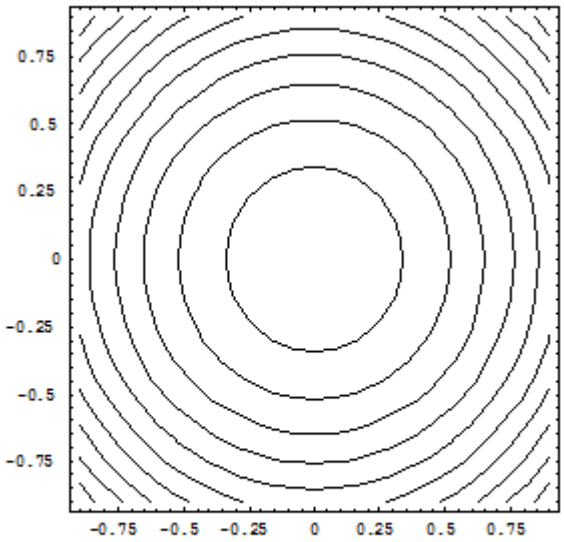

Figure (14)β=0, γ1=0,γ 3=0

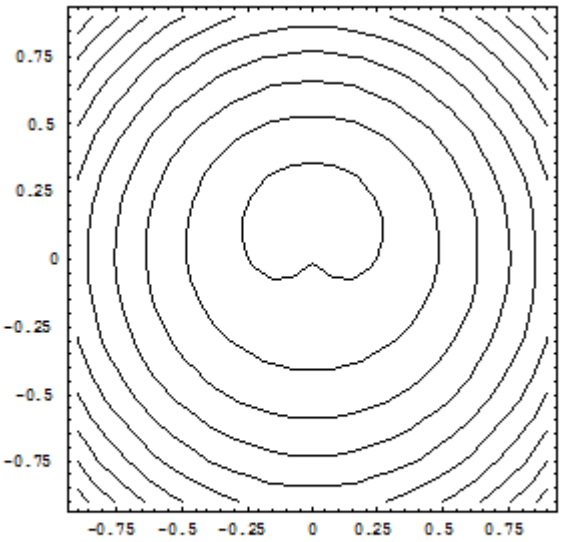

Figure (15) β=0.01, γ1=0, γ3=0.3,L=80

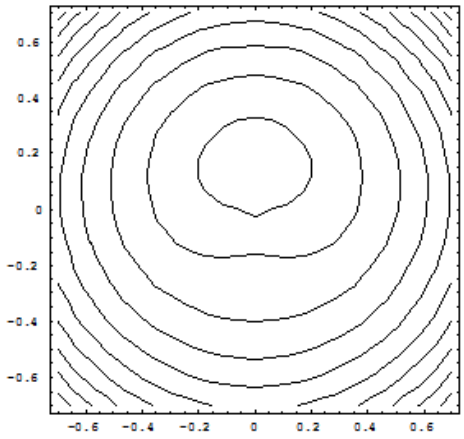

Figure (16) β=0.01, γ1=0, γ3=0.3,L=80

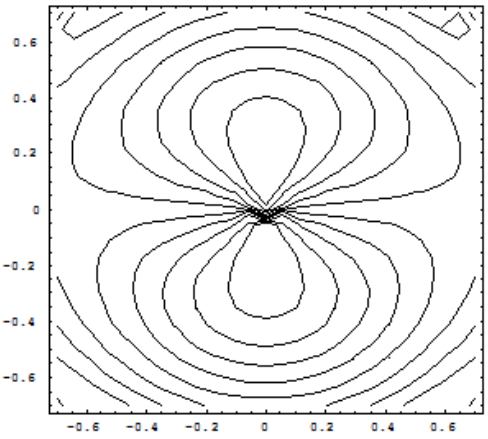

Figure (17) β=0.01, γ1=0, γ3=1,L=80

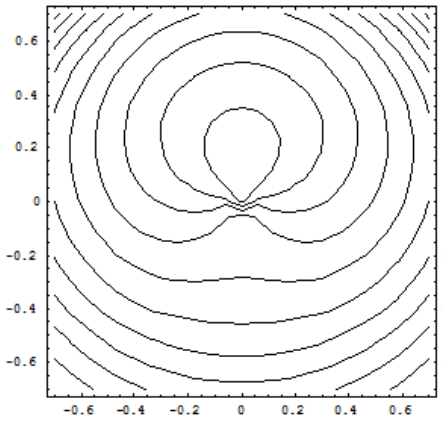

Figure (18) β=0.01, γ1=0.3, γ3=0.01,L=80

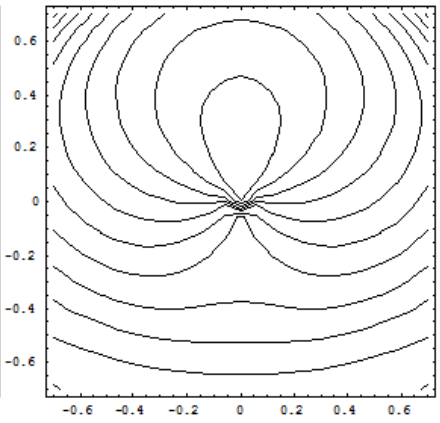

Figure (19) β=0.01, γ1=0.5, γ3=0.1,L=80

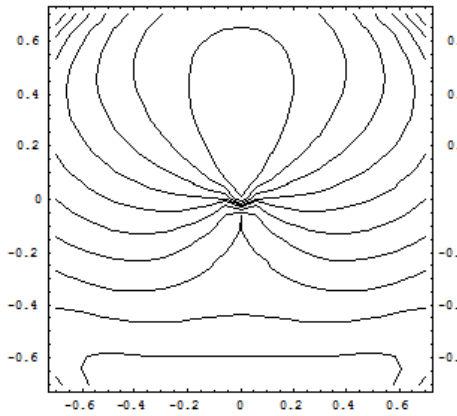

Figure (20) β=0.01, γ1=0.7, γ3=0.1,L=80

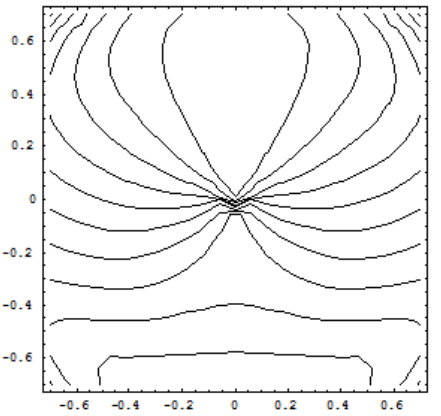

Figure (21) β=0.01, γ1=1.5, γ3=0.1,L=80

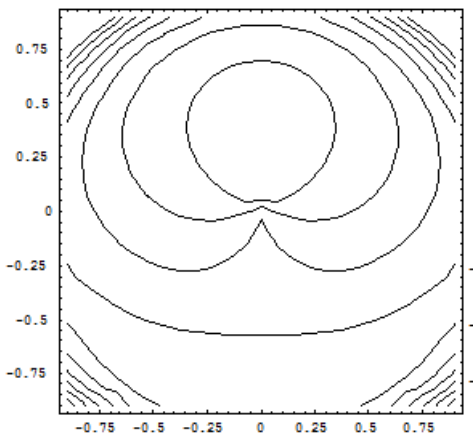

Figure (22) β=0.01, γ1=0.3, γ3=0.07,L=80

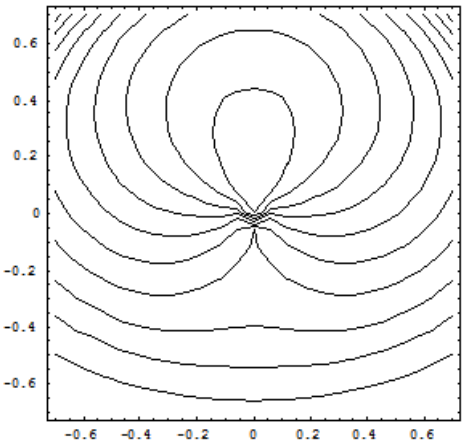

Figure (23) β=0.05, γ1=0.3, γ3=0.07, L=80

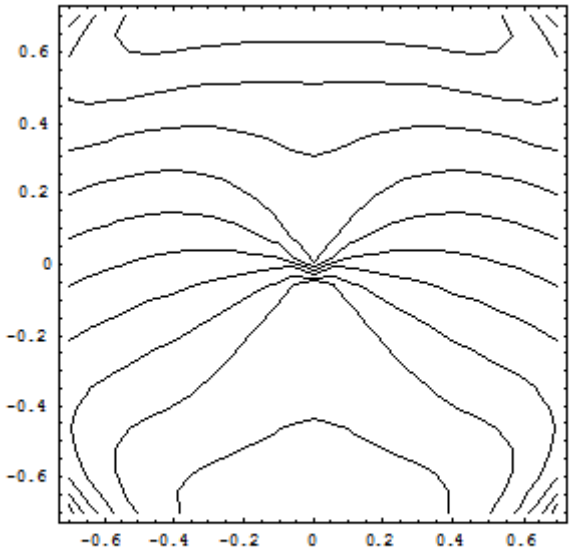

Figure (24) β=0.05, γ1=0.3, γ3=0.07, L=80

References

1. Ahmed, M. A. Hadi, (2000). "Flow Analysis Through Curved Pipes". Ph.D. Thesis submitted to university of Pune .
2. Anton, Bivens, and Davis, (2002). "Calculus".7th. Edition, John Wiley. Sons, Inc. New York .
3. Batchelor, C.K., (1967). "An introduction to fluid mech.". App. 2 Cambridge University Press.
4. Bolinder, C. J., (1996). "First and higher order effect of curvature and torsion on the flow in a helical rectangular duct". J. Fluid Mech. (108:185-194.
5. Chen, W. H., and Jan, R., (1992). " The characteristics of laminar flow in a helical circular pipe". J. Fluid Mech. (244): 241-256.
6. Dean, W. R., (1927). " Note on the motion of fluid in a curved pipe". Polilos. Mag. (20): 208-223.
7. Dean, W. R., (1928). "The stream line motion of fluid in a curved pipe". Polilos. Mag. (30): 673-693.
8. Fosdick, R. L., and Rajagopal, K. R., (1980). "Thermodynamics and

stability of fluids of third grade". Proc. R. Soc. London. A 339-351.

9. Germano, M., (1982). "On the effect to torsion on a helical pipe flow". J. Fluid Mech. (125):1-8.
10. Germano, M., (1989). "The Dean equations extended to a helical pipe flow". J. Fluid Mech. (20):289-305.
11. Jinsuo Zhang, Benzhao Zhang, and Huajun Chen, (2000). "Flow in helical a nnular pipe". J. Engineering Mech. Vol. 126 No.10.
12. Jones, J.R. (1960). "Flow of non –Newtonian liquid in a curved pipe". Q. J. Mech. App1.Math. (13): 428-443.
13. Lei Xue, (2002). "Study on laminar flow in helical circular pipes with Galerkin method". J. Computer and Fluids. (31):113-129.
14. Love, A. E. H., "Atreatise on the mathematics theory of elasticity". New York. Dover publications.
15. Tuttle, E. R., (1990). "Laminar flow in twisted pipes". J. Fluid Mech. (21):70-545.
16. VusudeVaiah, M., and Patturaj, R., (1994). "Effect of torsion in a a helical pipe flow". J. Math. and Math. Sci. (17) No.3:553-560.
17. Wang, C. Y., (1981). "On the low Reynolds number flow in a helical Pipe". J. Fluid Mech. (108):185-194.

The Scientific Approach in Designing a Virtual Reality Educational Program

Ayad Rifaat Raoof
University of Baghdad, College of Administration and Economics,
Computer Center, Baghdad Iraq (ayadraouf@hotmail.com)

Abstract

Educational Virtual Reality (VR) is an improved multimedia tool that creates a computer simulation learning environment which is very close to reality. It is realized a sufficient improvement level in several applications, such as education, research, and training. The implementation of virtual reality offers numerous educational benefits which leads to use it for more than the traditional instructions. But, the main limitation of using this technology is the cost. In this paper, the main concepts, bases, approaches, requirements, and components that are essential to create an educational virtual reality program and its main strength and weakness points are explored. In addition, the design making process of the virtual reality program and the use of fuzzy logic in the building of educational virtual reality program are described.

Keywords: Virtual Reality (VR); VRML; HMD; Educational units,

المستخلص

الواقع الافتراضي التعليمي (VR) هو أداة تحسين الوسائط المتعددة التي تخلق بيئة تعلم قريبة جدا من الواقع تحاكي الكمبيوتر. تم تحقيق مجموعة من مستويات التطور في هذا النظام ليشمل تطبيقات متعددة مثل التعليم والبحث والتدريب. تنفيذ الواقع الافتراضي يوفر العديد من الفوائد التعليمية التي تؤدي إلى استخدامه أكثر من الإرشادات التقليدية. لكن المشكلة الرئيسية لاستخدام هذه التكنولوجيا هي التكلفة. في هذا البحث، تم توضيح أهم المفاهيم والقواعد والمناهج والمتطلبات والمكونات المهمة لإنشاء برنامج الواقع الافتراضي التعليمي واهم نقاط قوة وضعف هذا البرنامج. بالإضافة إلى ذلك، تم شرح عملية صنع القرار لبرنامج الواقع الافتراضي التعليمي واستخدام المنطق الضبابي في بناء البرنامج.

I. Introduction

Recently, computers are widely used as an educational tool due to their flexibility, rapidity, and capability to make a decision and show several images. Improvements of computer systems as well as multimedia technologies facilitate the improvement of new education and training technologies. These new technologies are currently recognized and established to offer enhanced educational environments. Several issues must be taken into account in order to understand the complexity of these systems, such as recognized techniques of documentation, qualifications, design and implementation. [1, 2, 3]

Several educational and learning technologies are widely employed in order to improve the learning efficiency and enhance the proficiency in the nowadays complex technological environment. No one of these technologies is established to verify the technological environment meaning that is made by people with gradually more complicated equipment, complex operations and enlarged safety worries. The solution of these problems is the use of educational virtual reality technologies. [4, 5]

Recently, the main tools that are utilized in the storing and processing of data in the established educational systems are: Textbooks, individuals' minds and pencils. The most significant and valuable performer in the nowadays educational environment is the online learning or as called also virtual learning. [5, 6]

Virtual reality technology is the main educational technology that is used to enhance the interactivity. It is widely utilized in medical training, services training, entertainment and aerospace design in order to offer an appropriate environment for the analysis and evaluation of designs, decrease both the improvement time and cost and enhance the superiority as well as usability of several products. [7, 8, 9]

Several training and teaching material are used in the environment of educational virtual reality technologies due to the development of visualization techniques as well as computer hardware. Educational virtual reality technologies are utilized as training and educational tools since these technologies are secure, protected, inexpensive and completely controllable. In addition, these technologies improve learning since they offer learners with interactivity and practicality. [10]

This paper is divided into several sections as follows: Section I explores an introduction about the

virtual reality technologies, section II reviews some of the related works of the virtual reality program, section III explores the main concepts and bases of the educational virtual reality program, section IV explores the main approaches of building a virtual reality program, section V explores the main features of this program, section VI illustrates the main strength as well as weakness of the virtual reality program, section VII explains the requirements and components that are essential to create a virtual reality program, section VIII describes the basic concepts of designing a virtual reality program, section IX explores the design making process of this program, section X explores the use of fuzzy logic in the building of educational programs, section XI explores the main fuzzy set expressions, section XII gives a conclusion of this paper and section XIII illustrates some of the future improvements of the virtual reality program.

II. Related Works

Several researchers developed many computer education and learning technologies which offers opportunities for users to get real education and learning sense and to enhance their skills. Virtual reality technologies are interactive interfaces among persons and computers. Rheingold explored that the use of virtual reality technologies and defined them as practices where students are surrounded by computer formed demonstration. [11, 12]

Ashton explored that the virtual reality technologies are assistant educators that let students capable to visit several places and learn several cultures. Biocca contrasted among the beginning of virtual reality technology and television in the beginning of 1940s. [13, 14]

Nilan described the main cognitive space features in which virtual reality technology is utilized as illustrious to distinguish between these features and those of the physical space. Schwier supposed that the three-dimensional environment of virtual reality technology let both system and students equally adaptive which is considered as an essential issue in the learning improvement. [15, 16]

Smedley and Higgins supposed that virtual reality means anything. In other words, its definition can be ranged uncomplicated simulation program to complete fascination tools. This range of definition discovers the several virtual reality levels. The use of virtual reality in learning offers an important educational enhancement more than

the traditional techniques, since the virtual reality technology is an interactive tool and offers real educational environment. [17]

Miltenoff and Rogers compared among the PowerPoint software and virtual reality programs. PowerPoint program provides users with several reactive tools and allows the importing of images and creating conversions and animations among slides. In addition, PowerPoint program permits the use of sounds and music which in turn improve the presentations superiority. So, Miltenoff and Rogers explored that these two programs are extremely different in which the PowerPoint program shows pictures and the virtual reality program makes three-dimensional illusion. [18]

III. Concepts and Bases of an Educational Virtual Reality Program

Educational virtual reality program an improved model of the interface among students and computers. It facilitates the traveling of students to influence several objects and practice many consequences. It offers a generated sensory indication which is adequate to produce disposed suspension incredulity in students. Virtual reality program is a set of student computer interfaces, networking, sensor techniques and graphics. The use of virtual reality program let students believe that it is a real environment. Thus, this program is the most excellent way that is utilized to offer several experiences for students in a real environment. [19, 20]

Virtual reality program is a completely immersive and reactive experience of a reality by utilizing a computer where student reacts with several simulated objects. In addition, many students can see each other as well as react in a communal environment. Virtual reality program can be divided into two mean categories; immersive virtual reality and non-immersive virtual reality. The immersive virtual reality depends on immersive demonstration techniques, while the non-immersive virtual reality illustrates images in a typical screen and permits students to react with these images. [21]

In the virtual reality program, students influence in a real environment where they are completely engaged, wear gloves as well as a Head Mounted Display (HMD). These two components that used by students are utilized to sense and record the movements of students. Fiber optic cables are used also to transfer data to the computer which in turn reads data and transmits it into visual descriptions.

In this technique, students react with computers without using keyboards or mouse. In addition, students can wear a helmet which fully guarantees their ears and eyes. The used helmet consists of a video screen for each eye in which the virtual reality environment is seen in a three-dimensional way by these two screens. When a student looks at another direction, then computer will redraw what emerges in the helmet and make the delusion that the student is gazing around in a similar way to the real world. [17, 22]

IV. Approaches of Modeling a Virtual Reality Program

The model of the virtual reality program is shown in figure 1 below, this model consists of three main approaches; instruction design, educational content and development units.

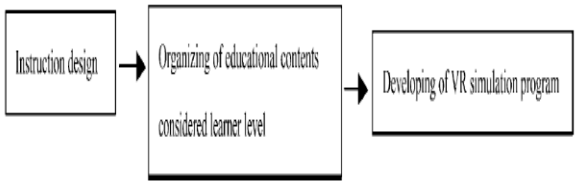

Figure 1 model of virtual reality program [23]

The instruction design approach consists of three stages, which are: Exploring of a given virtual environment by students in order to write their own comments and conclusions, discussing these comments and conclusions with teachers in which any wrong explanation is removed, using new ideas in the examination of another situation where the proposed educational cycle is repeated again. [23]

In the educational content approach, the educational contents are placed in the student's educational concept level structure. This structure is formulated with several analysis techniques of the examination level. The analysis of both concept level and examination level is followed by building the educational contents levels for several accepted, difficult and corrective courses. Investigational attributes and enactive demonstration between the educational types are used in the choosing of the learning contents by utilizing the virtual reality technology. [23]

In the development approach, the virtual reality simulation is improved by using several software programs, such as the three-dimensional webmaster which is a multifunctional tool. These programs help in the making of animated shapes, textures, clustered objects and uncluttered objects. In addition, these programs

make several viewpoints in order to observe and analyze the virtual reality world. [23]

The 3D webmaster is a Virtual Reality Modeling Language (VRML) that is similar to the HTML. It can ascertain common standards that make the virtual reality program simply language in the internet. This software creates a completely interactive environment in the web in two-dimensional pages. In addition, it offers rapid, practical and very interactive worlds. Various script languages can be used in order to create practical and helpful worlds to allocate performances to objects in the created world, carry out compound actions and adjust the virtual environments depending on the actions of the users. The interface of the software regulates the whole interaction, movement and object exploitation in the virtual environment via utilizing keyboard, mouse or joystick. [23]

The model of developing the virtual reality simulation program process is shown in figure 2 below. [23]

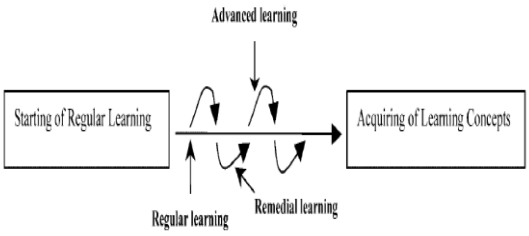

Figure 2. model of developing the virtual reality simulation program process [23]

V. Features of an Educational Virtual Reality Programs

The main features of virtual reality programs that make it an important educational tool are: [24, 25, 26]

A. Virtual reality program assists in the understanding of complicated, theoretical and non perceptive systems and perceptions. Virtual reality program utilizes several graphics as well as simulation techniques in the modeling and visualization illustrations of information, perceptions and events. In addition, this program facilitates the interaction of learners with three-dimensional models and helps them in the working with applicable parameters and employing of several viewpoints in real time.

B. Virtual reality program improves education by making the education like a game without changing fundamental contents. Due to the use of videogames, students

are extremely provoked to play these interactive games. Thus, students can master and preserve knowledge better than the traditional techniques since they are occupied with making the knowledge via studying though doing.

C. Virtual reality program permits the making of enhanced educational environments for students who cannot understand well by using the traditional techniques. This program can reengage students with learning outside the school.

VI. Strength and Weakness of Using the Virtual Reality Program as an Educational Tool

Virtual reality programs are new techniques that are suited with some applications and they are not with other ones. The main strength and weakness of these programs are: [22]

Strength:

Virtual reality programs provides several benefits for learners, such as experimental learning, capability to provide students with new styles of teaching, utilization of several systems that offer educational data and engagement of students in educational environments. Virtual reality programs can show spatial relations as well as discover environments which are unreachable.

Weaknesses:

The main critical significance of virtual reality programs is the effecting speed which requires cooperation in the precision of simulation and details in order to preserve sensible performance of the system. In addition, the limitation in accessing with the outside environment and the small declaration of learners are the main reasons of decreasing the efficiency of visual perception. Virtual reality programs are not suitable for showing equations, methods and texts at this time. Direction controls are not recognizable by all students as well as they are not obtainable for all computers.

VII. Requirements and Components of an Educational Virtual Reality Program

Virtual reality program is a simulation form that depends on the graphics of computers in order to make a virtual environment. This program allows students to compact with the created virtual environment by using simulation as well as several devices. The created virtual environment is a real time reactive system that acts in response with the inputs of students as well as change the created virtual environment along with the inputs of students. The

virtual reality program can modify and enhance the educational ways. [1, 27]

Hardware and Software Requirements:

The main hardware and software requirements which are essential in the building of a virtual reality program are: [28]

- Hardware requirements include: Displays, computers with multimedia services, actuators and sensors.
- Software requirements include: modeling software programs, such as AutoCAD, simulation systems, such as animation system and toolkits that sustain several applications.

Components of a Virtual Reality Program:

Virtual reality program consists of four main components that are shown in figure 3 below, these components are: [28]

- Virtual environment: In which a student can see and react with several units via a display screen and stereo spectacles.
- Virtual devices: The main devices are information acquisition and allocation unit which is the interface of computer with other devices, sensors that are utilized in the tracking of the student's hands and head direction and position in the three-dimensional space, gloves that are used to facilitate the communication of student with the virtual world by a finger control and stereo spectacles that permit the view of images in three-dimensional depth via students.
- Virtual real time modeling: It consists of algorithms which are used in the creation of a virtual environment and in the generation of three-dimensional graphs and mathematical models that are used to model the virtual reality environment.
- Virtual control software: The main functions of the used software are real time signal processing of virtual environment data, control of the modified virtual environment and communication among several virtual reality program components.

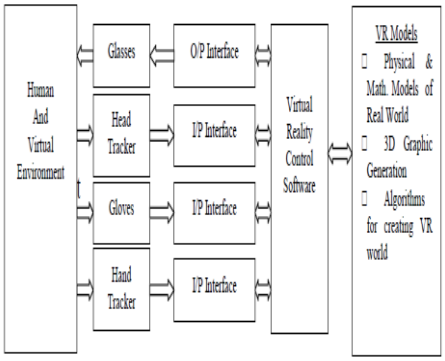

Figure 3 main components of virtual reality program [28]

Roles of Teachers:

The main roles of teachers in the virtual reality programs are: Describing the main educational outcomes and making a learning world with the purpose of addressing them, underlining contents instead of technology, offering notice and attention in order to sustain students' reactions and develop the learning community, changing the educational environment until achieving the required educational outcomes and considering the main process in order to expose the main principles of design which informs several investigators, instructors and expected projects. [5, 29]

VIII. Virtual Reality Program Design

The environment of a virtual reality program determines the popularity of this program. The most exciting characteristics that affect on the program popularity are: lights, music, colors and noises. Virtual reality program illustrates an educational environment which is simulated by using a computer. The majority of virtual reality programs are visual practices that are shown on a computer screen. [30]

Several programming languages can be used in the creation of virtual reality environments, such as the Virtual Reality Modeling Language (VRML). The use of this language facilitates the exploring of the three-dimensional world of the program, zooming and interacting with this environment. VRML contains several multimedia components, like images, sounds and videos. An example of virtual program architecture is shown in figure 4 below. [30, 31]

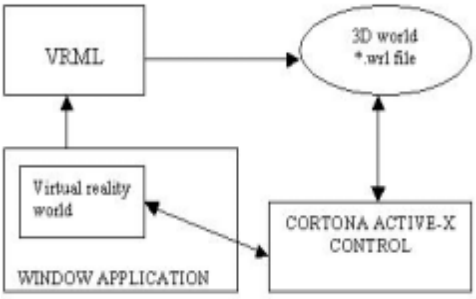

Figure 4 architecture of a virtual program [31]

The main programs that are used in order to offer a fundamental gratitude of the virtual reality educational applications are shown in the following table. The main purposes of using these programs in the virtual reality technologies varies from allowing students to visit the virtual environment to providing teachers who will utilize it in order to convene their learning objectives in the class with the virtual reality program. [32]

The main four stages of designing a virtual reality program are: [33]

- Stage one: Learn how to make a presentation.
- Stage two: Train with software and its psychoanalysis.
- Stage three: Build a virtual simulation that consists of several educational units.
- Stage four: Explore analysis of the designed virtual program that relates among practice and theory.

The virtual simulation aims to achieve four main findings, which are: [33]

- Visualization of educational processes.
- Enhancement of three-dimensional revelation as well as the spatial cleverness.
- Recognition of three-dimensional shapes.
- Solving several problems as well as enhancing the performance.

Table 1: Programs used in the creation of virtual reality program [32]

	Program Name	Participants
Outreach	Virtual Reality Roving Vehicle (VRRV)/Washington	Teachers and students grades 4-12
	VRRV/Nebraska, Phase I and II	Teachers and students
	Mobile Aeronautics Education Laboratory (MAEL)	Students grades 9-12
Web	—	Teachers
Teacher Education	VRRV/Nebraska, Phase III	Teachers
	Educators' VR Series	Teachers
	Virtual Reality in the Schools	Teachers
	Virtual Education - Science and Math of Texas (VESAMOTEX)	Teachers
	VR Concentration, M.A. in Education	Teachers
Collaborative	VR in Education	Teachers
	Virtual Reality in the Schools	Teachers

IX. Design Making Process of the Educational Virtual Reality Program

The educational virtual reality program offers a simple way to transform from one educational level to another one depending on the background of the student. The educational program can be divided into three main paths, which are:

– Educational path A which contains the learning unit review that is relatively adequate for expert students.
– Educational path B which contains the typical data which are offered by teachers to normal students.

– Educational path C which contains a full data that assists in the educational process for beginners.

Figure 5 below summarizes the proposed educational program.

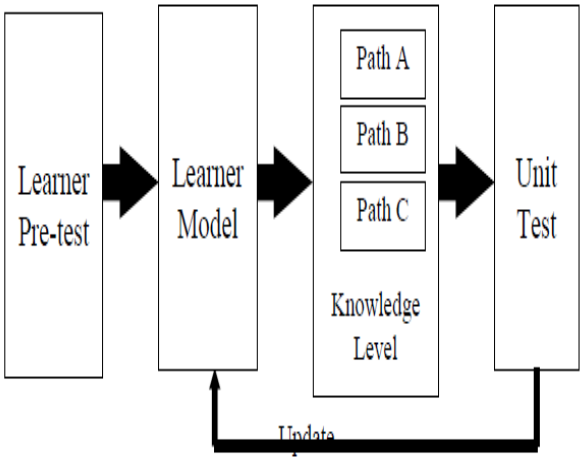

Figure 5 the proposed educational program [28]

The use of the proposed learning system permits expert students to go throughout the learning units with less time. In the other hand, beginners take long time with more effort to go throughout these units. By using this system, the course must be divided into different learning units depending on the course syllabus which is approved by the course instructor. This educational system operates as following: [28]

– A learner should take a pre-test in the beginning in order to indicate his learning level that let him go through the first learning unit.
– A Feed-forward education must be done depending on the recent student learning level.
– The student capability should be tested at each learning unit in order to inform the student's model as well as to find the next educational unit path.
– The obtained test determines the transformation of student form one level into another as shown in figure 6 below in which:

  - The student with grade very good or good is transformed to level A or is transformed from C to B in the next unit.
  - The student with grade fail is transformed from level A or B to C and continues in the same unit.
  - If the result of the test is unsatisfied, then the student will be transformed from level A or B to C and continues in the same unit regardless of his educational path.
  - If the result of the test is fail with level C, and then the student will be informed to leave the learning system.

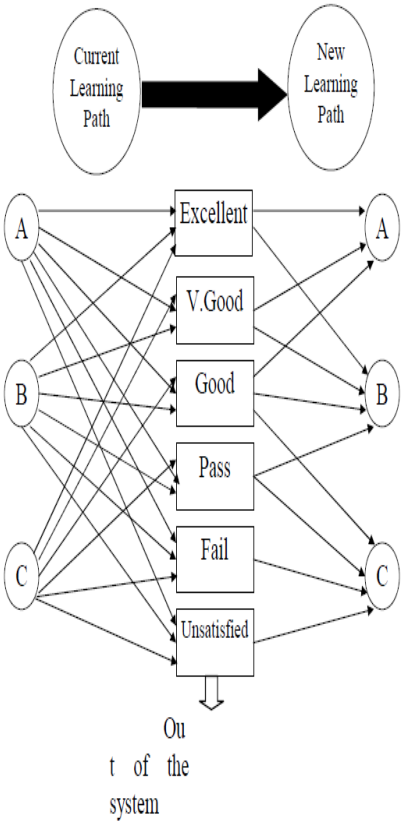

Figure 6 the educational decision making process [28]

X. Fuzzy theory in educational virtual reality systems

The main issue that must be taken into account in the building of an educational program is the use of appropriate methods for both the achievement of knowledge and making of virtual environment in real time. Actually, individual thoughts and analysis occupy indistinct data. Thus, educational programs must have the ability to manage this indistinctness which is cause by several sources, such as: [34]

- Offered data by students.
- The recent educational levels of students.
- Estimation of the student educational level.
- Teacher knowledge.
- Course objectives.

Educational virtual reality system design based in the first place on the demonstration of knowledge that is utilized in the controlling of decisions education. The educational system core is the knowledge of teachers, thus it should be modeled to make the educational programs more flexible and simple and to allow students to contract with the material of course which is appropriate to the student educational level. [26]

The modeling of teacher knowledge and course world is a difficult task due to the proposed vagueness. Thus, the use of a competent tool which is able to model the teacher knowledge and course world is an important issue in order to create flexible and simple rules of decision. The most competent tool is the fuzzy logic in which a linguistic variable employs words as values. [28]

The use of fuzzy theory in the building of educational virtual reality system can solve several problems that resulted from: [28]

- Modeling of student, teacher knowledge and virtual reality environments.

- Detection of the student's educational level in each learning unit.
- Algorithms for three-dimensional graphics and virtual environment production.
- Controlling variations in virtual reality programs.

Evaluation and estimation of students and their levels.

XI. Fuzzy Set Expressions

The main two fuzzy sets are the Interval Valued (IVFS(X)) and the Intuitionistic (IFS(X) fuzzy sets. For the intuitionistic fuzzy set that is a function of X in which X does not equal to zero and Card is also a function of X equals to K, the following formula describes its expression [35]:

$$A = \{< x, \mu_A(x), v_A(x) > | x \in X\}$$

Where: $\mu_A: X \to [0,1]$ and $v_A: X \to [0,1]$, $0 \leq \mu_A(x) + v_A(x) \leq 1$ for all $x \in X$, $\mu_A(x)$ represents the membership degree of element x to the set A and $v_A(x)$ represents the non-membership degree of element x to the set A. [35]

The main expressions for all A, B in the set X are: [35]

1.When $\mu_A(x) \leq \mu_B(x)$ and $v_A(x) \geq v_B(x)$ for $x \in X$, then A is less or equal to B

2.When $\mu_A(x) \leq \mu_B(x)$ and $v_A(x) \leq v_B(x)$ for $x \in X$, then $A \preccurlyeq B$

3. $A \vee B = \{< x, \mu_A(x) \vee \mu_B(x), v_A(x) \wedge v_B(x) > | x \in X\}$ and $A \wedge B = \{< x, \mu_A(x) \wedge \mu_B(x), v_A(x) \vee v_B(x) > | x \in X\}$ These two expressions are simply generalizable to the case of various intuitionistic suzzy sets

4. $A \leq B$ and $B \leq A$, then $B = A$

5. $A_c = \{< x,\} v_A(x), \mu_A(x) > | x \in X$

For all $| x \in X$, $\mu_A(x) + v_A(x) = 1$, thus A is considered as a fuzzy set. The following expression of the fuzzy set is considred as a the intuitionistic fuzzy set case:

$$A = \{< x, \mu_A(x) > | x \in X\} = \{< x, \mu_A(x), 1 - \mu_A(x) > | x \in X\}$$

Fuzzy sets are used widely in the provlems of decision making. The intuitionistic fuzzy set problem can be solved by considering an alternatives set and criteria sets as IFSs. In addition, the distance among the membership function and the non-membership function of a specific element is considred as a score function in relationship to both the criteria set and the alternatives set. This distance is called the Hamming fuzzy distance. The use of the Hamming fuzzy distance in the intuitionistic fuzzy set offers the following formula [35]:

$$2.\, d_{H_{IFSs(x)}}(A,B) = \sum_{k=1}^{K} |\mu_A(x_k) - \mu_B(x_k)| + |v_A(x_k) - v_B(x_k)|$$

By considering that A and B belong to IFSs(X) (x) and xi is an element in the set X, then the following expression represents $d(x_i)$: [35]

$$2.\, d(x_i) = |\mu_A(x_i) - \mu_B(x_i)| + |v_A(x_i) - v_B(x_i)|$$

This proofs that: [35]

$$d_{H_{IFSs}(X)}(A,B) = \sum_{i=1}^{K} d(x_i)$$

XII. Conclusion

Virtual reality program is an improved educational technology of the interface between students and computers that is used to enhance the learning process. It is used in the education and training in order to provide a suitable environment for the analysis and estimation of designs, reduce both the improvement time and cost and develop the superiority and usability of several products.

XIII. Future Improvements

Some of the future improvements of the educational virtual reality program are using it to sustain all categories of learning programs, looking more properly at the educational display and demonstration efficiency and comprising a speech identification technique that will help a student to get notes during his research.

References

1. Vince, “Virtual reality systems”, 1995
2. J.M. Francioni and A Kandel, “A software engineering tool for expert system design”, IEEE Expert, Vol.3, No.1, pp.33-41, 1988
3. T.T. Al-Naimi, K.M. Al-Aubidy and N.S. Al-Rawi, “Decision making in expert education systems”, Computer Research Magazine, UASRC, Vol.1, No.1, pp.5-13, 1997
4. J. J. Fitzpatrick, “Interactive virtual reality learning systems: Are they a better way to ensure proficiency?” March, 2007
5. Yukiko Inoue, ‘’ Concepts, Applications, and Research of Virtual Reality Learning Environments’’, International Journal of Human and Social Sciences, pp 1-7, 2007
6. B. Droste and A. Droste, “A virtual reality,” Independent School, Vol. 63, No. 4. February 26, 2007
7. A. Attridge, M. A. Williams, and C. Tennant “The role of physical modelling in the design verification stage of the automotive NPI process in the premium sector”, International Journal of Automotive Technology and Management, Vol. 7, No. 1, pp 32-54, 2007
8. M. Zyda “From visual simulation to virtual reality to games”, IEEE Computer Society, Vol. 38, No.9, pp 25-32, 2005
9. A. G. De Sa and G. Zachmann, “Virtual reality as a tool for verification of asembly and maintenance processes”, Computer Graphics, Vol.23, No. 3, pp 389-403, 1999
10. Abdul-Hadi G. Abulrub, Alex N. Attridge and Mark A.Williams, ‘’Virtual Reality in Engineering Education’’, IEEE Global Engineering Education Conference (EDUCON), pp 751-757, 2011
11. H. Rheingold, ‘’Virtual reality’’, 1991
12. X.D. Fang, “Application of computer animation of machining operations in support of a manufacturing course”, Intr. J. Eng. Educ., Vol.11, No.6, pp.435-440, 1998.
13. K. Ashton, “Technology and interactive multimedia: Identifying emerging issues and trends for special education”, 1992

14.F. Biocca, “Communication within virtual reality: Creating a space for research,” Journal of Communication, Vol. 42, No. 4, PP. 5-22, 1992.

15.M. S. Nilan, “Cognitive space: Using virtual reality for large information resource management problems,” Journal of Communication, Vol. 42, No. 4, pp. 115-135, 1992.

16.R. A. Schwier, “A taxonomy of interaction for instructional multimedia. Paper presented at the Annual Conference of the Association for Media and Technology in Education in Canada.” Vancouver, British Columbia, Canada, June 1993.

17.T. M. Smedley and K. Higgins, “Virtual technology: Brining the world into the special education classroom,” Intervention in School and Clinic, Vol. 41 No. 2, pp. 114-119, 2005.

18.P. Miltenoff and J. Rogers, “Teaching with technology: Multimedia and interactivity in social science education.” Multimedia Schools, Vol. 1, No. 2, 2007

19.P. A. Kommers and Z. Zhiming, “Virtual reality for education”, 2007

20.T. A. Mikropoulos, et al., “Virtual environments in biology teaching”, Journal of Biological Education, Vol. 37, No. 4, 2007

21.Information Database, “Virtual reality”, 2007

22.B. Winn, “Learning through virtual reality”, 2007

23.Young-Suk Shin, ‘’ Virtual Reality Simulations in Web-Based Science Education’’, 2002

24.Yonghui Wang, Yonggao Yang, Suxia Cui and Jian-ao Lian, ‘’ Virtual Reality Mathematic Learning Module for Engineering Students’’, the Technology Interface Journal, Vol. 10, No. 1, 2009

25.X. Wang, X. Han, and Y. Yang, “A Web-Based 3D Environment for Teaching and Learning,”, The 2005 Information Resources Management Association International Conference, San Diego, California, , pp 715- 717, May 2005

26.Y. Yang and A. Lodgher, "Use 3D Graphics Learning Environment to Help Comprehend Non-Intuitive Concepts," Computers in Education Journal, Vol. XVI, No. 4, pp.51-57, October/December 2006

27.V.S. Pantelidis, “Virtual reality and engineering education”, Computer Appl. Eng. Educ., Vol.5, No.1, pp.3-12, 1997.

28.Kasim M. Al-Aubidy, ‘’ A Virtual Reality Based Educational Module for Knowledge Learning and Skills Training’’

29.T. C. Reeves, J. Herrington, and R. Oliver, “Design research: A socially responsible approach to instructional technology research in higher education. Journal of Computing in Higher Education, Vol. 16, No. 2, pp. 97- 116, 2005.

30.George Katsionis and Maria Virvou, ‘’ A virtual reality user interface for learning in 3D’’

31.A. Ames, D. Nadeau, and J. Moreland, “VRML 2.0 Sourcebook”, 2nd Edition

32.Christine Youngblut, ‘’ Educational uses of virtual reality technology’’, 1998

33.Esther Zeretsky, ‘’ The Contribution of Virtual Reality Software to Design in Teaching Physical Education’’

34.K.M. Al-Aubidy & S.A. Gaed, “A fuzzy expert tool for educational system design”, Software Eng. Educ. Symp, pp.204-210, 1998

35.H. Bustince, 1995, ‘’ Handling multicriteria fuzzy decision making problems based on intuitionistic fuzzy set’’

Estimation the Activity of ADA in Individuals with Cataract and Glaucoma

Zainab Thamer Al-Asady

Biology department, College of Education/Ibn-Al-Haitham, University of Baghdad

Abstract

The activity of ADA was evaluated in the serum of (40) individuals (15 patients with cataract, 15 patients with glaucoma and 10 individuals as a control). The results showed significant reduction in ADA activity value in individuals with cataract and glaucoma comparing with control (147.86±2.4 Iu/mg), (164.06±2.5 Iu/mg) and (211.29±7.4 Iu/mg) respectively also there is a significant reduction in ADA activity value in individuals with cataract (147.86 ± 2.4) Iu/mg comparing with those with glaucoma (164.06 ± 2.5) Iu/mg that refer the effect of cataract on ADA activity is more than the glaucoma .

تقييم فعالية أنظيم الأدينوسين دي أمينيز عند الأشخاص المصابين بالماء الأبيض والماء الأسود

المستخلص

تم قياس فعالية أنظيم ADA لمصل 40 شخصاً (15 مصاب بالماء الابيض و15 مصاب بالماء الاسود و10 اشخاص اصحاء طبيعيين والذين يمثلون مجموعة السيطرة). أظهرت النتائج وجود إنخفاض معنوي في فعالية الأنظيم عند الأشخاص المصابين بالماء الأبيض والماء الأسود مقارنة بالسيطرة والتي بلغت فيها فعالية الأنظيم 211.29±7.4. كما وجد إن هناك إنخفاضاً معنوياً في فعالية الأنظيم عند الأشخاص المصابين بالماء الأبيض (147.86 ± 2.4) مقارنة مع الأشخاص المصابين بالماء الأسود (164.06 ± 2.5) مما يشير إلى تأثير الماء الأبيض على فعالية الأنظيم أكثر من تأثير الماء الأسود.

Introduction

Many enzymes are involved in the biosynthesis, interconversion and degradation of purine compound. These enzymes seem to play important roles in purine metabolism [1] .One of these enzymes is a adenosine deaminase (ADA) which is an important deamination enzyme , convert adenosine and 20-deoxy adenosine to inosine and 20-deoxyinosine, respectively.The genomic sequence of ADA gene spans 32k on the long arm of chromosome 20 [2] .

ADA is present in all tissues in mammals. the high activity of ADA enzyme was seen in thymes , spleen and duodenum while low activity was seen in blood , brain , muscles and pancreas [3], beside that ADA enzyme occur in other organ like liver , kidney , lung and in digestive tract that prove its role to clear the adenosine which enter the body from digestive tract .ADA enzyme also work in lung to clear the adenosine from the blood before its entrance to the heart .In serology , they measure its level in pleura fluid to detect Tuberculosis. Toxic levels of purine metabolites (adenosine, adenosine deoxyribonucleotides, due to deficiency of ADA which can cause hepatic, skeletal, neurologic and behavioral alteration [1], and sensorineural deafness [4] . A deficit of ADA enzyme causes cellular stress due to the unbalance of dNTPs leading to the inhibition of DNA replication and repair [5].After the deficit of ADA enzyme , the adenosine level is rising , linkage with its specific receptors ,singling transport is results according to this linkage , therefore there is increasing in the activity of AdeneylylCyclase enzyme which causes elevation in the level of cAmp inside the cells and enhance cell death mechanism through activation of endonucleases enzyme on Ca^{++} dependant [6].In similar way , when there is increasing in the level of deoxyadenosine , that enhance programmed death mechanism which activate Apo-1/fas mechanism which mediated cell death [7]. Therefore ADA deficiency is distinguished from other types of immunodeficiencies because it is metabolic disease causing immune dysfunction which failure to thrine impaired immunoresponses and recurrent infections [8,9]. Gene therapy is effective in patients with (SCID) like used mature hematopoietic stem cells engraftment in supporting the differential expansion of gene-Corrected cells especially in lymphoid lineages [10].

Many people sever from main eye diseases, like cataract and glaucoma, especially those people in older ages. A cataract is clouding in the lens that blocks some of the light and causes loss of vision [11] . Cataract formation is believed to involve damage to lens protein by free radicals, causing the lens to lose its transparency [12], while glaucoma is a group of diseases that damage the eye's optic nerve and can result in vision loss and blindness [13]. Several large studies have shown the elevated of intraocular pressure [eye pressure) is a major risk factor for optic nerve damage [14].

The people who suffer from age-related diseases, they have decline in the activity of many enzymes and proteins, therefore the purpose of this study to determine the impact the activity of ADA enzyme in people with cataract and glaucoma.

Materials and Methods

The serum of (40) individuals at age of (45 – 65) years old (male and female) were used in this research to evaluate ADA enzyme activity according to Giusti [15]. The sera were collected from Ibn-Al-Haitham hospital for eye diseases.

The individuals were divided into three group first group (15) individuals with cataract, second group (15) individuals with glaucoma , and third group (10) as control . At first total protein was estimated for each specimen according to Biuret kit (Randox , UK), then volume activity for ADA enzyme was evaluated for each specimen according to Giusti [15]. To estimate specific activity for ADA enzyme was used this formula:

$$\text{Specific activity (unit/mg protein)} = \frac{\text{Volume activity}}{\text{Total protein}}$$

The percentage from control value was estimated by this formula:

$$\frac{\text{The ADA activity in cataract or glaucoma}}{\text{The ADA activity in control}} \times 100$$

Statistical significances of differences between the groups were tested with two-tailed t test.

Results and Discussion

There are many mechanisms like oxidation and reduction have special importance in the eye damage which can result in a number of molecular changes that contribute to the development of glaucoma , cataract and other eye diseases [16,17] . Many studies about eye's diseases used plasma to measure many factors, because it was not possible to measure the status of factors in the eye itself [18], therefore we used

serum to measure the ADA activity in this study. The results of this research showed a significant reduction ($P<0.001$) in the percentage value of ADA activity in individual with cataract and glaucoma comparing with control. The percentage value of reduction in individuals with cataract was 70 .14 % while the percentage value of reduction in individuals with glaucoma was 76.78 % comparing with control which ADA activity value was 211.29 ± 7.4 Iu/mg (Fig. 1) The reduction in ADA enzyme activity in cataract and glaucoma groups is associated with age – related morbidit because there is a general consensus that cumulative oxidative and toxic damage is responsible for aging [19] and there is an age related rise in systemic oxidant which may be affected on the activity of ADA like the decreased in the activity of other enzymes (catalase , superoxide dismutase , peroxidase) which associated with cataract and glaucoma [4,20].

When we compared the results of ADA activity value between the individuals with cataract and other with glaucoma, we showed significant reduction ($P < 0.001$), the reduction value was presented in individuals with cataract 147.86 ± 2.4 Iu/mg comparing in individuals with glaucoma 164.06 ± 2.5 Iu/mg (fig.2).

The activity of ADA enzyme of the cataract group in this study was significantly decreased compared with its activity in individuals with glaucoma , like this result observed in the many studies about the activity value of antioxidant enzymes which was decreased in cataract group compared with glaucoma group which showed increased in the activity value of these enzymes [21] . That may be refer the effect of cataract on ADA activity is more thane the glaucoma . Any stress lead to accumulate the second messengers like diacylglycerol (DAG), Inositol triphosphate (IP_3) and the increasing of Ca^{++} concentration in the cell which effected on the biosynthesis and activity of different proteins and enzymes like ADA , this effect may be happen at molecular level and gene expression [22].

The results in this research showed that people with cataract and glaucoma appeared to have reduction in the activity of ADA which gives an indication of declined activity of immune system.

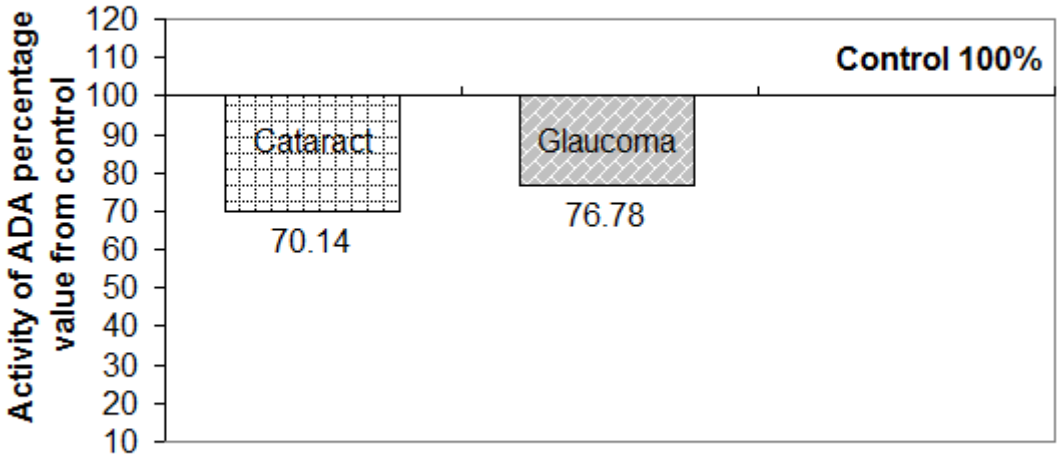

Fig.(1) The Activity of ADA enzyme in indivatulas with cataract and glaucoma comparing with control

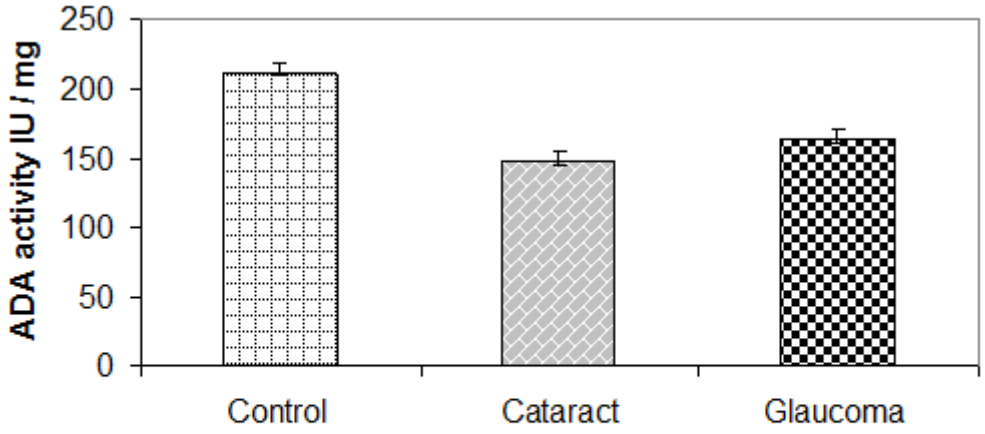

Fig.(2) Activity of ADA in cataract is lower than in glaucoma

References:

1. Moriwaki , y. ; yamamoto , T. ; Higashino, K. (1999). Enzymes involved in purine metabolism--a review of histochemical localization and functional implications.HistolHistopathol . 14(4): 1321 - 1340
2. Helani , A. ; Almassri , Nidal and Abu – Amero , k (2009) . A novel Mutation in the ADA gene causing severe combined immunodeficiency in an Arab patient : a case report . J. med . Case Report, 3: 6799.
3. Adams, A. and Harkness, R. (1976). Adenosindeaminase activity in thymus and other human tissues. Clin. Exp. Immunol., 26(3): 647-649.
4. Shenoy , T.S and Clifford , A.J. (1975) . Adenine nucleotide metabolism in relation to purine enzymes in liver, erythrocytes and cultured fibroblasts.BiochimBiophysActa. 411(1):133-43.
5. Tullo, A.; Mastropasqua , G.; Bourdon , J.C; Centorze , P; Leveoro , M.;Del Sal ; G.; Saccon , C. and Sbisa , E. (2003) Adenosine deaminaseakey enzyme in DNA percentage control , is a new P73 target . Oncogen, (22):8738-8748 .
6. Aldrich , M.B.;Blackburn , M.R. and Kellems , R.E. (2000) Breakthroughs and views . Biochem.Biophys.Res.Comm., 272: 311-315.
7. Ratter, F.; Germer, M.; Fischbach ,T.;Schulzerosthoff, K.; Peter , M.E.; Drage , W., Krammer, P.H. and Lehamann ,V. (1996) S-adenosylhomocysteine as a physiological modulator of Apo-1. Mediated apoptosis .Immunol.8:1139-1147.
8. Filanovskaia, L. I.; Vartanian, N. L.; Togo, A. V.; Samuskevich, I. G. and Blinov, M. N. (1985) .Enzymes of purine nucleotide catabolism in lymphocytes in normal states and in chronic lymphoid leukemia Vopr Med Khim., 31(3):48-53.
9. Levy, Y.; Hershfield, M. S.; Fernandez-Mejia, C., Polmar, S. H.; Scudiery, D.; Berger, M. and Sorensen, R.U. (1988)Adenosine deaminase deficiency with late onset of recurrent infections: response to treatment with polyethylene glycol-modified adenosine deaminase.J. Pediatr., 113(2):312-7.
10. Aiuti , A. ; Cattaneo , f . ; Galimberti , S . ; Benninghoff u. and cassani , B. (2009) Gene Therapy for Immunodeficiency Due to AdnosineDeaminase Deficiency . New Eng . J. Med . 360 : 447 – 458
11. British Colombia Medical Association (2005). Cataract – Treatment of Adults. (Article)

12.www.health-herbal.com cataract and the role of antioxdants (Percival, 1998)

13.www.nei.nih.gov. (Glaucoma.what you should know).

14.Yildirim , O:; Ates , N.A. ; Ercan , B- ; Muslu, N Ünlü , A.. ; Tamer , L . ; Atik , U . and kanik , (2005) . Role of Oxidative stress enzyme In open - angle glaucoma . Eye, 19 : 580 – 58.

15.Giusti , G. (1981) Adenosine deaminase In : Berg Meyer , H . U . (Ed) Methods of Enzymatic Analysis, 2nd Ed. Academic press. Vol . 2 : 1092 – 1099

16.Berman , E. R . (1991) *Biochemistry of the Eye* , plenum Press , New York: 476 pp.

17.Augusteyn , R.C. (1981) . Protein modification in cataract: possible Oxidative mechanisms . In: Duncan , G (ed) Mechanisms of Cataract formation in the Human lens . Academic press: (London) . pp 71 – 116

18.Belpoliti , M . ; Maraini , G . ; Alberti , G . Corona , R. and Crateri (1993) Enzyme Activities in Human lens Epithelium of Age – Related cataract . Invest . Ophthalmol. VISSCi , 34 : 2843 – 2847

19.Ferreira , S.M. ; Lerner , S.F , Brunzini , R . and Liesuy , S . F . (2010) . Glaucoma Damage Beyond the Eye : Oxidation stress Markers in Brain Homogenates . Invest . Ophthalmol VIS SCi, 51 : 6108 .

20.Chandrasena , G . ; Chackrewarthy , ; Teckla , P.; perera , M J . and silva , D. (2006). Erythrocyte antioxidant enzymes in patient with cataract. Ann. Clin. Lab. Sci., 36 (2): 201-204.

21.Ferreira , S. M . ; Lerner , S.F. ; Brunzini , R. ; Evelson , P.A. and Liesuy , S. F . (2004) Oxidative stress markers in a queous humor of glaucoma patient Am . J . Ophthalmol . 137 (1) : 62 – 69

22.Mckee, T. and Mckee, J.R. (1996) *Biochemistry* .Wm.C. Brown publishers. London : 638 pp.

EFFECT OF SUBLETHAL DOSE OF *Najanaja* SNAKE VENOM ON LEVELS OF SOME LIVER ENZYMES IN ALBINO MALE RATS

Taha Shawi Morad

Department of Human Anatomy ,Medical Biology, College of Medicine , Al-Naharin University

ABSTRACT

The effects of (*Najanaja*) snake cobra venom on some liver enzymes in albino male rats have been investigated. The effects of a single sublethal dose of *Najanaja* snake venom (0.04µg/g) body weight on the activities of certain serum enzymes levels: aspartate aminotransferase (AST), alanine aminotransferase (ALT) and alkaline phosphatase (ALP) were studied. Samples from the serum were collected 3 and 24 h following venom dose intraperitonealy injected in male albino rats. The activities of these enzymes showed significant elevation compared to the control. *Najanaja* snake venom caused damage and hepatic dysfunction in enevomated male rats.

Keywords: *Najanaja* venom, aspartate aminotransferase (AST), alanine aminotransferase (ALT), alkaline phosphate (ALP)**.**

تأثير الجرعة تحت المميتة لسم ألأفعى Najanaja على بعض إنزيمات الكبد في ذكور الجرذان البيض

المستخلص

تم في الدراسة الحالية التعرف على تأثير سم أفعى الكوبرا (*Najanaja*) في بعض أنزيمات الكبد في ذكور الجرذان البيض. تمت دراسة تأثير الجرعة المنفردة تحت المميتة (0.04 µg/g) لسم ألافعى المحقونة داخل الغشاء البريتوني لبعض الإنزيمات (ALT.AST & ALP). أخذت العينات من مصل الحيوانات بعد 3 و24 ساعة من الحقن. أظهر نشاط هذه ألانزيمات أرتفاعا معنويا عند مقارنتها بمجموعة السيطرة. سبب سم ألافعى تلف واختلال وظيفي للكبد في الحيوانات المحقونة بالسم.

Introduction

Snakes are cold-blooded vertebrates, and some species possess dangerous venoms. Cobras, which are widely distributed over the world, belong to the Elapidae family. *Najanaja*is one of the most dangerous snake species in the world , where it provokes a high number of human deaths due to envenomations [1]. *Najanaja*cobra venom contains a mixture of many different proteins, including a variety of enzymes (proteases and phospholipases), non-enzymatic polypeptide toxins (neurotoxins and cardiotoxins), and other substances [2,3]. Cobra envenoming is known to induce multiple-organ failure, leading to death in case of severe envenoming [4]. Liver is considered as one of the targets for cobra venom factor [5]. Moreover, the toxicity of the venoms of *Naja*species has been attributed to the presence of cardiotoxins or other cytotoxins (cytotoxin P4) and nigexine (basic phospholipase A2) [6]. There are reports showing the effects of various snake venomson ALT ,AST and ALP in rat that venom inceasing the level s of these enzyme and damage of the hepatocyes of the liver [7,8,9,]

The liver is a key organ actively involved in numerous metabolic and detoxifying functions. The objective of this study is to determine some biochemical changes in the liver of rats following snake cobra (*Najanaja*) envenomation in an attempt to improve our understanding of snake envenomation in rats .

Materials and Methods

Venom:

Lyomphilized*Najanaja*venom was obtained from India (Sigma loeate Ltd).Lyophilizedvenom was dissolved in phosphate buffered saline(PBS), pH 7.2.

Toxicological studies:

The determination of the median lethal dose LD_{50} of the snakevenom by intraperitoneally (i.p.) injection was carried on 40 adult healthy albino rats .The LD_{50} was determined in rats according to the method of Meier and Theakston[10], (Table 1).

Animals and Experimental design:

A total number of 24 adult healthy male albino rats weighing (180-200 g) obtained from the Institute of Embryo Researches and Infertility Treatment , AL-Nahrain University and used throughout this study. . All animals were given free access to standard laboratory chow and tap water. The animals were divided randomly into two main groups:

Group I- normal control (NC):

Eight normal healthy rats, each received a single i.p injection of 0.25 ml saline and remained intact serving as normal control.

Group II

This group includs 16 normal healthy rats, each received a single i.psublethal dose 0.04 µg/g body weight of snake venom in 0.25 ml phosphate buffered saline. These animals were divided into two subgroups (A and B). Each consisted of 8 rats, and was sacrificed by decapitation after 3 and 24 hours of the injection.

Blood Collection and handling:

At the end of the experimental period, the animals from the experimental groups together with the normal control group were decapitated, and the blood was collected by heart puncture and immediately placed into non heparinized tubes to obtain the serum for analysis of (ALT, AST,and ALP). Blood samples in the non- heparinezed tubes were allowed to clot at room temperature for 1h. Serum samples were obtained by centrifugation of non heparinized tubes at 3000 r.p.m. for 20 min. Clear serum was aspired and stored at refrigerator until used in the same day. The kinetic measurement of plasma ALT , AST and ALP by spectrophotometer using commercially available diagnostic kit (BioMareuix , France).

Statistical analysis

The results are given as mean ± standard error (X± S.E.). Significance of the differences was tested by analysis of variance (ANOVA) test. The levels of significance were taken at p <0.01.

Results and Discussion:

Venom Lethality:

The approximatei.p. LD_{50} for *Najanaja* snake was determined in rats to be equal to 0.05 µg/g body weight , as shown in table 1. the present results showed that the LD50 of *Najanaja*snake venom is approximately equal to 0.05µg/g body weight . Other investigators reported that the LD50 of the same venom is 0.066 µg/g body weight [11], 0.50 µg/g body weight [12] . These differences of LD50 could be attributed to differences in geographical distribution of *Najanaja* snake , seasonal variations in composition and potency of venoms (13,14,15].

Table 2 showed the effect of sublethal dose *Najanaja*snake venom on serum ALT, AST and ALP activity. There was significant elevation in serum ALT, AST, and ALP levels (P<0.01) in rats after 3 and 24 hrs treated with 0.04 µg/g (body weight) *Najanaja*snake venom in comparison with control group. Biochemical results showed that treatment with snake venom induced a significant increase in activity of serum ALT, AST and ALP activity. The principal marker enzymes include alanine (ALT) and aspartic (AST) aminotransferases, which catalyze the transfer of α-amino groups from alanine and aspartate to the α-keto group of ketoglutaric acid to produce pyruvic acid and oxaloacetic acid, respectively [16]. Other enzymes such as alkaline phosphatase (AP)

may also be used as markers of hepatic dysfunction [17]. Serum enzymes analysis proved to be very useful for liver diseases diagnosis . Serum alanine aminotransferase ALT), aspartate aminotrans- ferase (AST) and alkaline phosphatase (ALP) serve as markers for hepatocellular damage [18]. The result of this study is in agreement with that of [19] who reported that i.p of *Najahaje venom* to male rats induced changes in the activities of ALT , AST ALP activity . Elevated activities of ALT, ALP and AST have been reported due to envenoming with animals venom [20,21]. Rats treated with the *Najanaja*snake venom suffer from hepatocellular injury and dysfunction which are represented by significant elevations in the activities of serum ALT , AST and ALP. The present study was similar with previous studies which revealed harmful effects of venom on hepatocytes and induction of degenerative changes the liver [22]. The general rise in the activities of ALT, AST and ALP that indicate the damage of liver ,heart and other organs brought about by the venom [23,24].

Table (1). Determination of LD_{50} of *Najanaja* snake Cobra venom on rats.

Dose µg/g body weight	No. of animals	Survival (S)	Death (D)	% Mortality
0.02	8	8	0	**0%**
0.04	8	5	3	**37.5%**
0.06	8	3	5	**62.5%**
0.08	8	1	7	**%87.5**
0.1	8	0	8	**100%**

LD_{50} = 0.05 µg/g body weight rats

Table (2): Serum ALT, AST ,and ALP in rats of all groups

Parameters	No. of rats	Group 1	GroupII	
		Normal (Control)	Time after (i.p) venom injection	
			3 hours	24 hours
S ALT (U/L) Mean + S.E % change P <0.05	8	62.3±5.9	89.1±5.6 * 43.01	99.6±4.1 * 59.87
S AST (U/L) Mean + S.E % change P <0.05	8	123.7±6.3	143.8±4.8 * 16.24	167.9±3.4 * 35.73
S ALP (U/L) Mean + S.E % change P < 0.05	8	313.8±3.5	344.2±4.7 * 9.68	357.4±6.9 * 13.89

*P<0.01 (significantly different from the control)

REFERENCES

1. Li ,S.; Wang, J.; Zhang, X.; Yan, R.; Wang, N.; Zhao, K .(2004) . Proteomic characterization of two snake venoms: *Najanajaatra*and *Agkistrodonhalys* . Biochem J., 384(1):119-27.
2. Ponnappa, KC.; Saviour, P.; Ramachandra ,N .; Kini ,RM .; Gowda, TV. (2008). INN-toxin, a highly lethal peptide from the venom of Indian cobra (*Najanaja*)venom: isolation, characterization and pharmacological actions . Peptides. , 29(11):1893-900..
3. Binh ,DV.; Thanh, TT.;Chi ,PV. (2010) . Proteomic characterization of the thermostable toxins from *Najanaja*venom. J. Venom. Anim.Toxins. Incl. Trop. Dis. , 16 (4) : 631-638.
4. Cher, C.D.; Armugam, A.; Zhu, Y.Z.; Jeyaseelan, K. (2005). Molecular basis of cardiotoxicity upon cobra envenomation . Cell Mol. Life Sci ., 62(1): 105-118.
5. Fu, Q.L.; Satyaswaroop, P.G.; Gowda, D.C. (1997). Tissue targeting and plasma membrane clearance of cobra venom factor in mice . BiochemBiophys. Res. Commun.,231(2): 316-320.
6. Chwetzoff, S.; Tsunasawa, S.; Sakiyama, F.; Mènez, A. (1989):Nigexine, a phospholipase A2 from cobra venom with cytotoxic properties not related to esterase activity: Purification, amino acid sequence, and biological properties. *J. Biol. Chem*. 264(22):13289- 98.
7. Mohamed, A.H., Fouad, S.; EL-Assar, S.; Salem, A.M.; Abdel aal, A.;

Hassan,A.; Zahran, F.; Abbas, N. (1981). Effects of several snake venoms on serum and tissue transaminases, alkaline phosphatase and lactate dehydrogenase. *Toxicon*19 ,605 – 609.

8. Abdel-Aal, A.; (1998). Effect of *Cerastescerastes*venom on some biochemical parameters in serum and urine of rats. J. Egypt. Ger. Soc. Zool., 26 (A):41-58

9. Al-Sadoon1,M.; Fahim ,A. ; Safwat, F.; Gamal B . (2012). The effects of LD50 of *Walterinnesiaaegyptia*crude venom on blood parameters of male rats. African Journal of Microbiology Research 6(3): 653-659 .

10.Meier, J.; Theakston, R.D.G. (1986) .Approximate LD50 determinations of snake venoms using eight to ten experimental animals. Toxicon, 24(4): 395-401.

11.Lee,C.Y.;Lioe,C.; Lin,S.Y.(1971) .Identification of cholinesterase inactivating factor in cobra venom with cardiotoxin . Toxicon 9(1):429-433

12.Omale ,s.; Aguiyis ,JC.; Wannang ,NN.; Ogbole, E.; Amagon, KI. (2012) .Effects of the ethanolic extract of *Parinaricuratellifolia*on bloodclotting factors in rats pretreated with venom of *Najanajanigricolis* . Drug Invention Today .4(4):363-364 .

13.**13**-Jayanthi, G.P.;GWDA, TV. (1998) . Geographed variation in india in the composition and lethal potency of viper venom .Toxicon .26(30):257-264

14.Shashidharamuthy, R .; Jagadeesha ,D K.; Girish, KS . ;Kemparaiu ,K. (2002). Variations in biochemical and pharmacological properties of Indian cobra (Naja najanaja) venom due to geographical distribution. Mol .Cell Biochem. 229(1-2):93-101.

15.Shashidharamuthy, R .; Mahadeswarasamy ,YH .; Raqupathi ,L .;Kemparaiu ,K .(2010). Systemic pathological effects induced by cobra (Najanaja) venom from geographically distinct origins of Indian peninsula. Exp .ToxicolPathol. 62(6):587-92.

16.West, J. B. (1985): Blood and the plasma proteins: Function and composition blood. In: Best and Taylor's physiological basis of medical practice. 11th edt.Williams and Wilkins, Baltimore, pp. 334 – 340.

17.B urtis , C .; A shwood, E. (2001) .Tietz Textbook of Clinical Chemistry. 5.ed. Philadelphia . WB Saunders .USA.

18.Talwer, G.P.; Scrivastava, L.M.; Moudgil, K.D. (1989)**:** Text Bookof Biochemistry and Human Biology". 2nd ed ., Prentice Hall of Indian, New Delhi

19.Omran, M A.; Abdel Nabi, M.; El Naggar, M .H. (1997): Serum Biochemical and Hormonal parameters for the toxic effects of Egyptian Corba (Najahage) envenomation. J. Nat. Toxins, 6:69-83.

20.Mirakabadi, A.Z.; Jalali, A .; Vatanpur, H.; Akbary, A. (2006):Biochemical changes and manifestations of envenomation produced 75 by *odonthobuthusdoriae*venom in rabbits. J. Venom. Anim.Toxins. Incl. Trop. Dis. 12**:** 67-77.

21.C haves,F.;Guiterrez,JM.; Lomonte , B.; Cerdas, L. (1989)Histopathological and biochemical alterations induced by intramuscular injection of *Bothropsasper* (terciopelo) venom in mice.Toxicon. 27, 1085- 93**.**

22.Adzu, B. ; Abubakar, M.S.; Izebe, K.S. ; Akumka, D.D.; Gamaniel, K.S.(2005): Effect of *Annonasenegalensis*rootbark extracts on *Najanigricollisnigricollis*venom in rats. J Ethnopharmacol. 96(3): 507-513.

23.Abdel-Nabi,I.M .; Raafat ,A.; El-Shamy ,H .(1997).Biological effects of intraperitoneal injection of rats with venom of the snake *Echiscarinatus* .Egypt. J .Zool.,29:195-205.

24.Fahim ,A.(1998). Biological effects of the viper Bitisarietans ,crude venom on albino rats . Egypt. J .Zool. 30:35-54